PUCRS

SCHOOL OF TECHNOLOGY
GRADUATE PROGRAM IN ELECTRICAL ENGINEERING
MASTER'S DEGREE IN ELECTRICAL ENGINEERING

KAYOL SOARES MAYER

NMCMA-SDD CONCURRENT EQUALIZER

Porto Alegre
2018

PÓS-GRADUAÇÃO - *STRICTO SENSU*

Pontifícia Universidade Católica
do Rio Grande do Sul

PONTIFÍCIA UNIVERSIDADE CATÓLICA DO RIO GRANDE DO SUL
SCHOOL OF TECHNOLOGY
GRADUATE PROGRAM IN ELECTRICAL ENGINEERING

KAYOL SOARES MAYER

NMCMA-SDD CONCURRENT EQUALIZER

Advisor: Prof. Maria Cristina Felippetto de Castro, Ph.D.
Co-advisor: Prof. Fernando César Comparsi de Castro, Ph.D.

Porto Alegre – RS, Brazil
2018

KAYOL SOARES MAYER

NMCMA-SDD CONCURRENT EQUALIZER

Dissertation presented to the Graduate Program in Electrical Engineering of the Pontifícia Universidade Católica do Rio Grande do Sul, as requisite to obtain Master's degree in Electrical Engineering.

Concentration Area: Signals, Systems and Information Technology.

Research Area: Telecommunications.

ADVISOR: Prof. Maria Cristina Felippetto de Castro, Ph.D.

CO-ADVISOR: Prof. Fernando César Comparsi de Castro, Ph.D

Porto Alegre – RS, Brazil

2018

Ficha Catalográfica

M468n Mayer, Kayol Soares

NMCMA-SDD Concurrent Equalizer / Kayol Soares Mayer . – 2018.
130 f.
Dissertação (Mestrado) – Programa de Pós-Graduação em Engenharia Elétrica, PUCRS.

Orientadora: Profa. Dra. Maria Cristina Felippetto de Castro.
Co-orientador: Prof. Dr. Fernando César Comparsi de Castro.

1. Dynamic Communication Channels. 2. NMCMA. 3. SDD. 4. Concurrent Equalizer. I. de Castro, Maria Cristina Felippetto. II. de Castro, Fernando César Comparsi. III. Título.

Elaborada pelo Sistema de Geração Automática de Ficha Catalográfica da PUCRS
com os dados fornecidos pelo(a) autor(a).
Bibliotecário responsável: Marcelo Votto Texeira CRB-10/1974

Pontifícia Universidade Católica do Rio Grande do Sul
ESCOLA POLITÉCNICA
PROGRAMA DE PÓS-GRADUAÇÃO EM ENGENHARIA ELÉTRICA - PPGEE

NMCMA-SDD CONCURRENT EQUALIZER

CANDIDATO: KAYOL SOARES MAYER

Esta Dissertação de Mestrado foi julgada para obtenção do título de MESTRE EM ENGENHARIA ELÉTRICA e aprovada em sua forma final pelo Programa de Pós-Graduação em Engenharia Elétrica da Pontifícia Universidade Católica do Rio Grande do Sul.

DRA. MARIA CRISTINA F. DE CASTRO - ORIENTADORA

DR. FERNANDO CÉSAR COMPARSI DE CASTRO - CO-ORIENTADOR

BANCA EXAMINADORA

DR. DALTON SOARES ARANTES - PROGRAMA DE PÓS-GRADUAÇÃO EM ENGENHARIA ELÉTRICA - UNICAMP

DR. DARIO F. GUIMARÃES DE AZEVEDO - PROGRAMA DE PÓS-GRADUAÇÃO EM ENGENHARIA ELÉTRICA - PUCRS

ACKNOWLEDGMENTS

I would like to acknowledge and thank the following people who have supported me, not only during the course of this dissertation, however throughout my Master degree.

Firstly, I would like to extend my sincere gratitude to my advisor Prof. Maria Cristina Felippetto De Castro and my co-advisor Prof. Fernando César Comparsi de Castro for encouraging my research and for allowing me to grow as an academic researcher.

I would also like to thank Prof. Candice Müller, for her time, dedication, patience and faith that someday I will not write anymore in “Kayoleese” dialect.

And Finally, I would like to thank all my close friends and family. You have all encouraged and believed in me.

“Each dream you leave behind is a part of your future that will no longer exist."

(Steve Jobs)

ABSTRACT

In wireless digital communication systems, the transmitted signal may be affected by several sources of distortion, the most significant being Additive White Gaussian Noise (AWGN), multipath and Doppler effect. In environments where the impulse response of the communication channel is time variant, as in mobile communications, the multipath distortion is dynamic. Together with the Doppler effect, the dynamic multipath may even completely interrupt the wireless communication link. In order to solve this issue, blind channel equalizers are used to mitigate the multipath and Doppler effects. In this context, this dissertation proposes a novel blind channel equalizer, based on the Nonlinear Modified Constant Modulus Algorithm (NMCMA) and on the Soft Direct Decision (SDD) equalizers in a concurrent architecture. This novel NMCMA-SDD concurrent equalizer is compared with the state of the art, the Constant Modulus Algorithm (CMA)-SDD concurrent equalizer, over the so-called “Brazil channels A-E”, proposed by the International Telecommunication Union (ITU). The proposed equalizer presents significant results when compared with the state of the art, making possible its operation in wireless communication links for Unmanned Aerial Vehicles (UAVs), terrestrial vehicles, and others dynamic communication scenarios.

Keywords: Dynamic Communication Channels. NMCMA. SDD. Concurrent Equalizer.

RESUMO

Em sistemas de comunicação digital sem fio, o sinal transmitido pode ser afetado por várias fontes de distorção, sendo as mais significantes o ruído gaussiano branco aditivo (AWGN), multipercurso e efeito Doppler. Em ambientes onde a resposta de impulso do canal de comunicação é variável no tempo, como em comunicações móveis, a distorção por multipercurso é dinâmica. Juntamente com o efeito Doppler, o multipercurso dinâmico pode até mesmo eventualmente interromper completamente o link de comunicação sem fio. Para minimizar este problema, equalizadores de canais autodidatas são usados para mitigar os efeitos de multipercurso e Doppler. Neste contexto, esta dissertação propõe um novo equalizador de canal autodidata (*blind*), baseado no algoritmo de módulo constante modificado não linear (NMCMA) e no equalizador *Soft Direct Decision* (SDD) em uma arquitetura concorrente. Este novo equalizador concorrente NMCMA-SDD é comparado com o estado da arte, o equalizador concorrente com algoritmo de módulo constante (CMA)-SDD, operando sob os chamados "*Brazil channels A-E*", proposto pela União Internacional das Telecomunicações (UIT). O equalizador proposto apresenta resultados significativos em comparação com o estado da arte, possibilitando operação em links de comunicação sem fio entre veículos aéreos não tripulados (UAVs), veículos terrestres e em outros cenários de comunicação dinâmica.

Palavras-chave: Canais de Comunicação Dinâmicos. NMCMA. SDD. Equalizador Concorrente.

LIST OF FIGURES

LIST OF TABLES

LIST OF ABBREVIATIONS AND ACRONYMS

ATSC	Advanced Television Systems Committee
AWGN	Additive White Gaussian Noise
CIR	Channel Impulse Response
CMA	Constant Modulus Algorithm
DD	Direct Decision
FSE	Fractionally Spaced Equalizer
ISI	Intersymbol Interference
ITU	International Telecommunication Union
LMS	Least Mean Square
MCMA	Modified Constant Modulus Algorithm
MSE	Mean Squared Error
NMCMA	Nonlinear Modified Constant Modulus Algorithm
PDF	Probability Density Function
PMF	Probability Mass Function
PSK	Phase-Shift Keying
QAM	Quadrature Amplitude Modulation
SDD	Soft Direct Decision
SER	Symbol Error Rate
SGD	Stochastic Gradient Descent
SNR	Signal-to-Noise Ratio
UHF	Ultra High Frequency
VHF	Very High Frequency
WSS	Wide Sense Stationary
ZF	Zero Forcing

CONTENTS

1. INTRODUCTION

Mobile systems, such as satellite links with mobile ground stations (terrestrial, aerial and maritime vehicles), or links between mobile stations (aircrafts, Unmanned Aerial Vehicles (UAVs), terrestrial vehicles and so on) operate in highly dynamic propagation scenarios, not infrequently under severe multipath, particularly when one of the stations operates in urban environment or, in a less extent, in hilly environment. Single carrier systems like these usually adopt *M*-QAM (Quadrature Amplitude Modulation) or *M*-PSK (Phase-Shift Keying) modulation due to a good data throughput with a not excessive processing complexity.

In digital transmission over wireless communication channels, the transmitted signal may be corrupted by many distortions, such as Additive White Gaussian Noise (AWGN), Doppler effect and multipath (HAYKIN, 2013; PROAKIS; SALEHI, 2008). These channel distortions cause Intersymbol Interference (ISI) on the received signal at the receiver (HAYKIN, 2013; PROAKIS; SALEHI, 2008).

In order to reduce the multipath effect, a usual technique is the channel equalization. An equalizer is an inverse filter whose coefficients are adaptively adjusted such that the impulse response of the filter, convolved with the Channel Impulse Response (CIR), results in a single impulse in some determined instant of time. This process is used to minimize the amplitude of the echoes in the combined impulse response (filter-channel). The channel deconvolution operation, handled by the equalizer, minimizes the ISI effect due to multipath scenarios (HAYKIN, 2013). Adaptive equalization is based on the work of Widrow and Hoff (1960), which proposed an adaptive filtering process called Least Mean Square (LMS). The LMS adaptive filter is dependent upon a training sequence to iteratively adjust its coefficients (HAYKIN, 2013, 2014).

For a given transmitted signal spectrum bandwidth, the necessity of the transmission of a training sequence for channel equalization results in the reduction of the useful information transmission data rate. Specifically, the equalizer training sequence is spectrum consuming, given that the reduction of the useful data rate for an available signal bandwidth stems from the fact that an equalizer training sequence does not convey any useful data information but only information to specifically train the equalizer.

For such reason, it is imperative the optimization of the transmission signal bandwidth in order to avoid spectrum waste due to training sequences, which do not convey any useful information. To this end, blind equalizers are preferably used, since they do not depend on the transmission of training sequences known at the receiver end. Blind equalizers operation is based on the statistic properties of the signal distorted by the channel multipath but not on reference training signals.

The Constant Modulus Algorithm (CMA) (GODARD, 1980), in the fractionally spaced architecture, is perhaps one of the currently most used blind equalizers for QAM, according to Proakis and Salehi (2008). Nevertheless, the CMA has a slow convergence rate and a moderate residual Mean Squared Error (MSE). Besides, it does not recover the phase of the received signal distorted by multipath, inevitably occurring the rotation of the received symbols constellation with respect to the reference constellation (OH; CHIN, 1995).

In order to solve the CMA issues, Oh and Chin (1995) addressed a solution based on the partitioning of the Godard (1980) cost function in its real and imaginary components. The Modified Constant Modulus Algorithm (MCMA) corrects the CMA issue of phase recovery, as well as increases the convergence rate and reduces the residual MSE.

Another method used to work around the CMA problems was proposed by De Castro F. C. C., De Castro M. C. F. and Arantes (2001), where a concurrent architecture, composed by a CMA and a Direct Decision (DD) (MACCHI; EWEDA, 1984) equalizers, was addressed. This equalizer, CMA-DD, presents better results than the MCMA.

Using as reference the work of De Castro F. C. C., De Castro M. C. F. and Arantes (2001) work, Chen (2003) replaced the DD equalizer for a Soft Direct Decision (SDD) equalizer, thus achieving faster convergence rate with the CMA-SDD than with the CMA-DD equalizer.

Wang (2010) proposed a novel equalizer, the Nonlinear Modified Constant Modulus Algorithm (NMCMA). This equalizer is based on the nonlinear function presented by You and Hong (1998). The NMCMA presents better results than the MCMA due to the robustness provided by the well-marked region of decision.

In such context, the goal of this work is to contribute to the state of the art of single carrier mobile systems by proposing a new equalization technique that allows such systems to robustly operate in dynamic multipath scenarios. The proposed approach is based on the concurrent equalizer proposed by De Castro F. C. C., De Castro M. C. F. and Arantes (2001), with the replacement of the CMA for the NMCMA algorithm and with the replacement of the DD for the SDD algorithm. This dissertation has the objective of improving the performance of wireless communication systems over environments with dynamic multipath.

This dissertation is organized as follows: Chapter 2 presents the *M*-QAM digital modulation, the wireless channel distortions: AWGN, multipath, and Doppler shift. Chapter 2 also presents the main mathematical descriptions of the blind equalizers, and their features and issues as well. Chapter 3 then describes the NMCMA-SDD concurrent equalizer proposed in this dissertation. Going further, Chapter 4 depicts the simulation results obtained in this dissertation and compares the proposed approach to the CMA-SDD concurrent equalizer, which is the current state of the art. Finally, Chapter 5 delineates the final considerations of this dissertation and future research suggestions are presented.

2. BACKGROUND

This chapter presents to the reader the background of digital modulation, wireless channel distortions, and blind equalizer. In the digital modulation section, the single carrier *M*-QAM scheme is presented. Next, the wireless channel distortions: AWGN, multipath, and Doppler shift are depicted. Finally, the equalizer blind architectures: CMA, MCMA, NMCMA, SS, SDD, CMA-DD and CMA-SDD concurrent equalizers are mathematically described.

2.1. DIGITAL MODULATION

In digital communication systems, the transmitted information is a stream of bits that, if transmitted in a raw pulse waveform with steep edge transitions, would require a spectrum with infinite bandwidth for its representation (SMITH, 1999). Since the communication channels are limited in band and usually are shared among various transmitters (HAYKIN, 2013; PROAKIS; SALEHI, 2008), the transmission of a stream of bits through a raw pulse waveform sent across the channel is not a practical solution.

In order to limit the spectrum of the transmitted signal, the modulation process is used, where the stream of bits is converted in a waveform with restrained spectrum. In this conversion process, the stream of bits is partitioned into blocks of L bits, accordingly to the desired transmission bitrate.

In complex communication systems based on single carrier architecture, perhaps the most used modulation is the Quadrature Amplitude Modulation (QAM). In the QAM scheme, the stream of bits is mapped into a sequence of complex numbers $s[n] = I[n] + jQ[n]$, where each complex number of $s[n]$ denotes a IQ (In-Phase/Quadrature) symbol of the reference constellation $\mathcal{S}$ and $n = 0, 1, \dots, n \to \infty$. Figure 1 depicts the *M*-QAM constellations (PROAKIS; SALEHI, 2008), with $M = 4$, 8, 16, 32 and 64.

The set of possible IQ symbols is defined by the value of M for the desired M-QAM, where $M = 2^L$. The *M*-ary complex alphabet is given by $\mathcal{S}_{p,q} = \{[2p - \sqrt{M} - 1] + j[2q - \sqrt{M} - 1], 1 \leq p \leq \sqrt{M}, 1 \leq q \leq \sqrt{M}\}$. The interval of time between two

consecutives IQ symbols $s[n]$ and $s[n+1]$ is given by $T_S = 1/S_R$, being S_R the adopted symbol rate.

Figure 1 – M-QAM constellation for M = 4, 8, 16, 32 and 64.

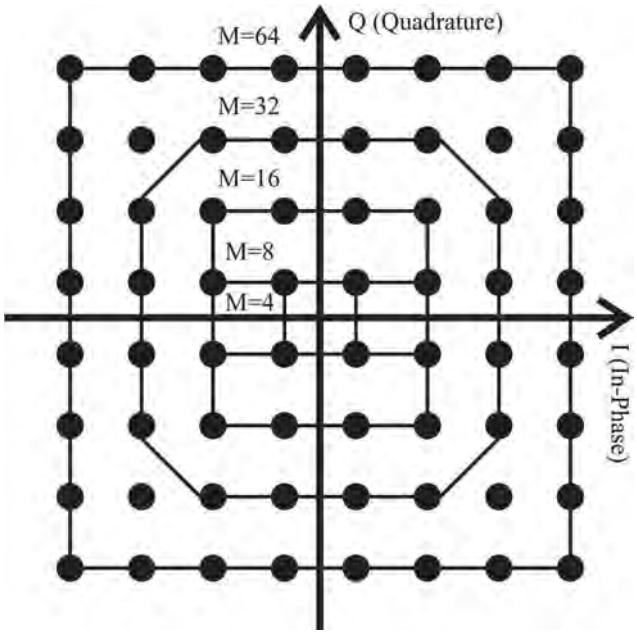

Source: Adapted from Proakis and Salehi (2008).

After upconversion to a passband channel with a central frequency f_0, the IQ symbols are transmitted through the magnitude and phase of the electromagnetic wave of frequency f_0 that propagates across the wireless channel between the transmitter and the receiver. The transmitted IQ symbol sequence $s[n]$ is distorted and interfered in the channel by a variety of sources of distortion and interference – mainly AWGN, Doppler and multipath.

The effect of the communication channel on the signal $r[n]$ that arrives at the receiver input can be represented as

$$r[n] = \sum_{i=0}^{L_{CH}-1} h_i[n]s[n-i] + a[n], \tag{2.1}$$

where $h_i[n]$ is the impulse response of the i^{th} propagation path on channel, $a[n]$ is the AWGN and L_{CH} is the channel dispersion. The sections that follow, discuss the main sources of distortion: Multipath, Doppler effect, and AWGN.

2.2. MULTIPATH

Multipath occurs when the input signal at the receiver antenna arises from the superposition of multiple inbound electromagnetic waves that impinge the antenna from multiple propagation paths on the channel, each path with different delay values (PROAKIS; SALEHI, 2008), as depicted by Figure 2. Thus, the multipath may be represented by the channel impulse response (CIR) vector $\underline{h}[n] = \left[h_0[n], h_1[n], \cdots, h_{L_{ch}-1}[n]\right]^T$, where $[\cdot]^T$ denotes the vector transpose operator.

In order to establish a standard set of multipath profiles for telecommunication researchers, the International Telecommunication Union (ITU), in March 2003, defined five different multipath scenarios, the so-called “Brazil channels” (ITU, 2008). This set of scenarios has been used as a benchmark for equalizers performance assessment, due to its similarity to real static multipath distortions. The Brazil channels are a set of five distinct multipath delay profiles designated as Brazil A, Brazil B, Brazil C, Brazil D, and Brazil E.

Figure 2 – Multipath scenario.

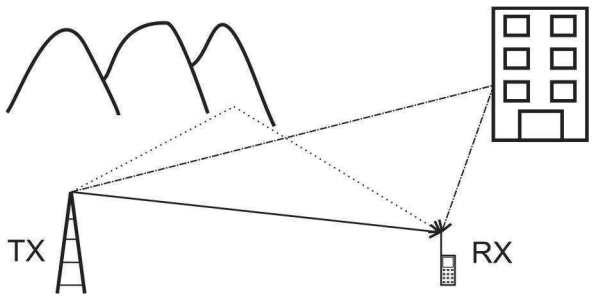

Source: Author (2018).

2.2.1. Static Brazil A

The delay profile of the static Brazil A channel is presented in Table 1.

Table 1 – Static Brazil A delay profile.

Channel parameters	Path 1 (main path)	Path 2	Path 3	Path 4	Path 5	Path 6
Delay (μs)	0.00	0.15	2.22	3.05	5.86	5.93
Attenuation (dB)	0.00	13.8	16.2	14.9	13.6	16.4

Source: ITU (2008).

Figure 3 illustrates the channel impulse response for a symbol rate $S_R = 10.7622377622$ MHz (symbol rate adopted by the ATSC digital television system) (ATSC, 2006) and for a fractionally sampling $\Upsilon = 2$. The magnitude and phase of the channel frequency response are presented in Figures 4 and 5, respectively.

Figure 3 – Channel impulse response of the static Brazil A.

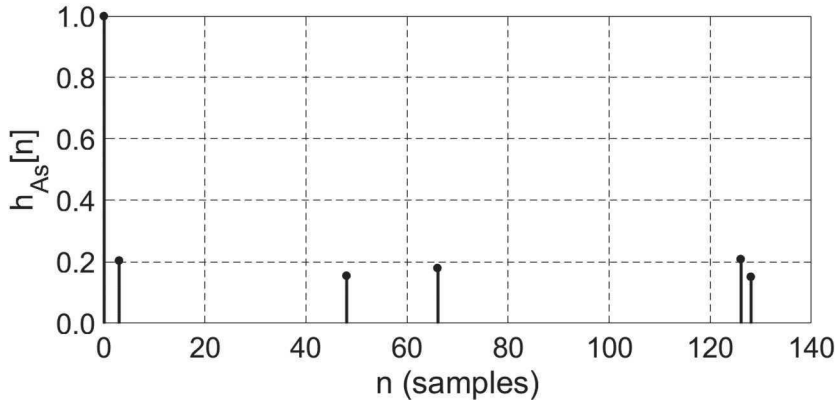

Source: Author (2018).

Figure 4 – Magnitude of the channel frequency response to the static Brazil A.

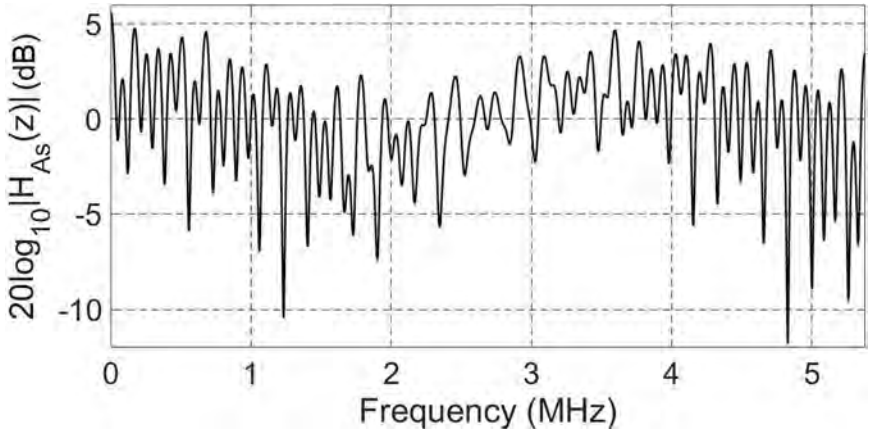

Source: Author (2018).

Figure 5 – Phase of the channel frequency response to the static Brazil A.

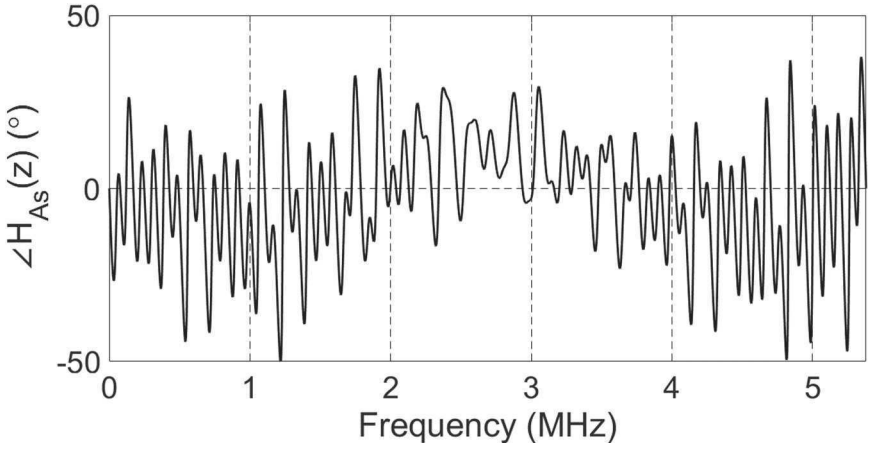

Source: Author (2018).

2.2.2. Static Brazil B

The delay profile of the static Brazil B channel is presented in Table 2.

Table 2 – Static Brazil B delay profile.

Channel parameters	Path 1 (main path)	Path 2	Path 3	Path 4	Path 5	Path 6
Delay (μs)	0.00	0.30	3.50	4.40	9.50	12.7
Attenuation (dB)	0.00	12.0	4.00	7.00	15.0	22.0

Source: ITU (2008).

The channel impulse response for a symbol rate $S_R = 10.7622377622$ MHz and a fractionally sampling $\Upsilon = 2$ is depicted in Figure 6. The magnitude and phase of the channel frequency response are presented in Figures 7 and 8, respectively.

Figure 6 – Channel impulse response of the static Brazil B.

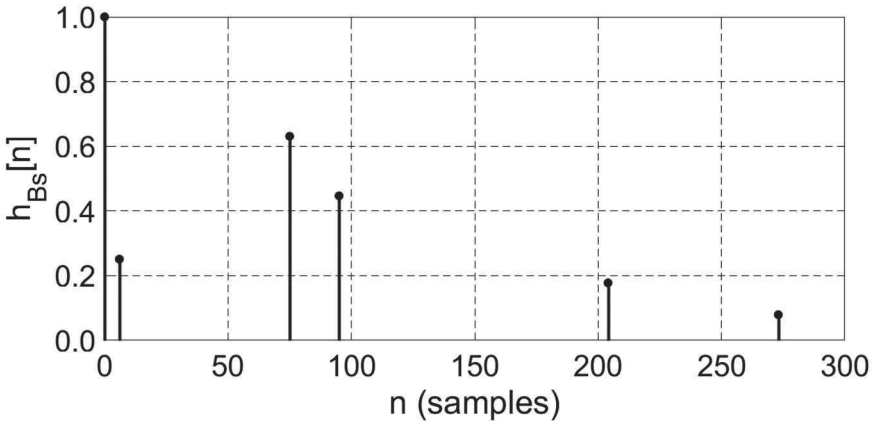

Source: Author (2018).

Figure 7 – Magnitude of the channel frequency response to the static Brazil B.

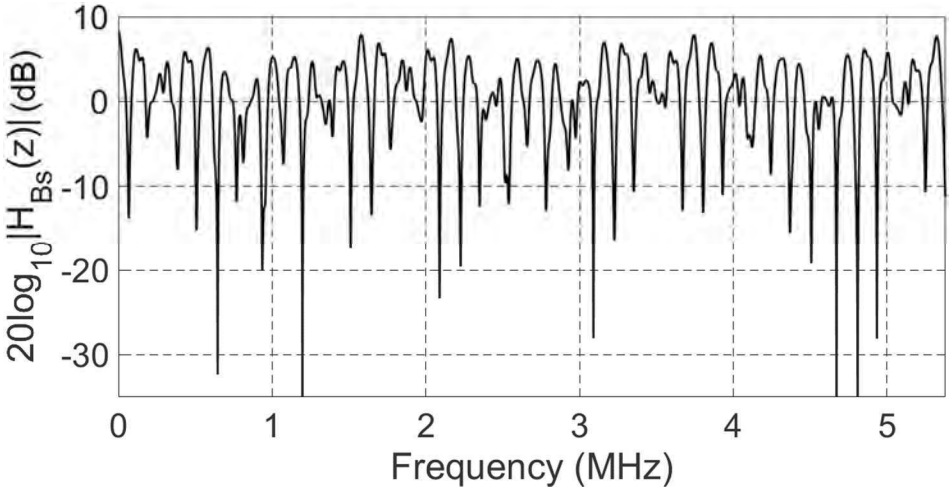

Source: Author (2018).

Figure 8 – Phase of the channel frequency response to the static Brazil B.

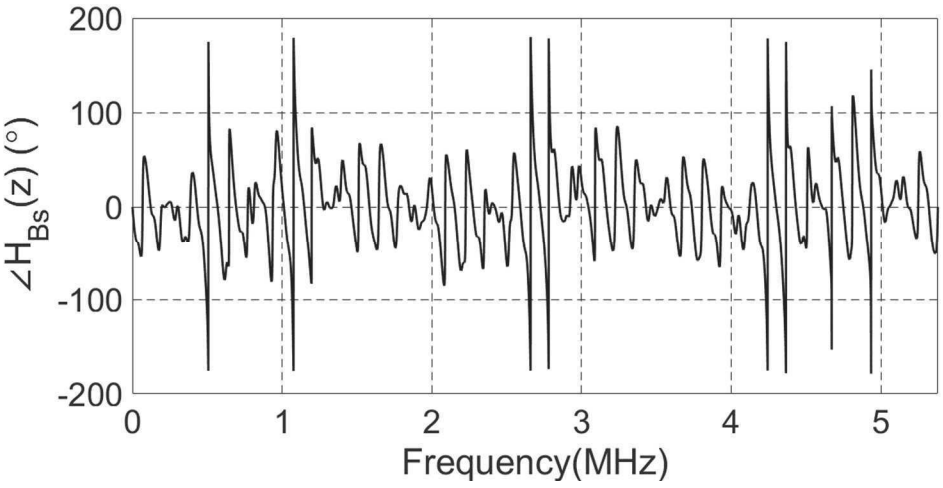

Source: Author (2018).

2.2.3. Static Brazil C

The delay profile of the static Brazil C channel is presented in Table 3.

Table 3 – Static Brazil C delay profile.

Channel parameters	Path 1	Path 2	Path 3 (main path)	Path 4	Path 5	Path 6
Delay (μs)	0.000	0.089	0.419	1.506	2.322	2.799
Attenuation (dB)	2.800	0.000	3.800	0.100	2.500	1.300

Source: ITU (2008).

The channel impulse response for a symbol rate $S_R = 10.7622377622$ MHz and a fractionally sampling $\Upsilon = 2$ is depicted in Figure 9. The magnitude and phase of the channel frequency response are presented in Figures 10 and 11, respectively.

Figure 9 – Channel impulse response of the static Brazil C.

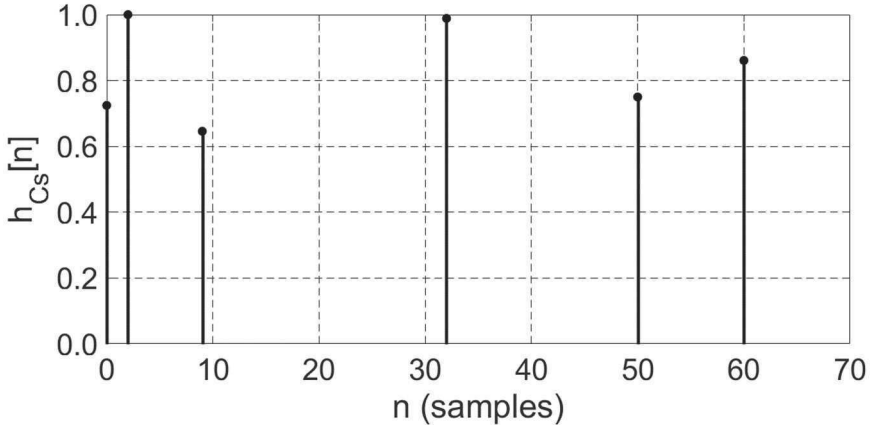

Source: Author (2018).

Figure 10 – Magnitude of the channel frequency response to the static Brazil C.

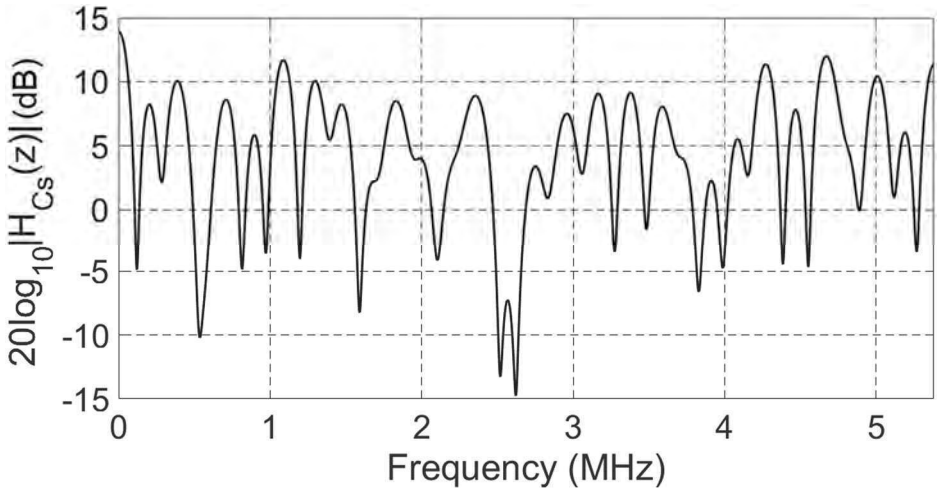

Source: Author (2018).

Figure 11 – Phase of the channel frequency response to the static Brazil C.

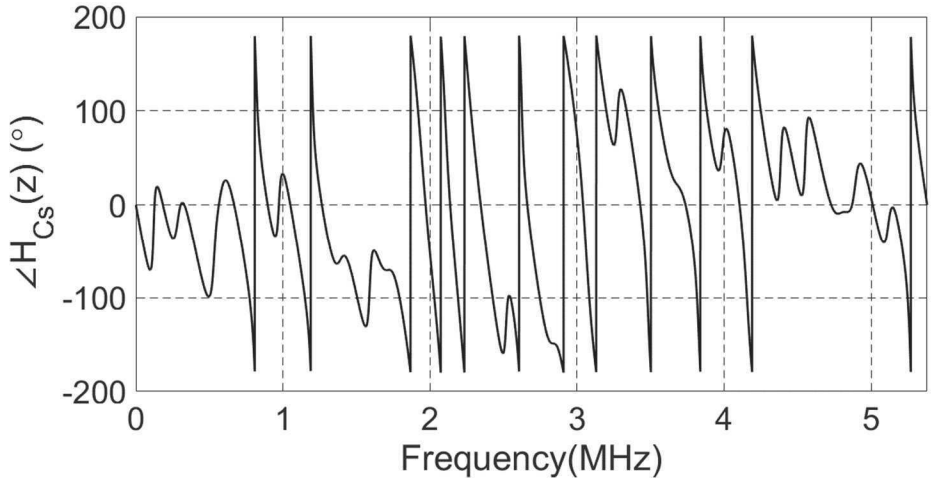

Source: Author (2018).

2.2.4. Static Brazil D

The delay profile of the static Brazil D channel is presented in Table 4.

Table 4 – Static Brazil D delay profile.

Channel parameters	Path 1 (main path)	Path 2	Path 3	Path 4	Path 5	Path 6
Delay (μs)	0.15	0.63	2.22	3.05	5.86	5.93
Attenuation (dB)	0.10	3.80	2.60	1.30	0.00	2.80

Source: ITU (2008).

The channel impulse response for a symbol rate $S_R = 10.7622377622$ MHz and a fractionally sampling $\Upsilon = 2$ is depicted in Figure 12. The magnitude and phase of the channel frequency response are presented in Figures 13 and 14, respectively.

Figure 12 – Channel impulse response of the static Brazil D.

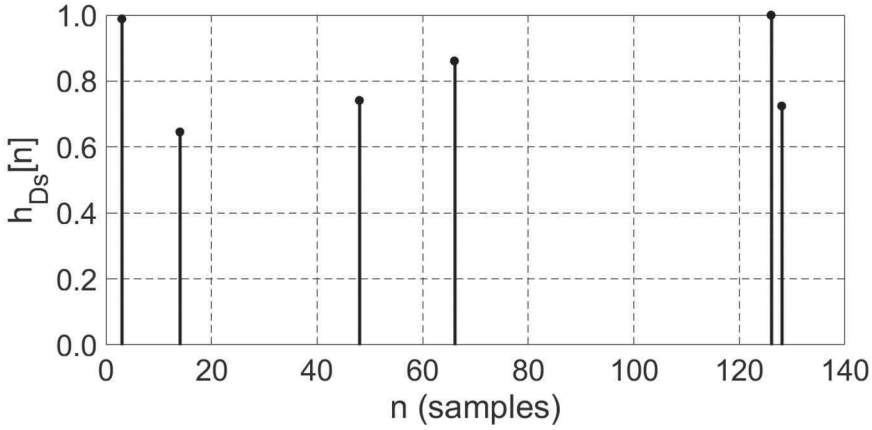

Source: Author (2018).

Figure 13 – Magnitude of the channel frequency response to the static Brazil D.

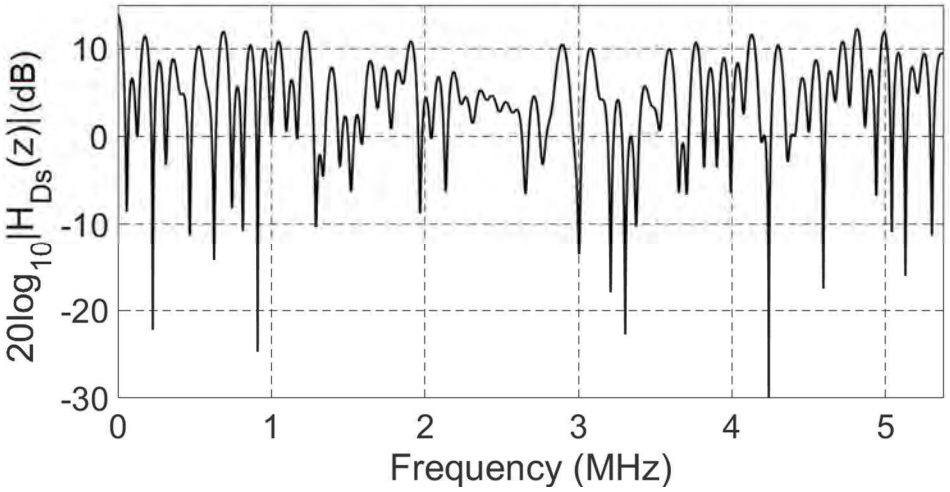

Source: Author (2018).

Figure 14 – Phase of the channel frequency response to the static Brazil D.

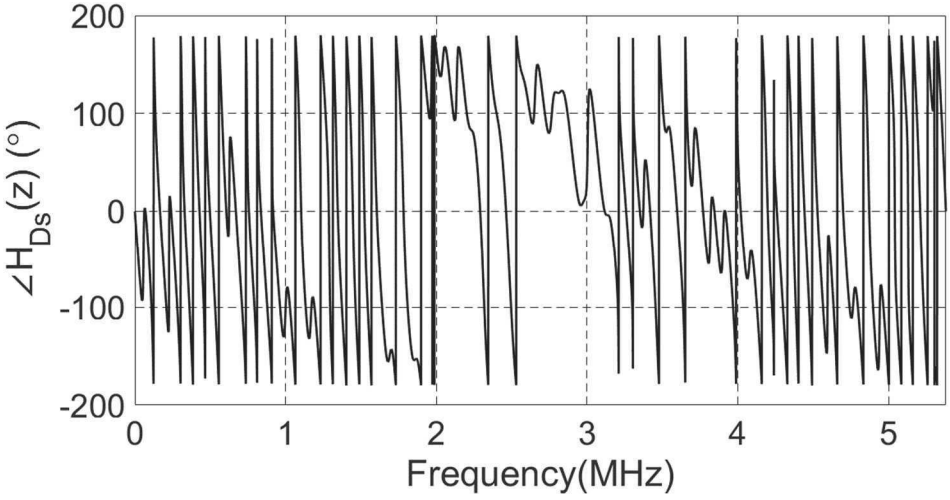

Source: Author (2018).

2.2.5. Static Brazil E

The delay profile of the static Brazil E channel is presented in Table 5.

Table 5 – Static Brazil E delay profile.

Channel parameters	Path 1	Path 2	Path 3 (main path)
Delay (μs)	0.0	1.0	2.0
Attenuation (dB)	0.0	0.0	0.0

Source: ITU (2008).

The channel impulse response for a symbol rate $S_R = 10.7622377622$ MHz and a fractionally sampling $\Upsilon = 2$ is depicted in Figure 15. The magnitude and phase of the channel frequency response are presented in Figures 16 and 17, respectively.

Figure 15 – Channel impulse response of the static Brazil E.

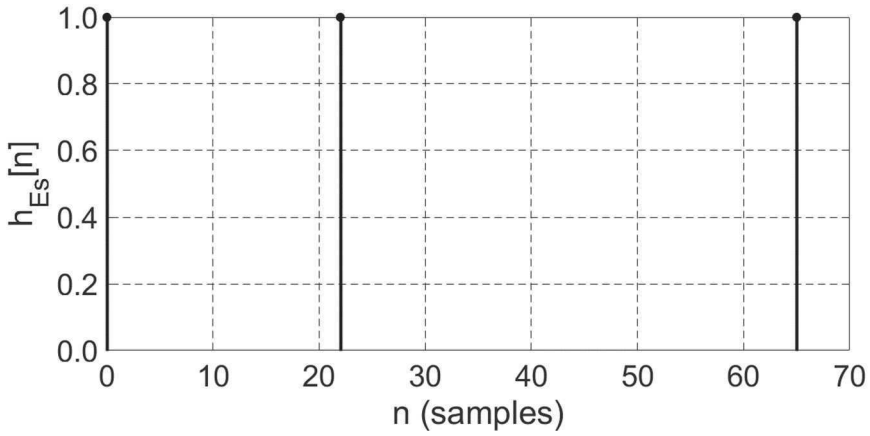

Source: Author (2018).

Figure 16 – Magnitude of the channel frequency response to the static Brazil E.

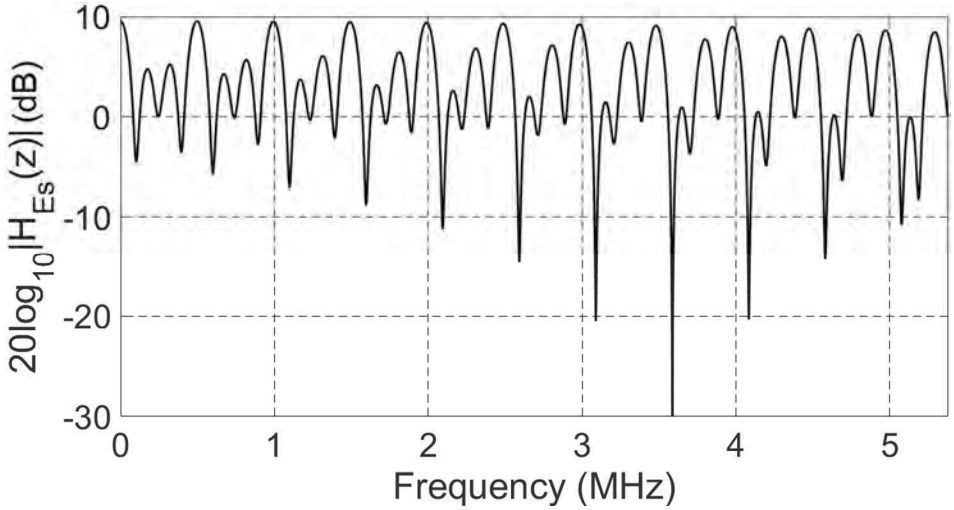

Source: Author (2018).

Figure 17 – Phase of the channel frequency response to the static Brazil E.

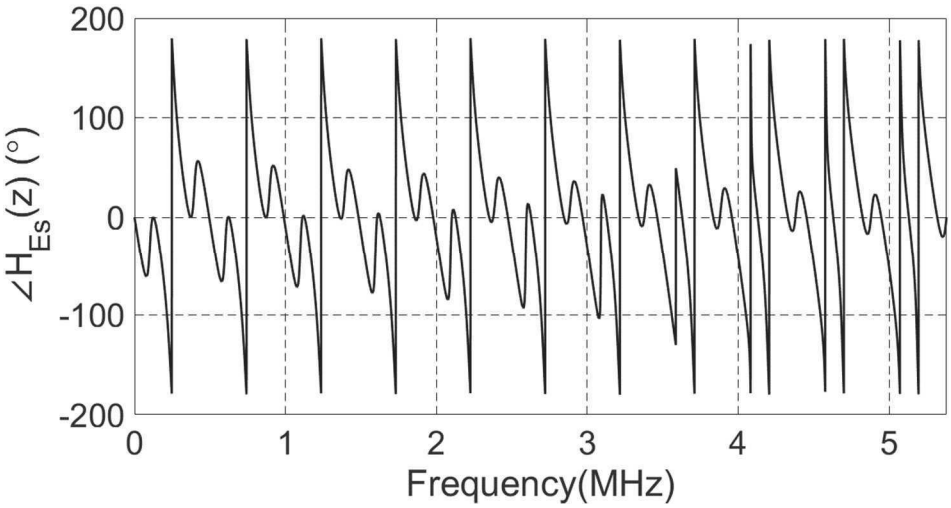

Source: Author (2018).

2.3. DOPPLER EFFECT

In a wireless link, the transmitted electromagnetic wave propagates across the transmission channel towards the wireless receiver antenna. The electromagnetic wave is reflected for each conductive object along its propagation path, thus propagating in a distinct path than the original one. Therefore, the input signal at the receiver antenna is a superposition of multiple inbound electromagnetic waves originated at the reflective objects. These inbound waves impinge the antenna from multiple respective propagation paths on the channel, each path with different delay values. Depending on the paths delay and attenuation, the superposition of multiple inbound electromagnetic waves may result in total destructive interference between the inbound waves (maximum fade), or result in total constructive interference between the inbound waves (maximum boost), or result in any wave interference scenario between the two previous ones. Thus, when one or more of these reflective objects moves in relation to the receptor and/or to the transmitter, or when the receiver and/or the transmitter moves in relation to the reflective objects, the magnitude and phase of the input signal at the receiver antenna become variable in time, since it results from the superposition of multiple inbound waves with variable magnitude and phase in time.

Any object moving with velocity v that reflect a wave of frequency f_c will shift the reflected wave frequency of an amount f_D due to the Doppler effect. Thus, the Doppler shift is an average measure of how fast the reflective objects, and/or the

transmitter and/or the receiver are moving in the transmission channel with respect each other. Specifically, any channel with multipath and without Doppler shift is called as static channel $\underline{h}$ and any channel with multipath and with Doppler shift is called as dynamic channel $\underline{h}[n] = \left[h_0[n], h_1[n], \cdots, h_{L_{CH}-1}[n]\right]^T$ (HAYKIN, 2013; PROAKIS; SALEHI, 2008).

Doppler shift is given by

$$f_D = \frac{f_c\, v}{c}, \tag{2.2}$$

where c is the speed of light.

In order to simulate the Doppler shift over the Brazil channels, an adaptation of the delay profile is necessary (NORONHA, 2012). The i^{th} path of the delay profile, with Doppler shift, is given by

$$h_i[n] = \begin{cases} b_i, & n = 0, \\ b_i \cos\left(\dfrac{2\pi n f_D}{\Upsilon S_R}\right), & n > 0, \end{cases} \tag{2.3}$$

where b_i is the i^{th} attenuation of the delay profile.

2.3.1. Dynamic Brazil A

The first dynamic Brazil channel adapted from the ITU (2008) is defined by a delay profile with five paths, besides the main one (first path), with the Doppler shift applied to the fourth path. The delay profile of the dynamic Brazil A is presented in Table 6.

Table 6 – Dynamic Brazil A delay profile.

Channel parameters	Path 1 (main path)	Path 2	Path 3	Path 4	Path 5	Path 6
Delay (μs)	0.00	0.30	3.50	4.40	9.50	12.7
Attenuation (dB)	0.00	12.0	4.00	7.00	15.0	22.0
Doppler Frequency (Hz)	0.00	0.00	0.00	20 or 50	0.00	0.00

Source: Adapted from ITU (2008).

Magnitude and phase of the channel frequency response, for a symbol rate $S_R =$ 10.7622377622 MHz and a fractionally sampling $\Upsilon =$ 2 are respectively

depicted in Figures 18 and 19, for a Doppler shift $f_D = 20$ Hz. Figures 20 and 21 present the magnitude and phase of the channel frequency response for $f_D = 50$ Hz, respectively.

Figure 18 – Magnitude of the channel frequency response to the dynamic Brazil A for $f_D = 20$ Hz.

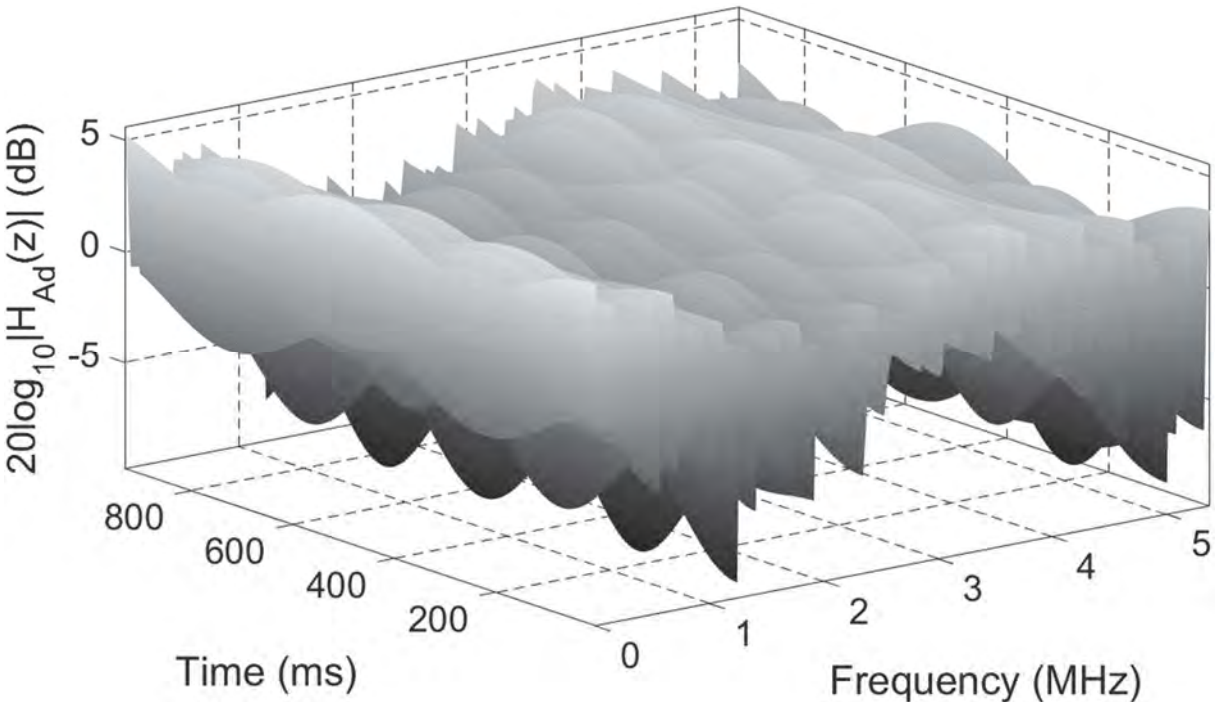

Source: Author (2018).

Figure 19 – Phase of the channel frequency response to the dynamic Brazil A for $f_D = 20$ Hz.

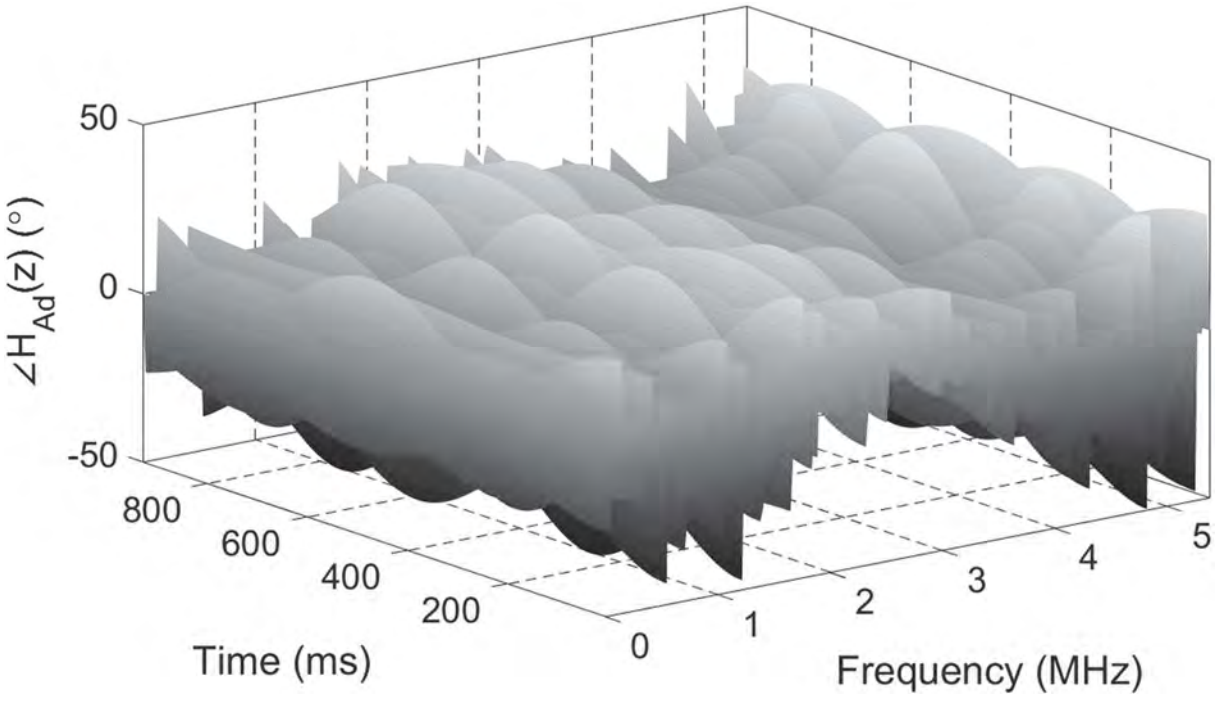

Source: Author (2018).

Figure 20 – Magnitude of the channel frequency response to the dynamic Brazil A for $f_D = 50$ Hz.

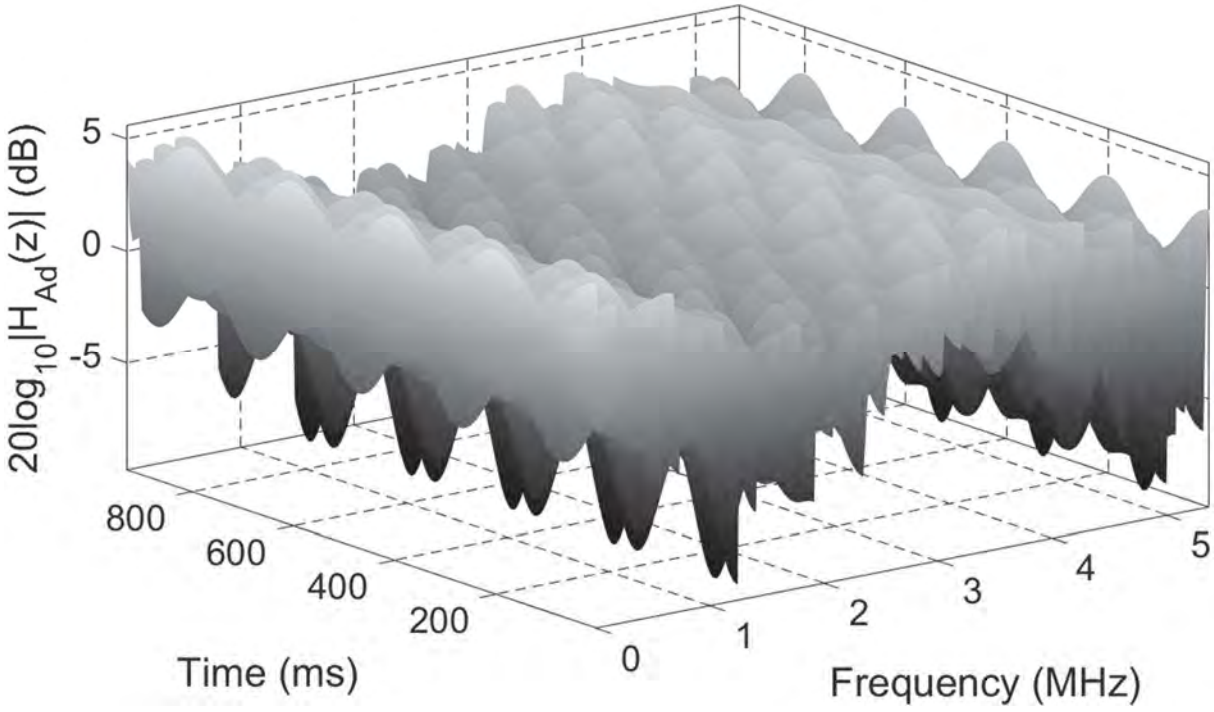

Source: Author (2018).

Figure 21 – Phase of the channel frequency response to the dynamic Brazil A for $f_D = 50$ Hz.

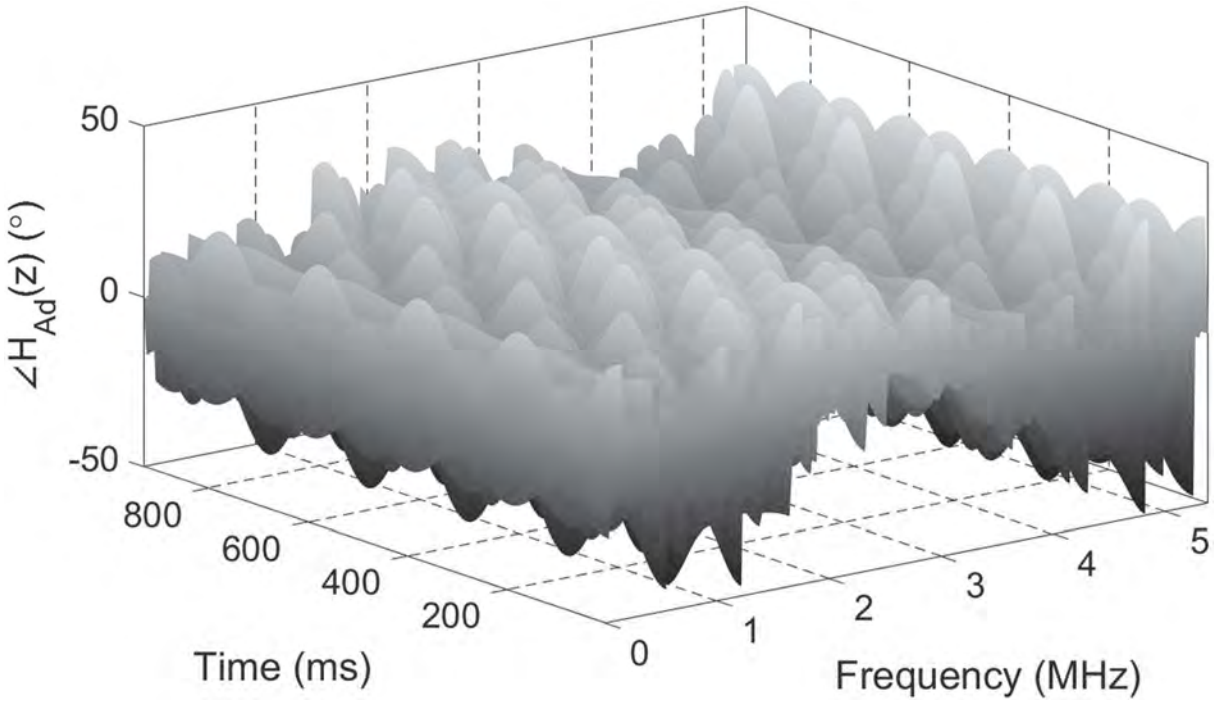

Source: Author (2018).

2.3.2. Dynamic Brazil B

The second dynamic Brazil channel adapted from the ITU (2008) is defined by a delay profile with five paths, besides the main one (first path), with the Doppler shift applied to the fourth path. The delay profile of the dynamic Brazil B is presented in Table 7.

Table 7 – Dynamic Brazil B delay profile.

Channel parameters	Path 1 (main path)	Path 2	Path 3	Path 4	Path 5	Path 6
Delay (μs)	0.00	0.30	3.50	4.40	9.50	12.7
Attenuation (dB)	0.00	12.0	4.00	7.00	15.0	22.0
Doppler Frequency (Hz)	0.00	0.00	0.00	20 or 50	0.00	0.00

Source: Adapted from ITU (2008).

Magnitude and phase of the channel frequency response, for a symbol rate $S_R = 10.7622377622$ MHz and a fractionally sampling $\Upsilon = 2$ are respectively depicted in Figures 22 and 23, for a Doppler shift $f_D = 20$ Hz. Figures 24 and 25 present the magnitude and phase of the channel frequency response for $f_D = 50$ Hz, respectively.

Figure 22 – Magnitude of the channel frequency response to the dynamic Brazil B for $f_D = 20$ Hz.

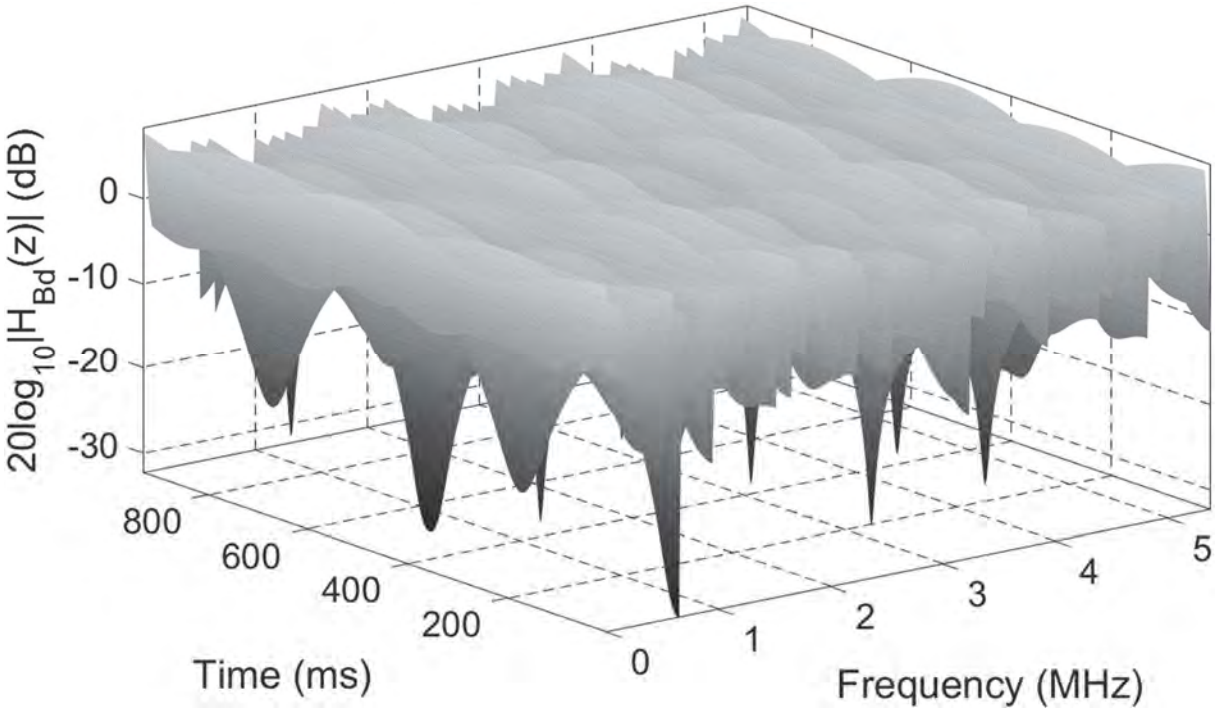

Source: Author (2018).

Figure 23 – Phase of the channel frequency response to the dynamic Brazil B for $f_D = 20$ Hz.

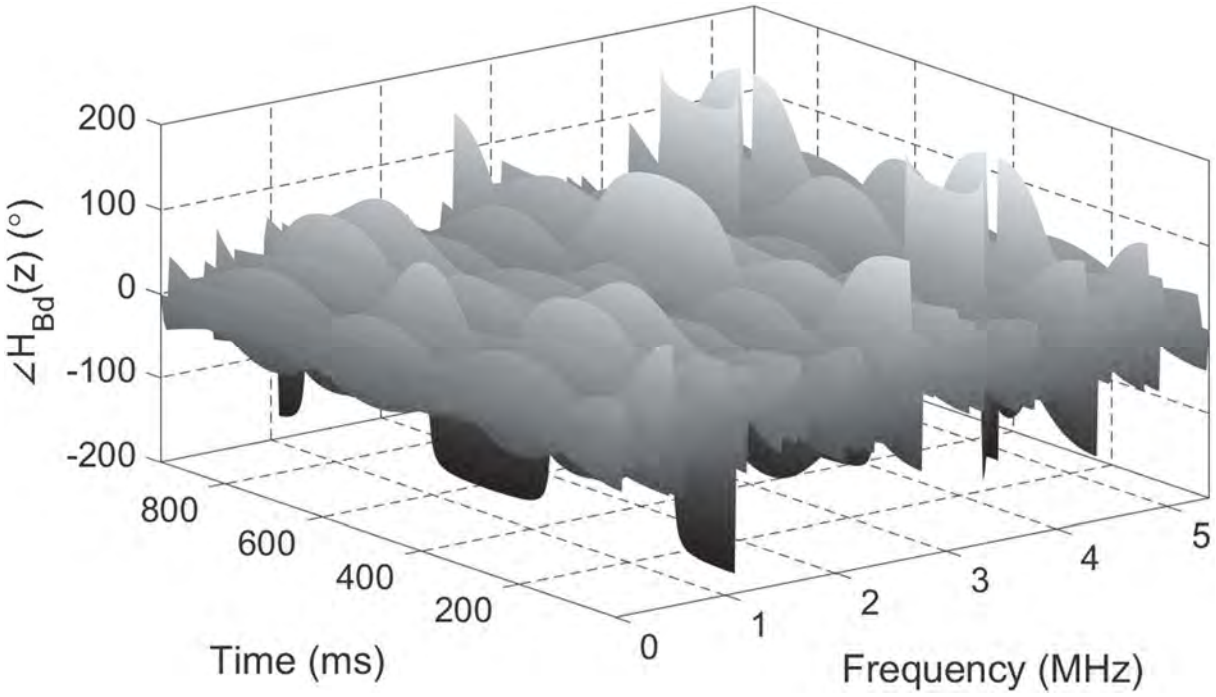

Source: Author (2018).

Figure 24 – Magnitude of the channel frequency response to the dynamic Brazil B for $f_D = 50$ Hz.

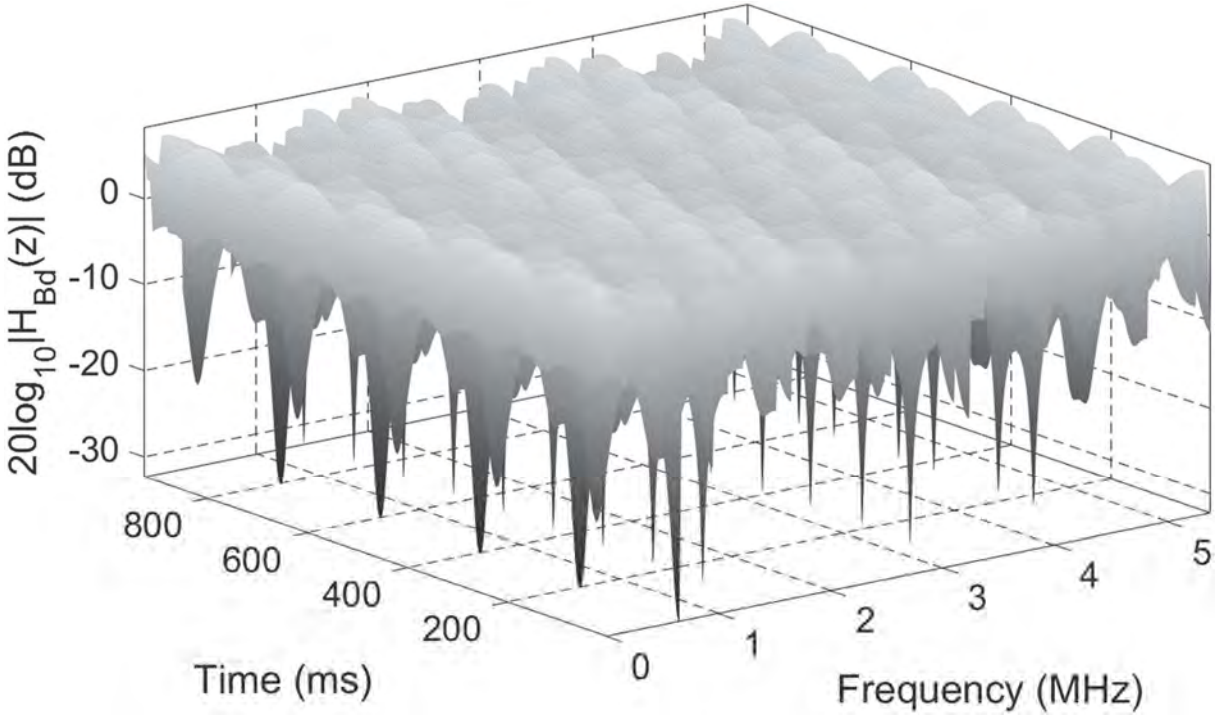

Source: Author (2018).

Figure 25 – Phase of the channel frequency response to the dynamic Brazil B for $f_D = 50$ Hz.

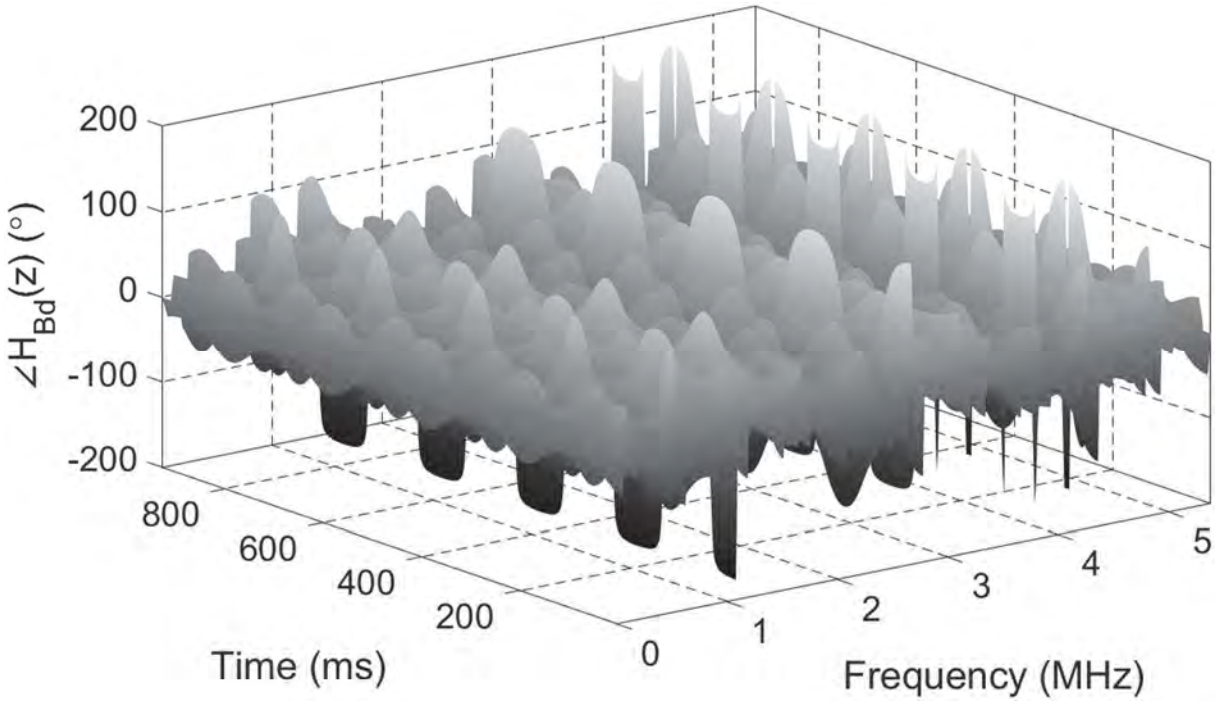

Source: Author (2018).

2.3.3. Dynamic Brazil C

The third dynamic Brazil channel adapted from the ITU (2008) is defined by a delay profile with five paths, besides the main one (third path), with the Doppler shift applied to the first path. The delay profile of the dynamic Brazil C is presented in Table 8.

Magnitude and phase of the channel frequency response, for a symbol rate $S_R = 10.7622377622$ MHz and a fractionally sampling $\Upsilon = 2$ are respectively depicted in Figures 26 and 27, for a Doppler shift $f_D = 20$ Hz. Figures 28 and 29 present the magnitude and phase of the channel frequency response for $f_D = 50$ Hz, respectively.

Table 8 – Dynamic Brazil C delay profile.

Channel parameters	Path 1	Path 2	Path 3 (main path)	Path 4	Path 5	Path 6
Delay (μs)	0.000	0.089	0.419	1.506	2.322	2.799
Attenuation (dB)	2.800	0.000	3.800	0.100	2.500	1.300
Doppler Frequency (Hz)	20 or 50	0.00	0.00	0.00	0.00	0.00

Source: Adapted from ITU (2008).

Figure 26 – Magnitude of the channel frequency response to the dynamic Brazil C for $f_D = 20$ Hz.

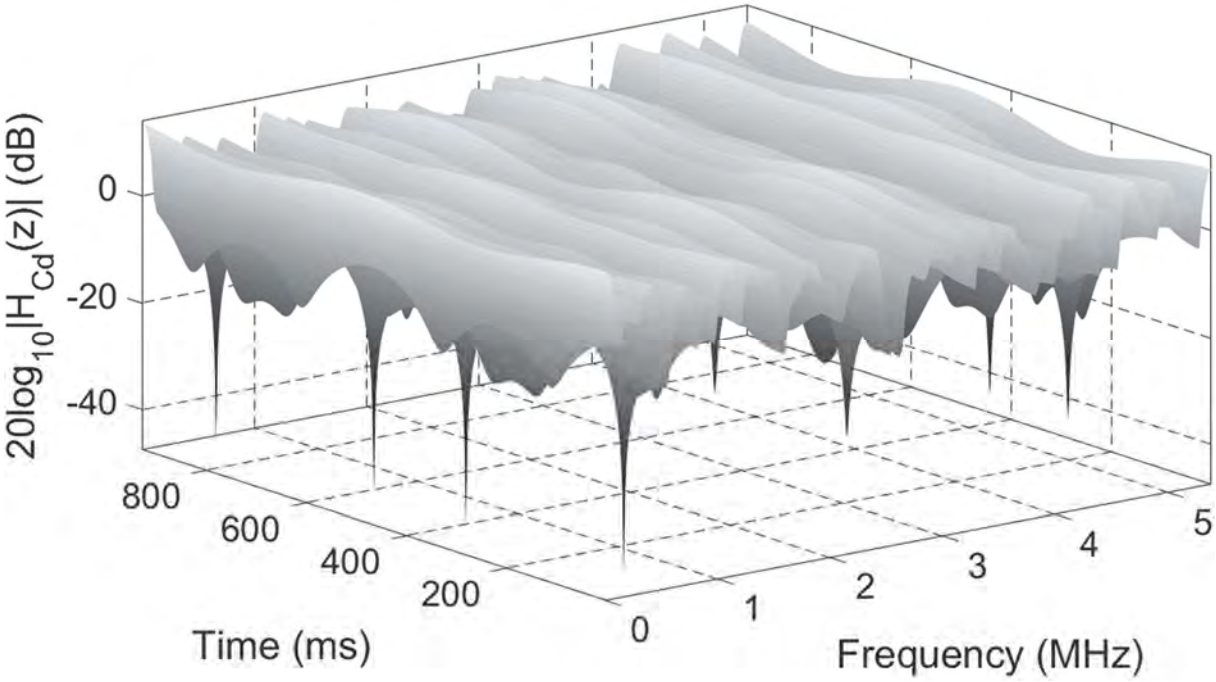

Source: Author (2018).

Figure 27– Phase of the channel frequency response to the dynamic Brazil C for $f_D = 20$ Hz.

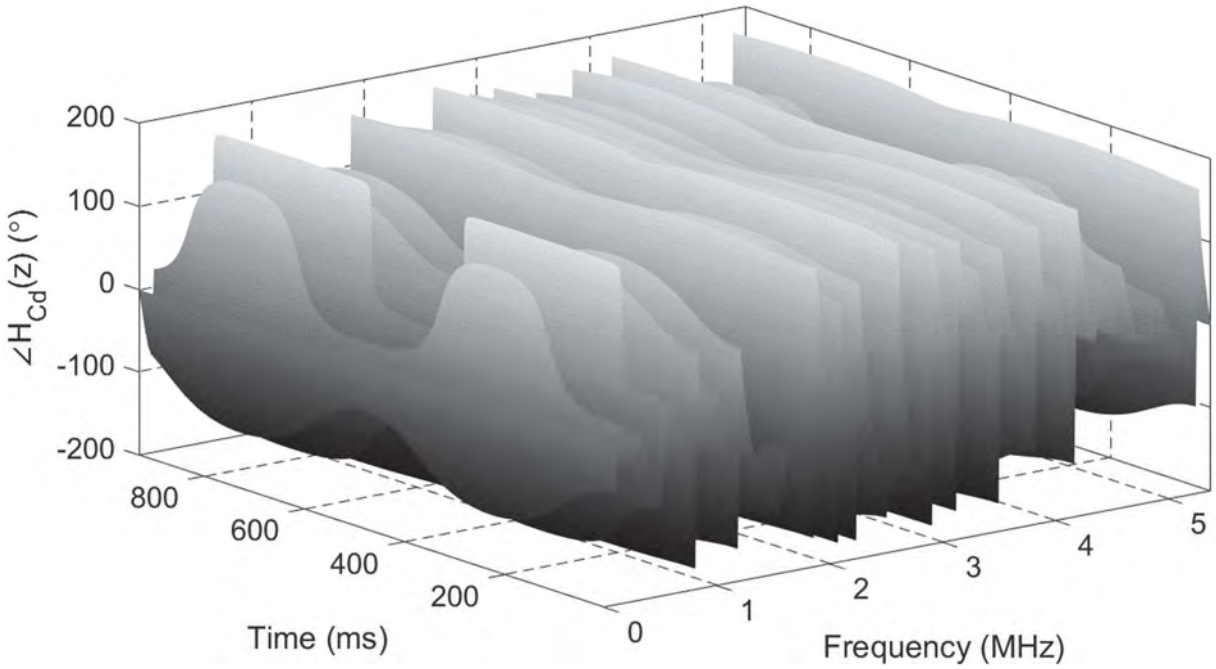

Source: Author (2018).

Figure 28 – Magnitude of the channel frequency response to the dynamic Brazil C for $f_D = 50$ Hz.

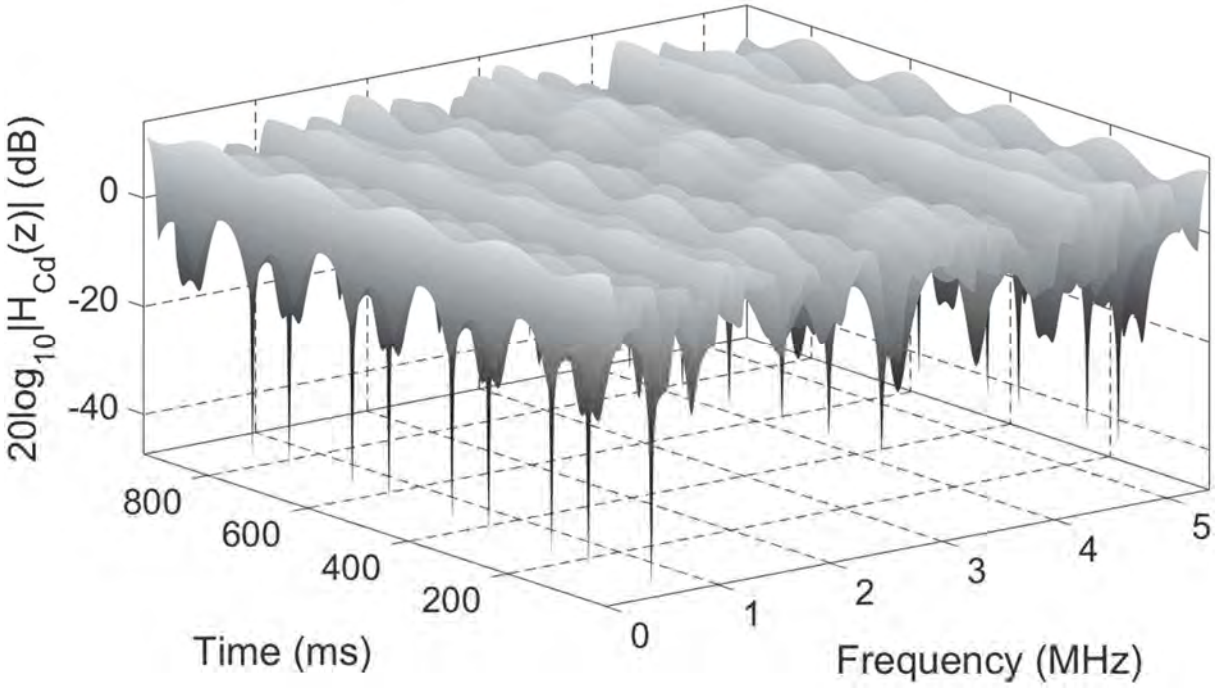

Source: Author (2018).

Figure 29 – Phase of the channel frequency response to the dynamic Brazil C for $f_D = 50$ Hz.

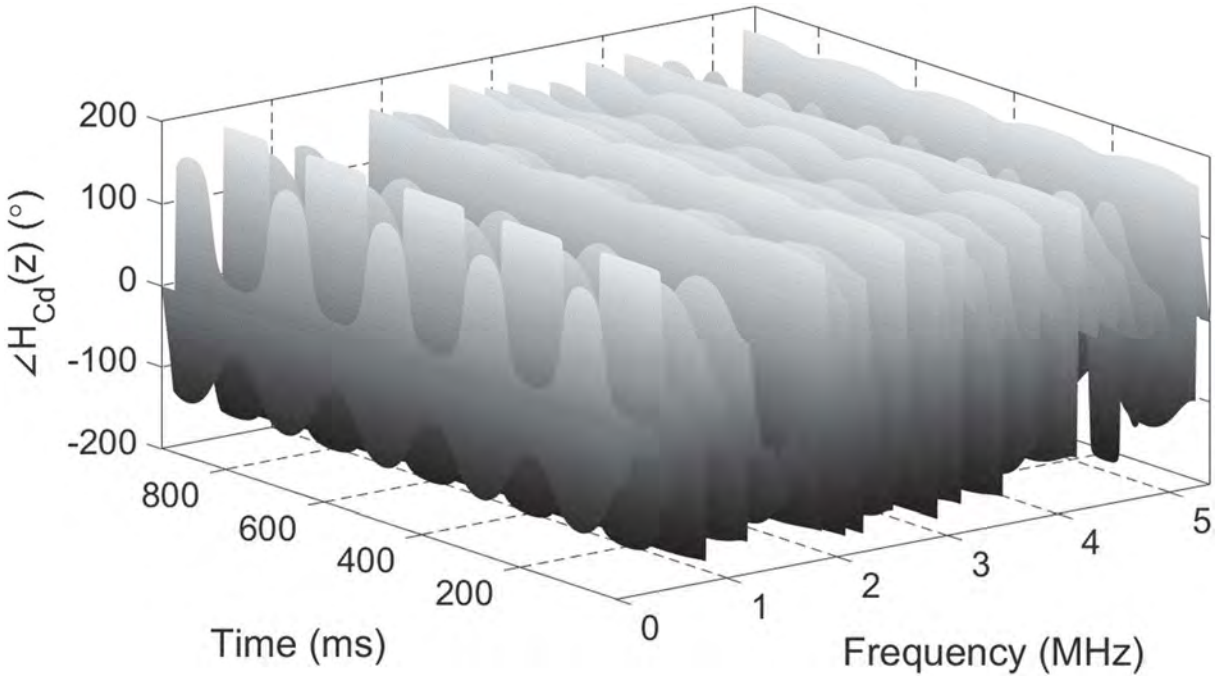

Source: Author (2018).

2.3.4. Dynamic Brazil D

The first fourth Brazil channel adapted from the ITU (2008) is defined by a delay profile with five paths, besides the main one (first path), with the Doppler shift

applied to the fourth path. The delay profile of the dynamic Brazil D is presented in Table 9.

Magnitude and phase of the channel frequency response, for a symbol rate $S_R =$ 10.7622377622 MHz and a fractionally sampling $\Upsilon = 2$ are respectively depicted in Figures 30 and 31, for a Doppler shift $f_D = 20$ Hz. Figures 32 and 33 present the magnitude and phase of the channel frequency response for $f_D = 50$ Hz, respectively.

Table 9 – Dynamic Brazil D delay profile.

Channel parameters	Path 1	Path 2	Path 3 (main path)	Path 4	Path 5	Path 6
Delay (μs)	0.15	0.63	2.22	3.05	5.86	5.93
Attenuation (dB)	0.10	3.80	2.60	1.30	0.00	2.80
Doppler Frequency (Hz)	0.00	0.00	0.00	20 or 50	0.00	0.00

Source: Adapted from ITU (2008).

Figure 30 – Magnitude of the channel frequency response to the dynamic Brazil D for $f_D = 20$ Hz.

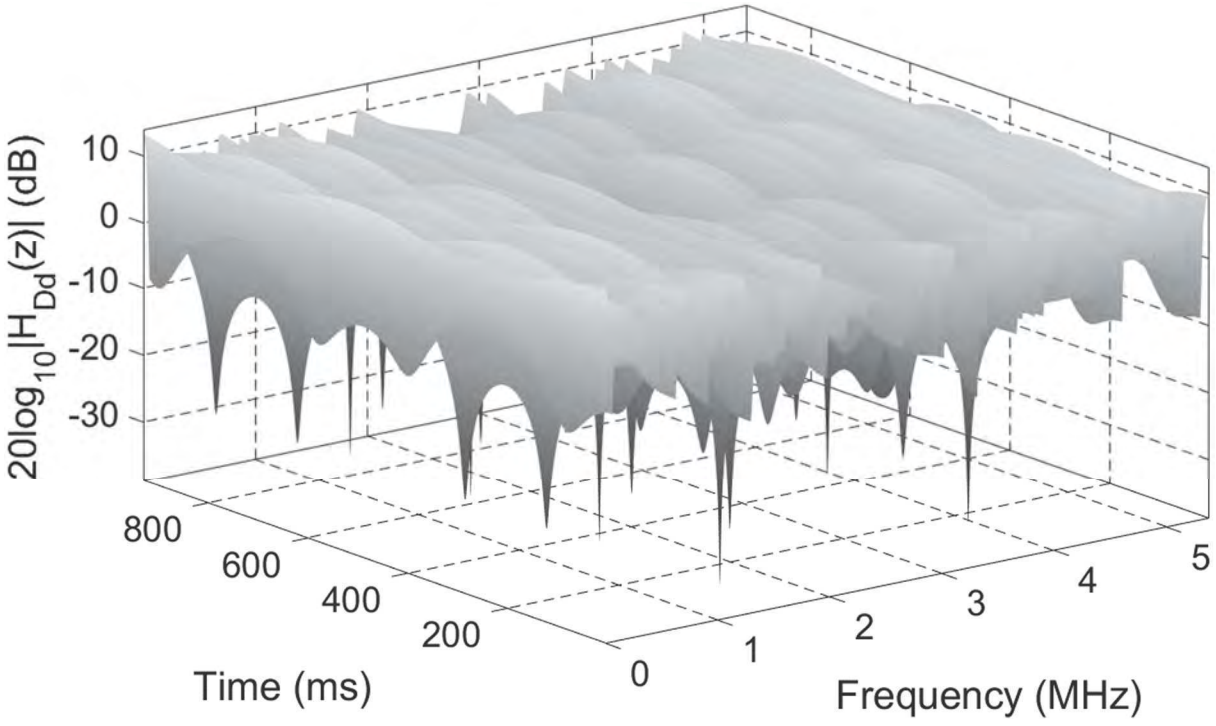

Source: Author (2018).

Figure 31 – Phase of the channel frequency response to the dynamic Brazil D for $f_D = 20$ Hz.

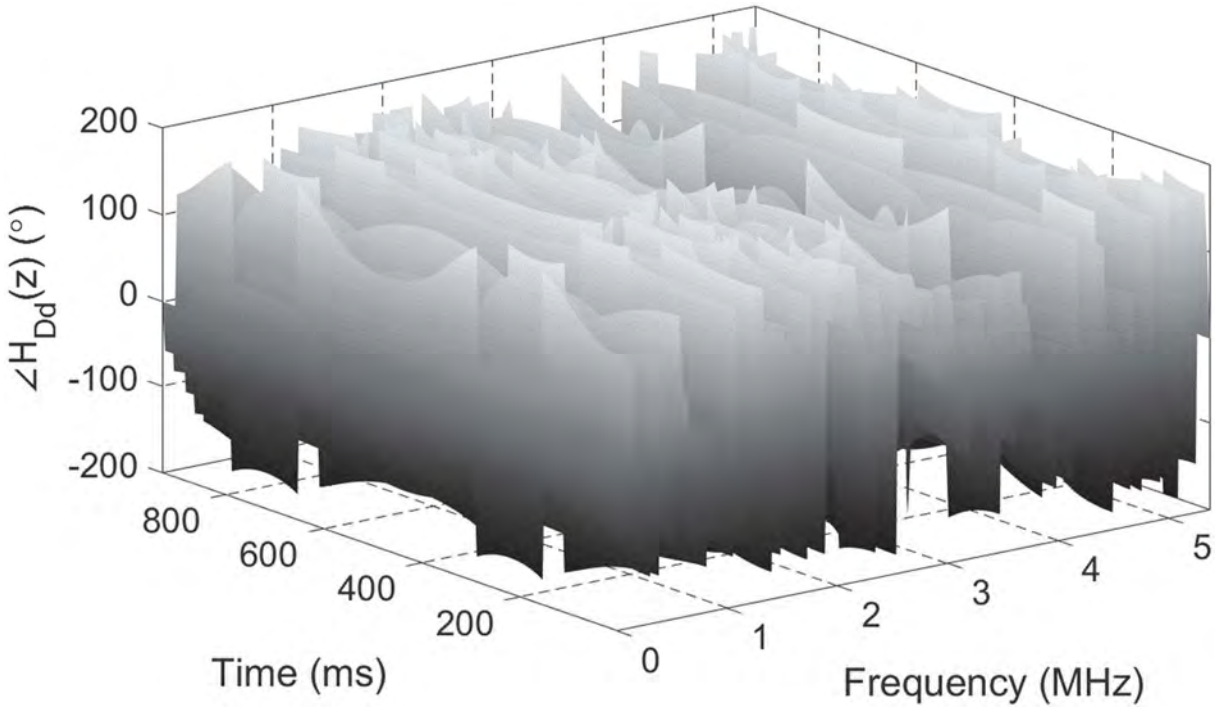

Source: Author (2018).

Figure 32 – Magnitude of the channel frequency response to the dynamic Brazil D for $f_D = 50$ Hz.

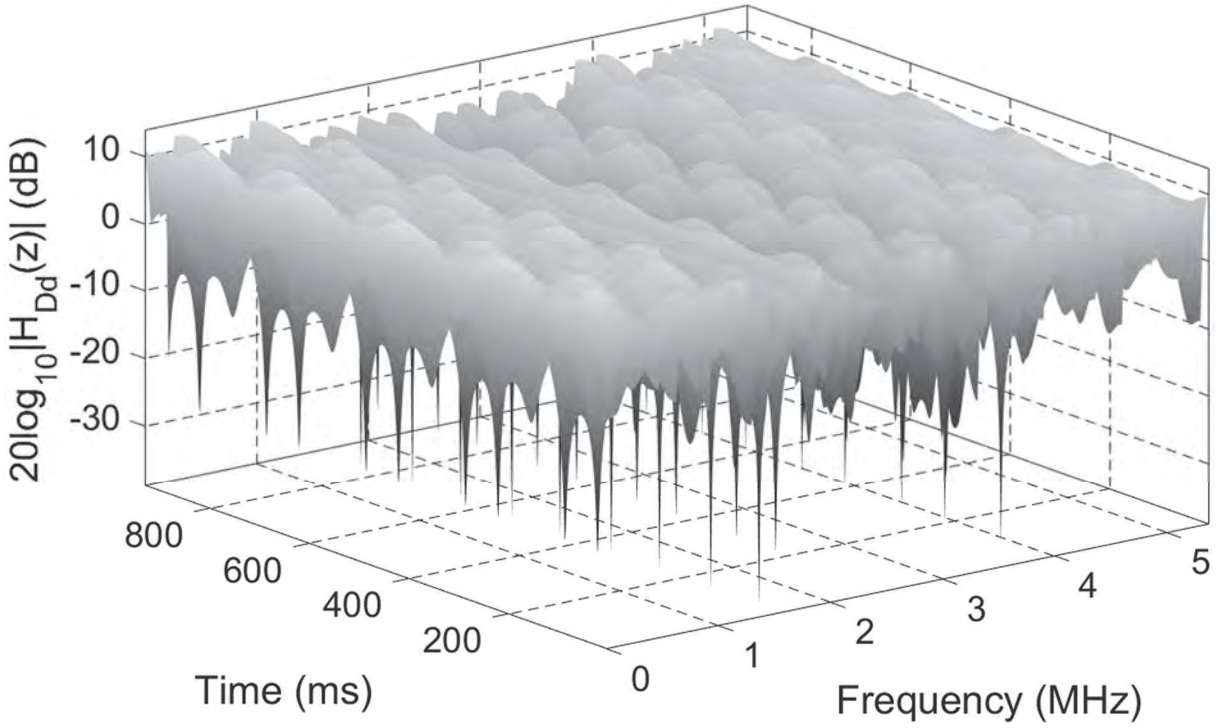

Source: Author (2018).

Figure 33 – Phase of the channel frequency response to the dynamic Brazil D for $f_D = 50$ Hz.

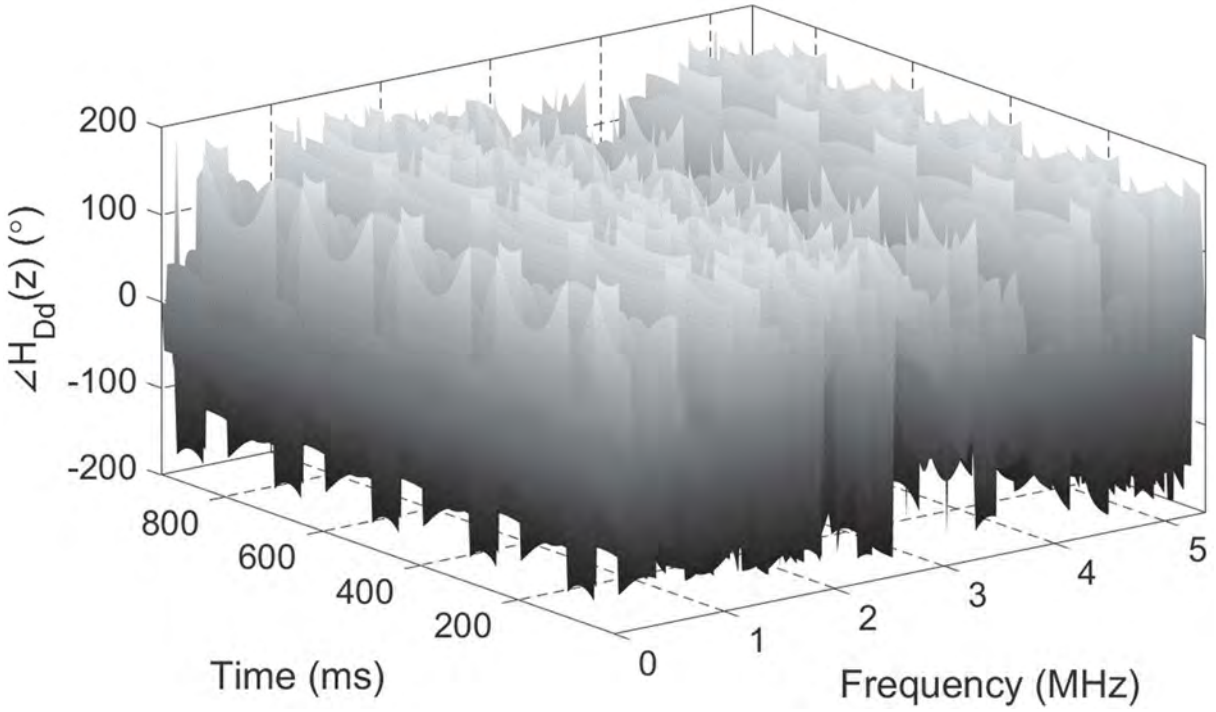

Source: Author (2018).

2.3.5. Dynamic Brazil E

The fifth dynamic Brazil channel adapted from the ITU (2008) is defined by a delay profile with two paths, besides the main one (third path), with the Doppler shift applied to the first path. The delay profile of the dynamic Brazil E is presented in Table 10.

Magnitude and phase of the channel frequency response, for a symbol rate $S_R = 10.7622377622$ MHz and a fractionally sampling $\Upsilon = 2$ are respectively depicted in Figures 34 and 35, for a Doppler shift $f_D = 20$ Hz. Figures 36 and 37 present the magnitude and phase of the channel frequency response for $f_D = 50$ Hz, respectively.

Table 10 – Dynamic Brazil E delay profile.

Channel parameters	Path 1	Path 2	Path 3 (main path)
Delay (μs)	0.00	1.00	2.00
Attenuation (dB)	0.10	3.80	2.60
Doppler Frequency (Hz)	20 or 50	0.00	0.00

Source: Adapted from ITU (2008).

Figure 34 – Magnitude of the channel frequency response to the dynamic Brazil E for $f_D = 20$ Hz.

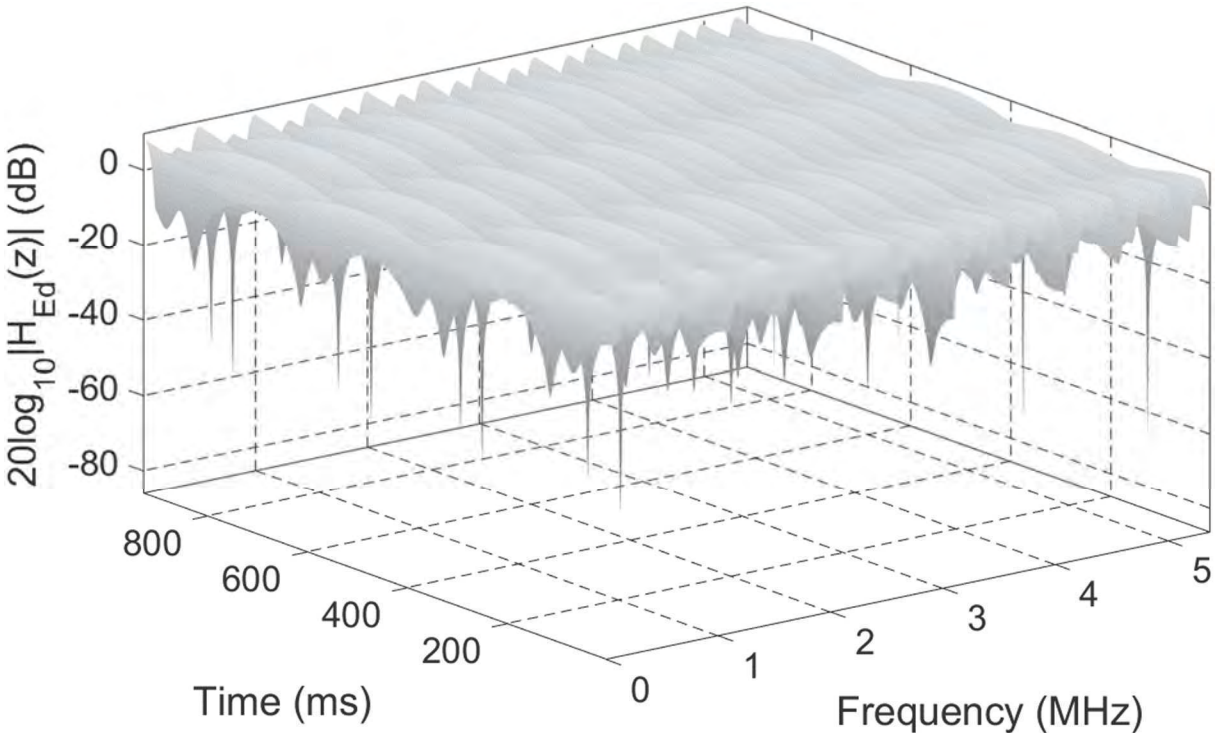

Source: Author (2018).

Figure 35 – Phase of the channel frequency response to the dynamic Brazil E for $f_D = 20$ Hz.

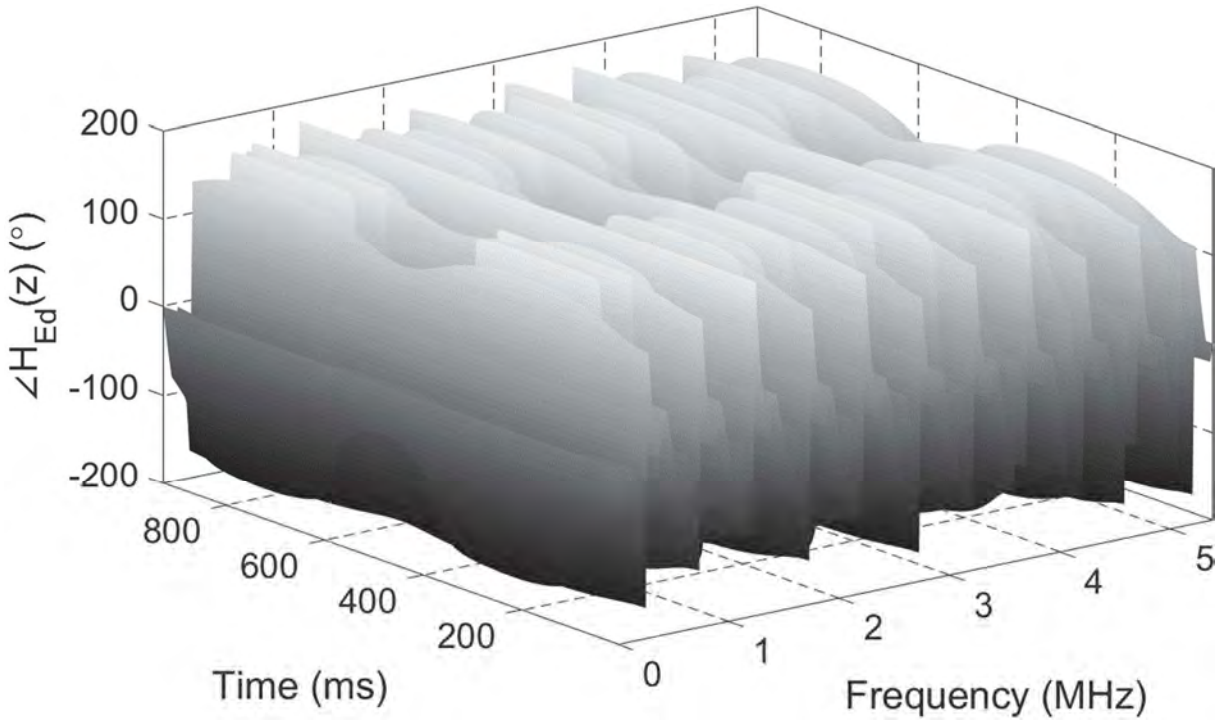

Source: Author (2018).

Figure 36 – Magnitude of the channel frequency response to the dynamic Brazil E for $f_D = 50$ Hz.

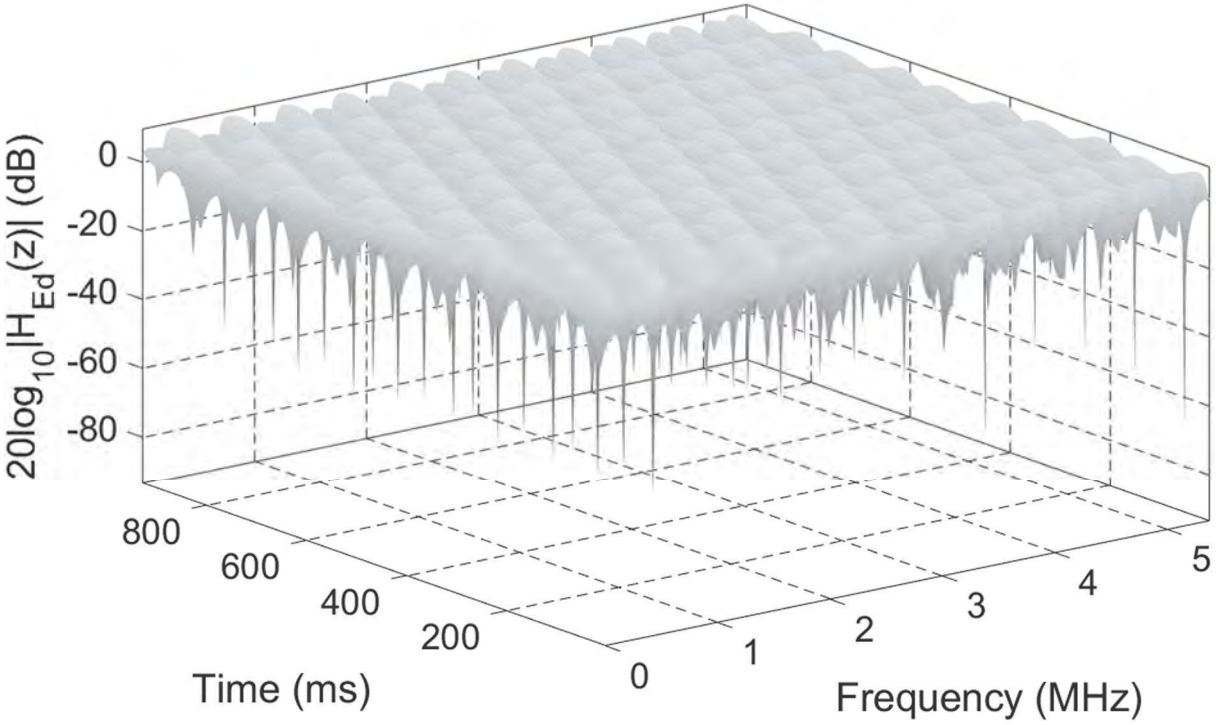

Source: Author (2018).

Figure 37 – Phase of the channel frequency response to the dynamic Brazil E for $f_D = 50$ Hz.

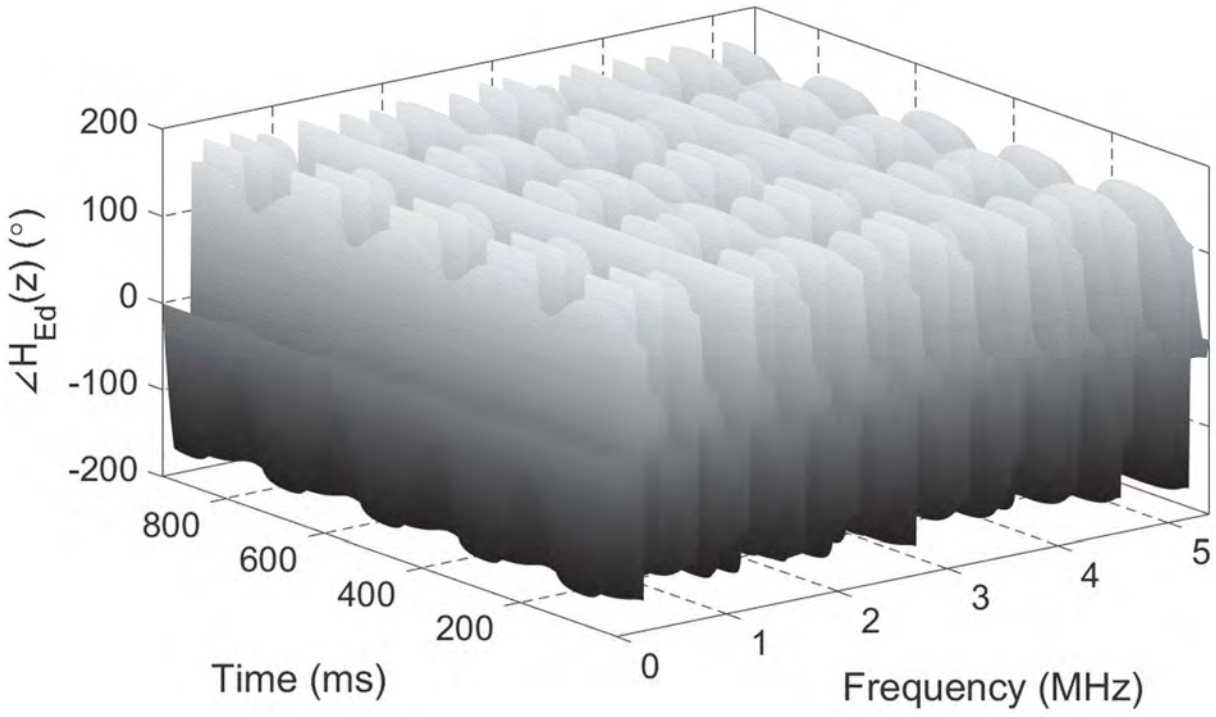

Source: Author (2018).

2.4. ADDITIVE WHITE GAUSSIAN NOISE

The transmitted signal over a wireless channel may be corrupted by noise from an infinity of sources. The noise from these sources can be originated by human activity (e.g., ignition of a car) or by nature (e.g., lightning, thermal noise). In order to simplify the representation of these diverse noise sources, using as base the central limit theorem (PAPOULIS; PILLAI, 2002), it is considered that the sum of the noise generated from these sources can be approximated by an AWGN with mean $\mu = 0$ and variance $\sigma_N^2 = N_0/2$, where N_0 is the noise spectral density (HAYKIN, 2013; PROAKIS; SALEHI, 2008).

AWGN channel model is the principal impairment for deep space communications, although it is a limited model (PROAKIS; SALEHI, 2008). In terrestrial communication, the AWGN model is used as a background noise source for others sources of distortion with more corruption capability, such as the multipath and the Doppler effect.

In order to represent the AWGN in a computer simulation, pseudorandom numbers can be created to approximate the mean and the variance of this noise. A useful method to create pseudorandom numbers, with normal distribution (PAPOULIS; PILLAI, 2002), is the Box-Muller transformation given by the pseudocode presented in the Algorithm 1 (PRESS et al., 2007).

Algorithm 1: Box-Muller transformation algorithm.

Variables: v_1, v_2, rsq, fac
Outputs: ξ_1, ξ_2

```
1.  do{
2.      v1 = 2.0 * (rand() - 0.5);
3.      v2 = 2.0 * (rand() - 0.5); /*rand() returns a number with uniform distribution between 0.0 and 1.0*/
4.      rsq = v1*v1 + v2*v2;
5.  } while(rsq > 1.0 or rsq == 0.0);
6.  fac = sqrt(-2.0*log(rsq)/rsq);
7.  ξ1 = v1*fac;
8.  ξ2 = v2*fac;
9.  Return ξ1 and ξ2
```

The pseudorandom variables ξ_1 and ξ_2, with 50,000 samples, have a normal distribution presented in the Probability Mass Function (PMF) at the Figures 38 and 39, respectively. The cross-correlation (PAPOULIS; PILLAI, 2002) of ξ_1 and ξ_2, results in a single impulse in the sample time equals to zero, as depicted in Figures 40 and 41.

Figure 38 – Probability mass function of the variable ξ_1 with 50,000 samples.

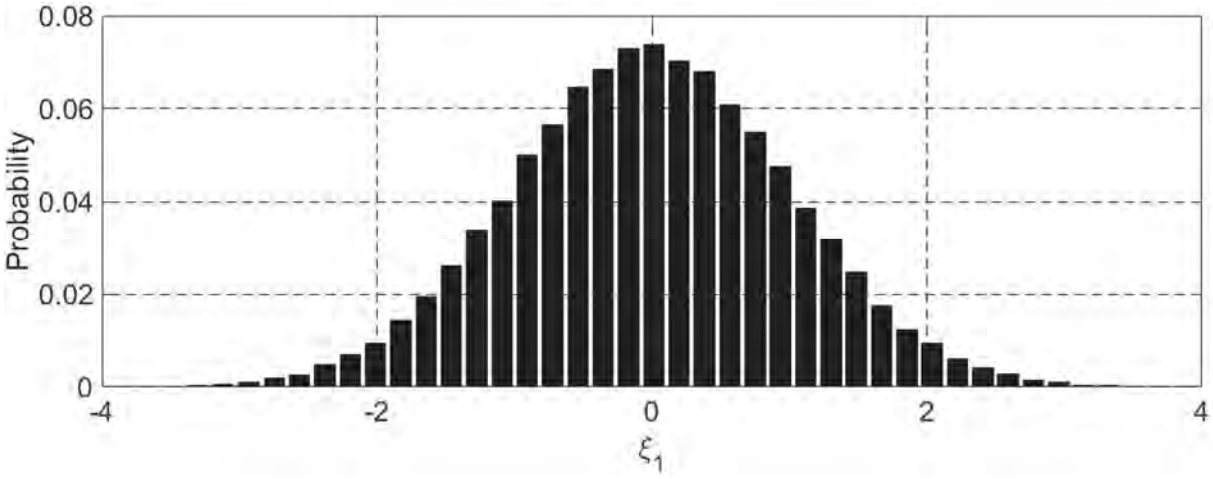

Source: Author (2018).

Figure 39 – Probability mass function of the variable ξ_2 with 50,000 samples.

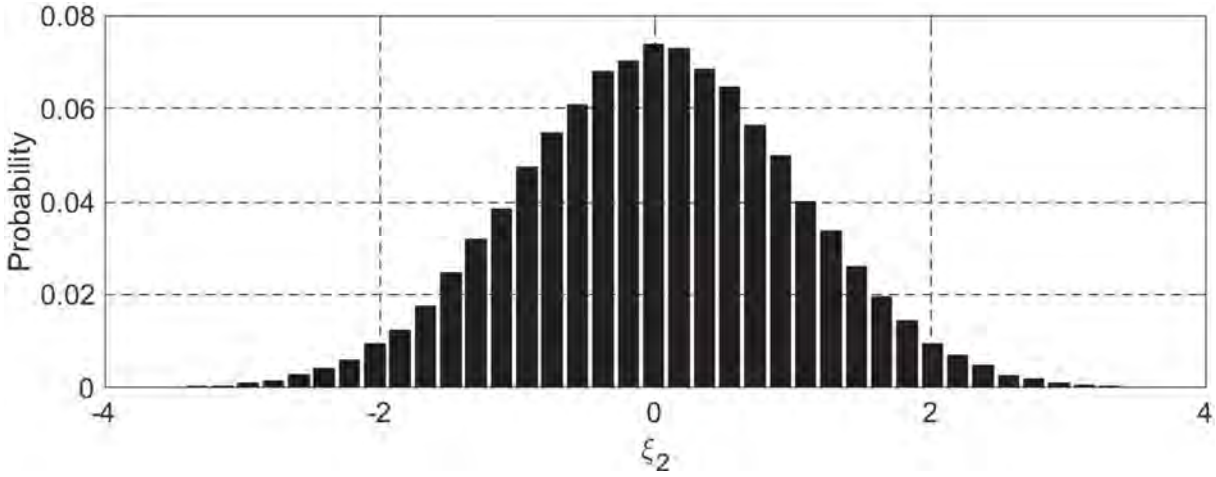

Source: Author (2018).

Figure 40 – Cross correlation of the variable ξ_1 with 50,000 samples.

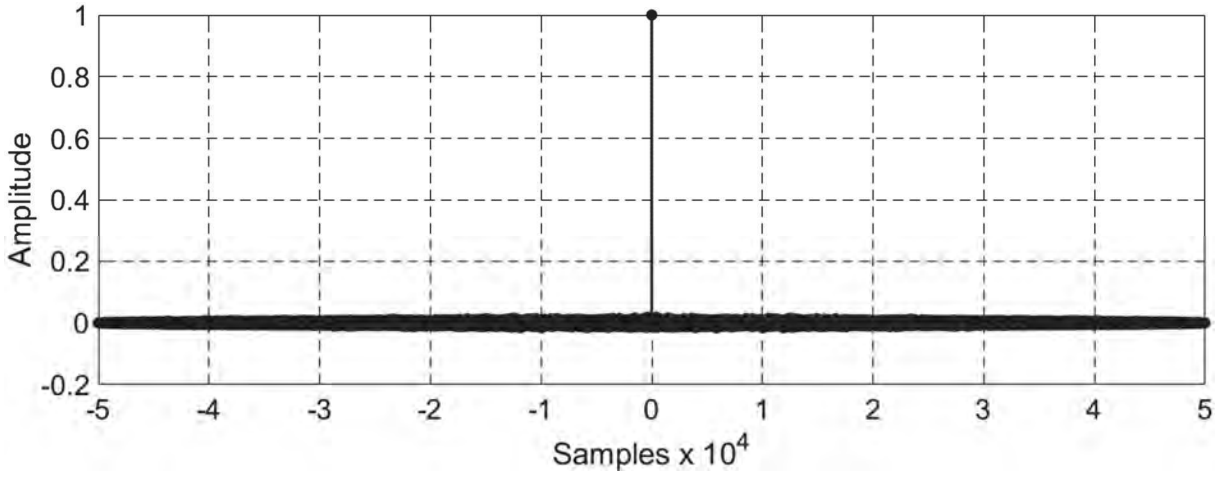

Source: Author (2018).

Figure 41 – Cross correlation of the variable ξ_2 with 50,000 samples.

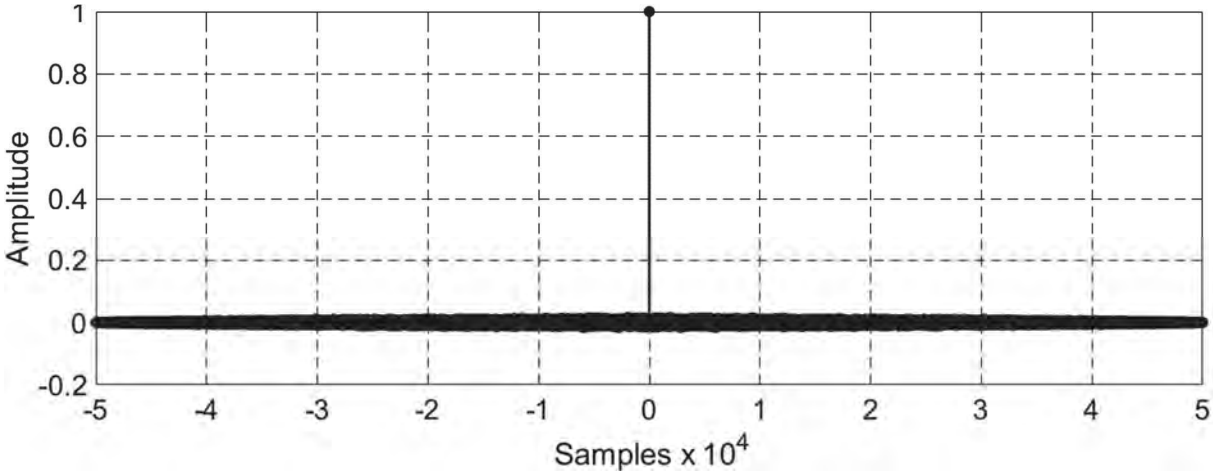

Source: Author (2018).

In a complex M-QAM system, over an AWGN channel, with multipath and Doppler shift, as represented in Figure 42, the effects of the distortions can be approximated by the Signal-to-Noise Ratio (SNR) (CHEN et al., 2010) as

$$\mathrm{SNR} = \left(\sum_{i=0}^{L_{CH}-1} |h_i[n]| \sigma_S^2 \right) \Big/ \sigma_N^2, \tag{2.4}$$

where $\sigma_S^2 = \mathrm{E}\{|s[n]|^2\}$ is the energy of the M-QAM signal and $\mathrm{E}\{\cdot\}$ is the expectancy operator.

Figure 42 – Channel representation with AWGN, multipath and Doppler shift.

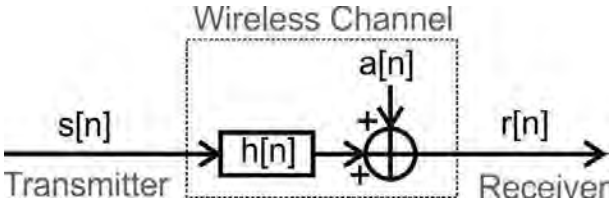

Source: Author (2018).

2.5. BLIND EQUALIZERS

The channel equalization process attempts to mitigate the multipath effects, via the adaptive adjust of the transfer function, in the frequency domain, of the equalizer filter, in order to approximate the inverse transfer function of the transmission channel. Similarly, in the time domain analysis, an equalizer is a filter, whose coefficients adapt themselves in order that the filter impulse response

convolved with the CIR result in a single impulse (HAYKIN, 2013; PROAKIS; SALEHI, 2008).

Nevertheless, the CIR is unknown by the receiver, and, in addition, it may be time-variant. Thus, the determination of the inverse CIR is not trivial. Due this issue, many adaptive algorithms for channel equalization have been proposed in the last decades, such as LMS, DD, SDD, CMA, MCMA, NMCMA, among others.

For static channels, LMS equalizers, supported by a DD, presents a satisfactory efficiency operating with few data on the training sequence, achieving the situation of Zero Forcing (ZF) (HAYKIN, 2013; PROAKIS; SALEHI, 2008), when the DD is initiated with a low MSE value. On the other hand, for dynamic channels, the training sequence sent by the transmitter at some point usually in the beginning of each transmission frame must be significantly long in order to cope with the time varying CIR. For a given transmitted signal spectrum bandwidth, the necessity of the transmission of a long training sequence for channel equalization results in a significant reduction of the useful information transmission data rate, since the equalizer training sequence does not convey any useful data information but only information to specifically training the equalizer. In order to overcome this issue, blind equalizers are widely employed.

Blind equalizers, which work with sample rate (S_S) equal to the symbol rate (S_R), are generally convergent, provided the information source has a uniform distribution and the equalizer has a dimension larger than the infinites past samples of the channel (GODARD, 1980). In a practical application, the number of equalizer taps is defined as large as necessary for an acceptable situation of convergence.

On the contrary, if the equalizer works with sample rate $S_S = \Upsilon\, S_R$, it is called Fractionally Spaced Equalizer (FSE) (GITLIN; WEINSTEIN, 1981; JOHNSON et al., 1998). The FSE has the property of to transform the stochastic process of the received signal from Wide Sense Stationary (WSS) to cyclostationary (GARDNER, 1991). This stochastic transformation permits the equalizer to achieve the ZF condition with a finite number of channel past samples. The ZF condition is easier achieved for some particular conditions (e.g., statistical characteristic of the signal, channel without additive noise and subchannel disparities, and the equalizer with a dimension larger than the delay spread of the channel) (LEBLANC et al., 1995). For

any $\Upsilon > 1$, the received signal statistics is transformed into cyclostationary (GARDNER, 1991). In a practical approach, the equalizer oversampling is defined as $\Upsilon = 2$. Indeed, a $\Upsilon > 2$ only increases the computational complexity.

In the discrete frequency domain analysis, the oversampling aims to avoid the noise enhancement effect that occurs when the equalizer is not fractionally spaced and the transmission channel presents zeros on the unit circle of the z-plane (GITLIN; WEINSTEIN, 1981).

2.5.1. CMA Equalizer

The CMA equalizer proposed by Godard (1980), depicted in Figure 43, is based on the statistic properties of the transmitted signal over a communication channel.

Figure 43 – Block diagram of the CMA equalizer.

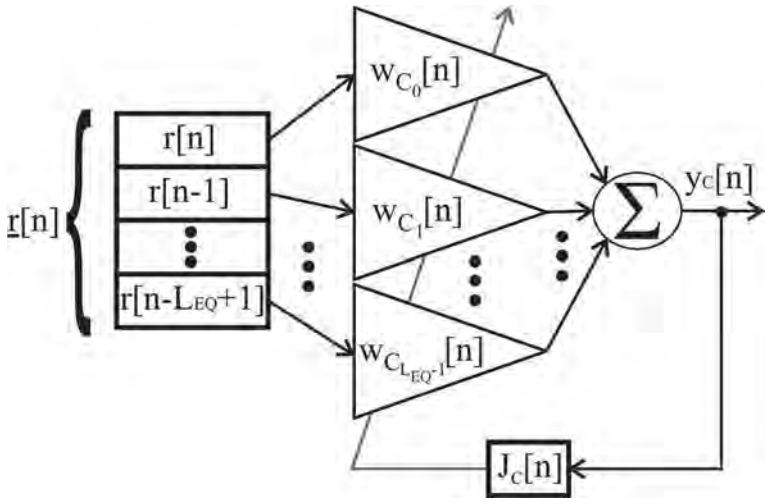

Source: Author (2018).

The CMA output ($y_C[n]$) is given by

$$y_C[n] = \sum_{i=0}^{L_{EQ}-1} w_{C_i}[n] r[n-i] = \underline{w_C}[n]^T \underline{r}[n], \tag{2.5}$$

where $L_{EQ} \geq L_{CH} - 1$ is the number of coefficients of the CMA equalizer, $\underline{w_C}[n] = \left[w_{C_0}[n], w_{C_1}[n], \cdots, w_{C_{L_{EQ}-1}}[n]\right]^T$ is the coefficient vector of the CMA, and $\underline{r}[n] = \left[r[n], r[n-1], \cdots, r\left[n - L_{EQ} + 1\right]\right]^T$ is the CMA input vector, also called as channel regressor (DE CASTRO; DE CASTRO; ARANTES, 2001).

Equation (2.5) can be similarly represented as

$$y_C[n] = \left\{ \sum_{i=0}^{L_{EQ}-1} \mathrm{Re}\{w_{C_i}[n]\}\mathrm{Re}\{r[n-i]\} - \mathrm{Re}\{w_{C_i}[n]\}\mathrm{Re}\{r[n-i]\} \right\} +$$

$$+ j \left\{ \sum_{i=0}^{L_{EQ}-1} \mathrm{Re}\{w_{C_i}[n]\}\mathrm{Im}\{r[n-i]\} + \mathrm{Im}\{w_{C_i}[n]\}\mathrm{Re}\{r[n-i]\} \right\}, \quad (2.6)$$

where $\mathrm{Re}\{\cdot\}$ and $\mathrm{Im}\{\cdot\}$ return the real and imaginary component of their arguments, respectively.

The principal objective of the CMA equalizer is to mitigate the channel multipath distortion, through the $\underline{w_C}[n]$ coefficients update, obtained by the Stochastic Gradient Descent (SGD) (HAYKIN, 2014) as

$$\underline{w_C}[n+1] = \underline{w_C}[n] + \eta_C(-\nabla J_C[n]), \quad (2.7)$$

where ∇ is the gradient operator, $\eta_C > 0$ is the adaptive step of the CMA, and $J_C[n]$ is the Godard cost function, given by

$$J_C[n] = \frac{1}{4}[(|y_C[n]|^2 - \gamma)^2], \quad (2.8)$$

where $\gamma = \mathrm{E}\{|\mathcal{S}|^4\}/\mathrm{E}\{|\mathcal{S}|^2\}$ is the dispersion constant of second order (GODARD, 1980).

Applying the gradient operator to Eq. (2.8), considering the i^{th} variation of the coefficient vector $\underline{w_C}[n]$:

$$\nabla_i J_C[n] = \nabla_i^R J_C[n] + j\nabla_i^I J_C[n] = \frac{\partial J_C[n]}{\partial \mathrm{Re}\{w_{C_i}[n]\}} + j\frac{\partial J_C[n]}{\partial \mathrm{Im}\{w_{C_i}[n]\}}, \quad (2.9)$$

where ∇_i^R and ∇_i^I are the gradient operator applied on the real and imaginary component of the i^{th} CMA coefficient $w_{C_i}[n]$, respectively.

Substituting Eq. (2.8) into Eq. (2.9)

$$\nabla_i J_C[n] = \frac{1}{2}(|y[n]^2 - \gamma|)\left[\frac{\partial |y_C[n]|^2}{\partial \mathrm{Re}\{w_{C_i}[n]\}} + j\frac{\partial |y_C[n]|^2}{\partial \mathrm{Im}\{w_{C_i}[n]\}}\right]. \quad (2.10)$$

However, $|y_C[n]|^2$ is

$$|y_C[n]|^2 = \mathrm{Re}\{y_C[n]\}^2 + \mathrm{Im}\{y_C[n]\}^2, \tag{2.11}$$

and applying Eq. (2.6) into Eq. (2.11)

$$|y_C[n]|^2 = \left\{ \sum_{i=0}^{L_{EQ}-1} \mathrm{Re}\{w_{C_i}[n]\}\mathrm{Re}\{r[n-i]\} - \mathrm{Re}\{w_{C_i}[n]\}\mathrm{Re}\{r[n-i]\} \right\}^2 +$$

$$+ \left\{ \sum_{i=0}^{L_{EQ}-1} \mathrm{Re}\{w_{C_i}[n]\}\mathrm{Im}\{r[n-i]\} + \mathrm{Im}\{w_{C_i}[n]\}\mathrm{Re}\{r[n-i]\} \right\}^2. \tag{2.12}$$

Hence, the Eq. (2.12) referenced to Eq. (2.10)

$$\frac{\partial |y_C[n]|^2}{\partial \mathrm{Re}\{w_{C_i}[n]\}} = 2(\mathrm{Re}\{y_C[n]\}\mathrm{Re}\{r[n-i]\} + \mathrm{Im}\{y_C[n]\}\mathrm{Im}\{r[n-i]\}), \tag{2.13}$$

$$\frac{\partial |y_C[n]|^2}{\partial \mathrm{Im}\{w_{C_i}[n]\}} = 2(\mathrm{Im}\{y_C[n]\}\mathrm{Re}\{r[n-i]\} - \mathrm{Re}\{y_C[n]\}\mathrm{Im}\{r[n-i]\}). \tag{2.14}$$

Substituting Eqs. (2.13) and (2.14) into (2.10) and multiplying by -1

$$\nabla_i J_C[n] = (\gamma - |y[n]^2|)[(\mathrm{Re}\{y_C[n]\}\mathrm{Re}\{r[n-i]\} + \mathrm{Im}\{y_C[n]\}\mathrm{Im}\{r[n-i]\}) +$$

$$+ j(\mathrm{Im}\{y_C[n]\}\mathrm{Re}\{r[n-i]\} - \mathrm{Re}\{y_C[n]\}\mathrm{Im}\{r[n-i]\})], \tag{2.15}$$

however:

$$y[n]r[n-i]^* = (\mathrm{Re}\{y_C[n]\}\mathrm{Re}\{r[n-i]\} + \mathrm{Im}\{y_C[n]\}\mathrm{Im}\{r[n-i]\}) +$$

$$+ j(\mathrm{Im}\{y_C[n]\}\mathrm{Re}\{r[n-i]\} - \mathrm{Re}\{y_C[n]\}\mathrm{Im}\{r[n-i]\}), \tag{2.16}$$

where $[\cdot]^*$ returns the conjugate operator.

Substituting Eq. (2.16) into (2.15)

$$\nabla_i J_C[n] = y_C[n](\gamma - |y[n]^2|)r[n-i]^*, \tag{2.17}$$

and finally, substituting Eq. (2.17) into (2.7)

$$\underline{w}_C[n+1] = \underline{w}_C[n] + \eta_C y_C[n](\gamma - |y[n]^2|)\underline{r}[n]^*, \tag{2.18}$$

being $e_C[n] = y_C[n](\gamma - |y[n]^2|)$ called as error function of the CMA (LEBLANC et al., 1995).

2.5.2. MCMA Equalizer

When the multipath imposes a phase shift on the received signal $\underline{r}[n]$, the CMA equalizer does not recovery the phase signal at the output $y_C[n]$, resulting in a rotated constellation. This effect is due to the CMA cost function, which is based on the $|y_C[n]|$, thus the phase component of $y_C[n]$ is suppressed by the modulus operator (OH; CHIN, 1995). The MCMA equalizer, presented in Figure 44, circumvent this phase issue.

Figure 44 – Block diagram of the MCMA equalizer.

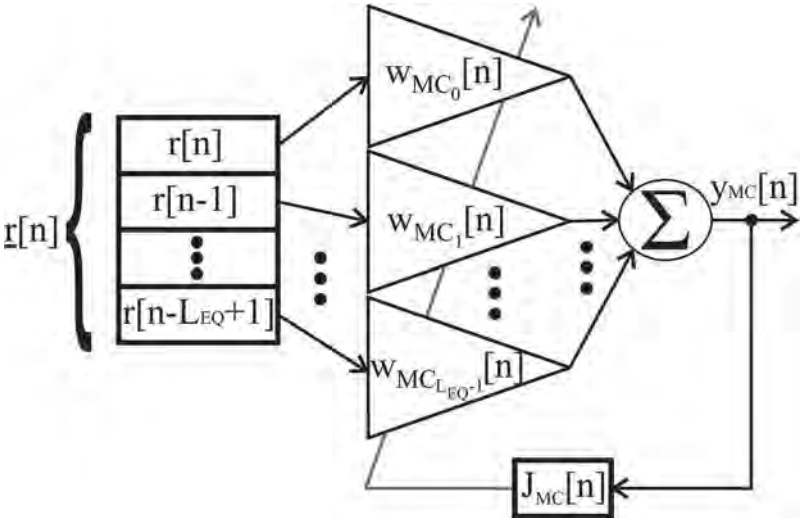

Source: Author (2018).

Using the CMA equalizer as a starting point, Oh and Chin (1995) separated the CMA cost function presented in Eq. (2.8) in real and imaginary components, thus defining with this the MCMA cost function ($J_{MC}[n]$), which is

$$J_{MC}[n] = \frac{1}{4}[(\mathrm{Re}\{y_{MC}[n]\}^2 - \gamma_R)^2 + (\mathrm{Im}\{y_{MC}[n]\}^2 - \gamma_I)^2], \tag{2.19}$$

where $\gamma_R = \mathrm{E}\{\mathrm{Re}\{\mathcal{S}\}^4\}/\mathrm{E}\{\mathrm{Re}\{\mathcal{S}\}^2\}$ and $\gamma_I = \mathrm{E}\{\mathrm{Im}\{\mathcal{S}\}^4\}/\mathrm{E}\{\mathrm{Im}\{\mathcal{S}\}^2\}$ are the real and imaginary dispersion constants proposed by Oh and Chin (1995), respectively.

The MCMA output ($y_{MC}[n]$) is given by

$$y_{MC}[n] = \sum_{i=0}^{L_{EQ}-1} w_{MC_i}[n] r[n-i] = \underline{w}_{MC}[n]^T \underline{r}[n], \tag{2.20}$$

where $\underline{w}_{MC}[n] = \left[w_{MC_0}[n], w_{MC_1}[n], \cdots, w_{MC_{L_{EQ}-1}}[n]\right]^T$ is the coefficient vector of the MCMA equalizer.

The SGD for the $\underline{w}_{MC}[n]$ update is

$$\underline{w}_{MC}[n+1] = \underline{w}_{MC}[n] + \eta_{MC}(-\nabla J_{MC}[n]), \tag{2.21}$$

where $\eta_{MC} > 0$ is the adaptive step of the MCMA equalizer.

Applying the gradient operator to Eq. (2.19), considering the i^{th} variation of the coefficient vector $\underline{w}_{MC}[n]$:

$$\nabla_i J_{MC}[n] = \nabla_i^R J_{MC}[n] + j\nabla_i^I J_{MC}[n] = \frac{\partial J_{MC}[n]}{\partial \mathrm{Re}\{w_{MC_i}[n]\}} + j\frac{\partial J_{MC}[n]}{\partial \mathrm{Im}\{w_{MC_i}[n]\}}. \tag{2.22}$$

Hence, the Eq. (2.19) referenced to Eq. (2.22)

$$\nabla_i^R J_{MC}[n] = \frac{1}{4}\left\{\frac{\partial(\mathrm{Re}\{y_{MC}[n]\}^2 - \gamma_R)^2}{\partial \mathrm{Re}\{w_{MC_i}[n]\}} + \frac{\partial(\mathrm{Im}\{y_{MC}[n]\}^2 - \gamma_I)^2}{\partial \mathrm{Re}\{w_{MC_i}[n]\}}\right\}, \tag{2.23}$$

$$\nabla_i^I J_{MC}[n] = \frac{1}{4}\left\{\frac{\partial(\mathrm{Re}\{y_{MC}[n]\}^2 - \gamma_R)^2}{\partial \mathrm{Im}\{w_{MC_i}[n]\}} + \frac{\partial(\mathrm{Im}\{y_{MC}[n]\}^2 - \gamma_I)^2}{\partial \mathrm{Im}\{w_{MC_i}[n]\}}\right\}. \tag{2.24}$$

The derivatives of Eqs. (2.23) and (2.24) leads to

$$\nabla_i^R J_{MC}[n] = \mathrm{Re}\{y_{MC}[n]\}(\mathrm{Re}\{y_{MC}[n]\}^2 - \gamma_R)\frac{\partial \mathrm{Re}\{y_{MC}[n]\}}{\partial \mathrm{Re}\{w_{MC_i}[n]\}} + \\ + \mathrm{Im}\{y_{MC}[n]\}(\mathrm{Im}\{y_{MC}[n]\}^2 - \gamma_I)\frac{\partial \mathrm{Im}\{y_{MC}[n]\}}{\partial \mathrm{Re}\{w_{MC_i}[n]\}}, \tag{2.25}$$

$$\nabla_i^I J_{MC}[n] = \mathrm{Re}\{y_{MC}[n]\}(\mathrm{Re}\{y_{MC}[n]\}^2 - \gamma_R)\frac{\partial \mathrm{Re}\{y_{MC}[n]\}}{\partial \mathrm{Im}\{w_{MC_i}[n]\}} + \\ + \mathrm{Im}\{y_{MC}[n]\}(\mathrm{Im}\{y_{MC}[n]\}^2 - \gamma_I)\frac{\partial \mathrm{Im}\{y_{MC}[n]\}}{\partial \mathrm{Im}\{w_{MC_i}[n]\}}, \tag{2.26}$$

being $e_{MC}[n]$ the error function of the MCMA, given by

$$e_{MC}[n] = \mathrm{Re}\{e_{MC}[n]\} + j\mathrm{Im}\{e_{MC}[n]\}, \tag{2.27}$$

where

$$\mathrm{Re}\{e_{MC}[n]\} = \mathrm{Re}\{y_{MC}[n]\}(\mathrm{Re}\{y_{MC}[n]\}^2 - \gamma_R), \tag{2.28}$$

$$\mathrm{Im}\{e_{MC}[n]\} = \mathrm{Im}\{y_{MC}[n]\}(\mathrm{Im}\{y_{MC}[n]\}^2 - \gamma_I). \tag{2.29}$$

Therefore, substituting Eqs. (2.28) and (2.29) into Eqs. (2.25) and (2.26)

$$\nabla_i^R J_{MC}[n] = \mathrm{Re}\{e_{MC}[n]\}\frac{\partial \mathrm{Re}\{y_{MC}[n]\}}{\partial \mathrm{Re}\{w_{MC_i}[n]\}} + \mathrm{Im}\{e_{MC}[n]\}\frac{\partial \mathrm{Im}\{y_{MC}[n]\}}{\partial \mathrm{Re}\{w_{MC_i}[n]\}}, \quad (2.30)$$

$$\nabla_i^I J_{MC}[n] = \mathrm{Re}\{e_{MC}[n]\}\frac{\partial \mathrm{Re}\{y_{MC}[n]\}}{\partial \mathrm{Im}\{w_{MC_i}[n]\}} + \mathrm{Im}\{e_{MC}[n]\}\frac{\partial \mathrm{Im}\{y_{MC}[n]\}}{\partial \mathrm{Im}\{w_{MC_i}[n]\}}, \quad (2.31)$$

however

$$\mathrm{Re}\{y_{MC}[n]\} = \mathrm{Re}\{w_{MC_i}[n]\}\mathrm{Re}\{r[n-i]\} - \mathrm{Im}\{w_{MC_i}[n]\}\mathrm{Im}\{r[n-i]\}, \quad (2.32)$$

$$\mathrm{Im}\{y_{MC}[n]\} = \mathrm{Re}\{w_{MC_i}[n]\}\mathrm{Im}\{r[n-i]\} + \mathrm{Im}\{w_{MC_i}[n]\}\mathrm{Re}\{r[n-i]\}, \quad (2.33)$$

substituting Eqs. (2.32) and (2.33) into Eqs. (2.30) and (2.31) and solving the derivatives

$$\nabla_i^R J_{MC}[n] = \mathrm{Re}\{e_{MC}[n]\}\mathrm{Re}\{r[n-i]\} + \mathrm{Im}\{e_{MC}[n]\}\mathrm{Im}\{r[n-i]\}, \quad (2.34)$$

$$\nabla_i^I J_{MC}[n] = \mathrm{Im}\{e_{MC}[n]\}\mathrm{Re}\{r[n-i]\} - \mathrm{Re}\{e_{MC}[n]\}\mathrm{Im}\{r[n-i]\}. \quad (2.35)$$

Applying Eqs. (2.34) and (2.35) into Eq. (2.22)

$$\nabla_i J_{MC}[n] = (\mathrm{Re}\{e_{MC}[n]\}\mathrm{Re}\{r[n-i]\} + \mathrm{Im}\{e_{MC}[n]\}\mathrm{Im}\{r[n-i]\}) + \\ + j(\mathrm{Im}\{e_{MC}[n]\}\mathrm{Re}\{r[n-i]\} - \mathrm{Re}\{e_{MC}[n]\}\mathrm{Im}\{r[n-i]\}), \quad (2.36)$$

which results in

$$\nabla_i J_{MC}[n] = e_{MC}[n]r[n-i]^*. \quad (2.37)$$

Finally, substituting Eq. (2.37) into (2.21)

$$\underline{w}_{MC}[n+1] = \underline{w}_{MC}[n] - \eta_{MC}\, e_{MC}[n]\underline{r}[n]^*. \quad (2.38)$$

2.5.3. NMCMA Equalizer

In order to improve the MCMA results of Oh and Chin (1995), Wang (2010) proposed a modification in the MCMA output $y_{MC}[n]$ by inserting a nonlinear function whose output is $Y_{NC}[n]$, as described by You Hong (1998). The nonlinear function aims to minimize the symbol dispersion around the reference symbols of the digital modulation constellation. Figure 45 presents the block diagram of the NMCMA equalizer.

The NMCMA equalizer output $Y_{NC}[n]$ is given by

$$Y_{NC}[n] = [\mathrm{Re}\{y_{NC}[n]\} + \alpha \sin(\pi \mathrm{Re}\{y_{NC}[n]\})] + \\ + j[\mathrm{Im}\{y_{NC}[n]\} + \alpha \sin(\pi \mathrm{Im}\{y_{NC}[n]\})], \quad (2.39)$$

where $0 < \alpha \leq 1/\pi$ is the constant parameter that controls the nonlinear component, and $y_{NC}[n]$ is the linear component of the NMCMA output presented in Figure 45, obtained as

$$y_{NC}[n] = \sum_{i=0}^{L_{EQ}-1} w_{NC_i}[n] r[n-i] = \underline{w}_{NC}[n]^T \underline{r}[n], \quad (2.40)$$

where $\underline{w}_{NC}[n] = \left[w_{NC_0}[n], w_{NC_1}[n], \cdots, w_{NC_{L_{EQ}-1}}[n] \right]^T$ is the coefficient vector of the NMCMA equalizer.

Figure 45 – Block diagram of the NMCMA equalizer.

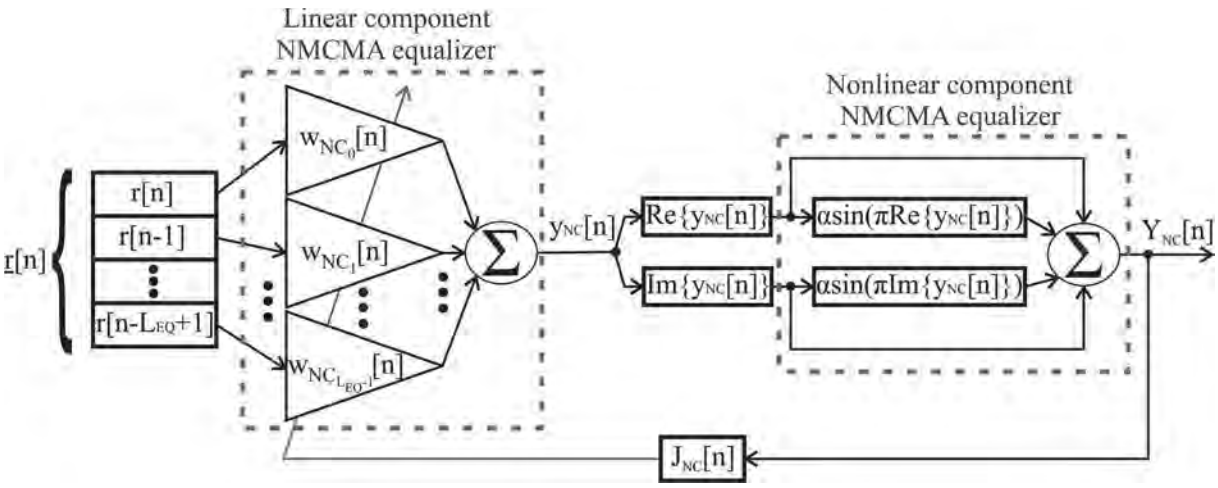

Source: Author (2018).

The NMCMA cost function ($J_{NC}[n]$) is the same presented by Oh and Chin (1995), and it is

$$J_{NC}[n] = \frac{1}{4}[(\mathrm{Re}\{Y_{NC}[n]\}^2 - \gamma_R)^2 + (\mathrm{Im}\{Y_{NC}[n]\}^2 - \gamma_I)^2]. \quad (2.41)$$

The SGD for the $\underline{w}_{NC}[n]$ update is

$$\underline{w}_{NC}[n+1] = \underline{w}_{NC}[n] + \eta_{NC}(-\nabla J_{NC}[n]), \quad (2.42)$$

where $\eta_{NC} > 0$ is the adaptive step of the NMCMA equalizer.

Applying the gradient operator to Eq. (2.41), considering the i^{th} variation of the coefficient vector $\underline{w}_{NC}[n]$:

$$\nabla_i J_{NC}[n] = \nabla_i^R J_{NC}[n] + j\nabla_i^I J_{NC}[n] = \frac{\partial J_{NC}[n]}{\partial \mathrm{Re}\{w_{NC_i}[n]\}} + j\frac{\partial J_{NC}[n]}{\partial \mathrm{Im}\{w_{NC_i}[n]\}}. \quad (2.43)$$

Hence, the Eq. (2.41) referenced to Eq. (2.43)

$$\nabla_i^R J_{NC}[n] = \frac{1}{4}\left\{\frac{\partial(\mathrm{Re}\{Y_{NC}[n]\}^2 - \gamma_R)^2}{\partial \mathrm{Re}\{w_{NC_i}[n]\}} + \frac{\partial(\mathrm{Im}\{Y_{NC}[n]\}^2 - \gamma_I)^2}{\partial \mathrm{Re}\{w_{NC_i}[n]\}}\right\}, \quad (2.44)$$

$$\nabla_i^I J_{NC}[n] = \frac{1}{4}\left\{\frac{\partial(\mathrm{Re}\{Y_{NC}[n]\}^2 - \gamma_R)^2}{\partial \mathrm{Im}\{w_{NC_i}[n]\}} + \frac{\partial(\mathrm{Im}\{Y_{NC}[n]\}^2 - \gamma_I)^2}{\partial \mathrm{Im}\{w_{NC_i}[n]\}}\right\}. \quad (2.45)$$

The derivatives of Eqs. (2.44) and (2.45) leads to

$$\nabla_i^R J_{NC}[n] = \mathrm{Re}\{Y_{NC}[n]\}(\mathrm{Re}\{Y_{NC}[n]\}^2 - \gamma_R)\frac{\partial \mathrm{Re}\{Y_{NC}[n]\}}{\partial \mathrm{Re}\{w_{NC_i}[n]\}} + \\ + \mathrm{Im}\{Y_{NC}[n]\}(\mathrm{Im}\{Y_{NC}[n]\}^2 - \gamma_I)\frac{\partial \mathrm{Im}\{Y_{NC}[n]\}}{\partial \mathrm{Re}\{w_{NC_i}[n]\}}, \quad (2.46)$$

$$\nabla_i^I J_{NC}[n] = \mathrm{Re}\{Y_{NC}[n]\}(\mathrm{Re}\{Y_{NC}[n]\}^2 - \gamma_R)\frac{\partial \mathrm{Re}\{Y_{NC}[n]\}}{\partial \mathrm{Im}\{w_{NC_i}[n]\}} + \\ + \mathrm{Im}\{Y_{NC}[n]\}(\mathrm{Im}\{Y_{NC}[n]\}^2 - \gamma_I)\frac{\partial \mathrm{Im}\{Y_{NC}[n]\}}{\partial \mathrm{Im}\{w_{NC_i}[n]\}}. \quad (2.47)$$

Hence, the Eq. (2.39) referenced to the derivatives of Eqs. (2.46) and (2.47)

$$\frac{\partial \mathrm{Re}\{Y_{NC}[n]\}}{\partial \mathrm{Re}\{w_{NC_i}[n]\}} = \frac{\partial \mathrm{Re}\{y_{NC}[n]\}}{\partial \mathrm{Re}\{w_{NC_i}[n]\}} + \frac{\partial \alpha \sin(\pi \mathrm{Re}\{y_{NC}[n]\})}{\partial \mathrm{Re}\{w_{NC_i}[n]\}}, \quad (2.48)$$

$$\frac{\partial \mathrm{Im}\{Y_{NC}[n]\}}{\partial \mathrm{Re}\{w_{NC_i}[n]\}} = \frac{\partial \mathrm{Im}\{y_{NC}[n]\}}{\partial \mathrm{Re}\{w_{NC_i}[n]\}} + \frac{\partial \alpha \sin(\pi \mathrm{Im}\{y_{NC}[n]\})}{\partial \mathrm{Re}\{w_{NC_i}[n]\}}, \quad (2.49)$$

$$\frac{\partial \mathrm{Re}\{Y_{NC}[n]\}}{\partial \mathrm{Im}\{w_{NC_i}[n]\}} = \frac{\partial \mathrm{Re}\{y_{NC}[n]\}}{\partial \mathrm{Im}\{w_{NC_i}[n]\}} + \frac{\partial \alpha \sin(\pi \mathrm{Re}\{y_{NC}[n]\})}{\partial \mathrm{Im}\{w_{NC_i}[n]\}}, \quad (2.50)$$

$$\frac{\partial \mathrm{Im}\{Y_{NC}[n]\}}{\partial \mathrm{Im}\{w_{NC_i}[n]\}} = \frac{\partial \mathrm{Im}\{y_{NC}[n]\}}{\partial \mathrm{Im}\{w_{NC_i}[n]\}} + \frac{\partial \alpha \sin(\pi \mathrm{Im}\{y_{NC}[n]\})}{\partial \mathrm{Im}\{w_{NC_i}[n]\}}. \quad (2.51)$$

The Eqs. (2.48), (2.49), (2.50) and (2.51) leads to

$$\frac{\partial \mathrm{Re}\{Y_{NC}[n]\}}{\partial \mathrm{Re}\{w_{NC_i}[n]\}} = [1 + \alpha\pi \cos(\pi \mathrm{Re}\{y_{NC}[n]\})] \frac{\partial \mathrm{Re}\{y_{NC}[n]\}}{\partial \mathrm{Re}\{w_{NC_i}[n]\}}, \tag{2.52}$$

$$\frac{\partial \mathrm{Im}\{Y_{NC}[n]\}}{\partial \mathrm{Re}\{w_{NC_i}[n]\}} = [1 + \alpha\pi \cos(\pi \mathrm{Im}\{y_{NC}[n]\})] \frac{\partial \mathrm{Im}\{y_{NC}[n]\}}{\partial \mathrm{Re}\{w_{NC_i}[n]\}}, \tag{2.53}$$

$$\frac{\partial \mathrm{Re}\{Y_{NC}[n]\}}{\partial \mathrm{Im}\{w_{NC_i}[n]\}} = [1 + \alpha\pi \cos(\pi \mathrm{Re}\{y_{NC}[n]\})] \frac{\partial \mathrm{Re}\{y_{NC}[n]\}}{\partial \mathrm{Im}\{w_{NC_i}[n]\}}, \tag{2.54}$$

$$\frac{\partial \mathrm{Im}\{Y_{NC}[n]\}}{\partial \mathrm{Im}\{w_{NC_i}[n]\}} = [1 + \alpha\pi \cos(\pi \mathrm{Im}\{y_{NC}[n]\})] \frac{\partial \mathrm{Im}\{y_{NC}[n]\}}{\partial \mathrm{Im}\{w_{NC_i}[n]\}}. \tag{2.55}$$

The error function of the NMCMA $e_{NC}[n]$ is

$$e_{NC}[n] = \mathrm{Re}\{e_{NC}[n]\} + j\mathrm{Im}\{e_{NC}[n]\}, \tag{2.56}$$

where

$$\mathrm{Re}\{e_{NC}[n]\} = \mathrm{Re}\{Y_{NC}[n]\}(\mathrm{Re}\{Y_{NC}[n]\}^2 - \gamma_R)[1 + \alpha\pi \cos(\pi \mathrm{Re}\{y_{NC}[n]\})], \tag{2.57}$$

$$\mathrm{Im}\{e_{NC}[n]\} = \mathrm{Im}\{Y_{NC}[n]\}(\mathrm{Im}\{Y_{NC}[n]\}^2 - \gamma_I)[1 + \alpha\pi \cos(\pi \mathrm{Im}\{y_{NC}[n]\})]. \tag{2.58}$$

Therefore, substituting Eqs. (2.52) and (2.53) into Eq. (2.46), and Eqs. (2.54) and (2.55) into Eq. (2.47)

$$\nabla_i^R J_{NC}[n] = \mathrm{Re}\{e_{NC}[n]\} \frac{\partial \mathrm{Re}\{y_{NC}[n]\}}{\partial \mathrm{Re}\{w_{NC_i}[n]\}} + \mathrm{Im}\{e_{NC}[n]\} \frac{\partial \mathrm{Im}\{y_{NC}[n]\}}{\partial \mathrm{Re}\{w_{NC_i}[n]\}}, \tag{2.59}$$

$$\nabla_i^I J_{NC}[n] = \mathrm{Re}\{e_{NC}[n]\} \frac{\partial \mathrm{Re}\{y_{NC}[n]\}}{\partial \mathrm{Im}\{w_{NC_i}[n]\}} + \mathrm{Im}\{e_{NC}[n]\} \frac{\partial \mathrm{Im}\{y_{NC}[n]\}}{\partial \mathrm{Im}\{w_{NC_i}[n]\}}. \tag{2.60}$$

Expanding $\mathrm{Re}\{y_{NC}[n]\}$ and $\mathrm{Im}\{y_{NC}[n]\}$

$$\mathrm{Re}\{y_{NC}[n]\} = \mathrm{Re}\{w_{NC_i}[n]\}\mathrm{Re}\{r[n-i]\} - \mathrm{Im}\{w_{NC_i}[n]\}\mathrm{Im}\{r[n-i]\}, \tag{2.61}$$

$$\mathrm{Im}\{y_{NC}[n]\} = \mathrm{Re}\{w_{NC_i}[n]\}\mathrm{Im}\{r[n-i]\} + \mathrm{Im}\{w_{NC_i}[n]\}\mathrm{Re}\{r[n-i]\}, \tag{2.62}$$

consequently, applying Eqs. (2.61) and (2.62) into Eqs. (2.59) and (2.60), and solving the derivatives

$$\nabla_i^R J_{NC}[n] = \mathrm{Re}\{e_{NC}[n]\}\mathrm{Re}\{r[n-i]\} + \mathrm{Im}\{e_{NC}[n]\}\mathrm{Im}\{r[n-i]\}, \tag{2.63}$$

$$\nabla_i^I J_{NC}[n] = \mathrm{Im}\{e_{NC}[n]\}\mathrm{Re}\{r[n-i]\} - \mathrm{Re}\{e_{NC}[n]\}\mathrm{Im}\{r[n-i]\}. \quad (2.64)$$

Substituting Eqs. (2.63) and (2.64) into Eq. (2.43)

$$\nabla_i J_{NC}[n] = (\mathrm{Re}\{e_{NC}[n]\}\mathrm{Re}\{r[n-i]\} + \mathrm{Im}\{e_{NC}[n]\}\mathrm{Im}\{r[n-i]\}) + \\ +j(\mathrm{Im}\{e_{NC}[n]\}\mathrm{Re}\{r[n-i]\} - \mathrm{Re}\{e_{NC}[n]\}\mathrm{Im}\{r[n-i]\}), \quad (2.65)$$

which results in

$$\nabla_i J_{NC}[n] = e_{NC}[n] r[n-i]^*. \quad (2.66)$$

Finally, substituting Eq. (2.66) into (2.42)

$$\underline{w}_{NC}[n+1] = \underline{w}_{NC}[n] - \eta_{NC}\, e_{NC}[n]\underline{r}[n]^*. \quad (2.67)$$

2.5.4. DD Equalizer

Differently of equalizers based on the CMA properties, which are able to operate in standalone mode, the DD requires another equalizer to minimize the error below to a specified value for its correct operation (MACCHI; EWEDA, 1984). Figure 46 depicts the block diagram of the DD equalizer.

Figure 46 – Block diagram of the DD equalizer.

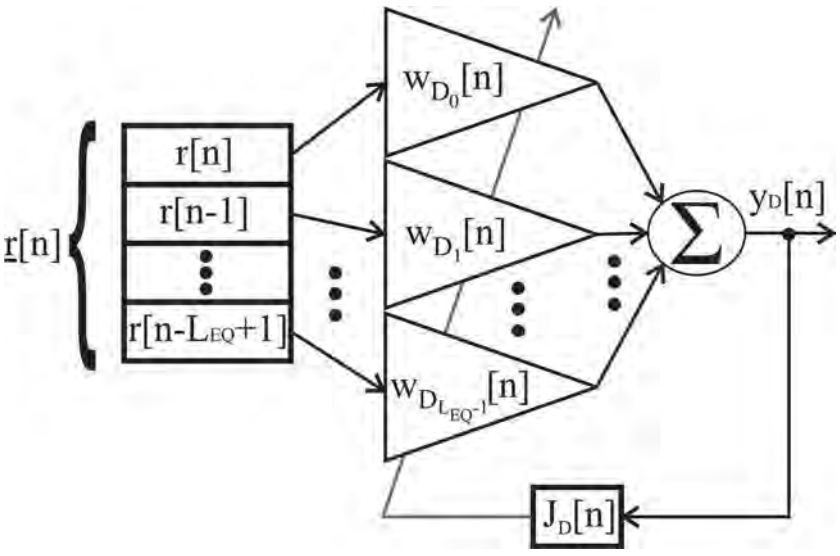

Source: Author (2018).

The DD output ($y_D[n]$) is given by

$$y_D[n] = \sum_{i=0}^{L_{EQ}-1} w_{D_i}[n] r[n-i] = \underline{w}_D[n]^T \underline{r}[n], \quad (2.68)$$

where $\underline{w_D}[n] = \left[w_{D_0}[n], w_{D_1}[n], \cdots, w_{D_{L_{EQ}-1}}[n]\right]^T$ is the coefficient vector of the DD.

Equation (2.68) can be similarly represented as

$$y_D[n] = \left\{\sum_{i=0}^{L_{EQ}-1} \mathrm{Re}\{w_{D_i}[n]\}\mathrm{Re}\{r[n-i]\} - \mathrm{Re}\{w_{D_i}[n]\}\mathrm{Re}\{r[n-i]\}\right\} + \\ + j\left\{\sum_{i=0}^{L_{EQ}-1} \mathrm{Re}\{w_{D_i}[n]\}\mathrm{Im}\{r[n-i]\} + \mathrm{Im}\{w_{D_i}[n]\}\mathrm{Re}\{r[n-i]\}\right\}. \quad (2.69)$$

The SGD for the $\underline{w_D}[n]$ update is

$$\underline{w_D}[n+1] = \underline{w_D}[n] + \eta_D(-\nabla J_D[n]), \quad (2.70)$$

where $\eta_D > 0$ is the adaptive step of the DD, and $J_D[n]$ is the DD cost function, given by

$$J_D[n] = \frac{1}{2}[|\mathrm{Q}\{y_D[n]\} - y_D[n]|^2], \quad (2.71)$$

where $\mathrm{Q}\{\cdot\}$ is the complex quantizier operator (DE CASTRO; DE CASTRO; ARANTES, 2001), which returns the reference constellation IQ symbol with the smallest Euclidean distance from its argument.

Applying the gradient operator to Eq. (2.71), considering the i^{th} variation of the coefficient vector $\underline{w_D}[n]$:

$$\nabla_i J_D[n] = \nabla_i^R J_D[n] + j\nabla_i^I J_D[n] = \frac{\partial J_D[n]}{\partial \mathrm{Re}\{w_{D_i}[n]\}} + j\frac{\partial J_D[n]}{\partial \mathrm{Im}\{w_{D_i}[n]\}}. \quad (2.72)$$

Substituting Eq. (2.71) into Eq. (2.72)

$$\nabla_i J_D[n] = \frac{1}{2}\left[\frac{\partial |\mathrm{Q}\{y_D[n]\} - y_D[n]|^2}{\partial \mathrm{Re}\{w_{D_i}[n]\}} + j\frac{\partial |\mathrm{Q}\{y_D[n]\} - y_D[n]|^2}{\partial \mathrm{Im}\{w_{D_i}[n]\}}\right]. \quad (2.73)$$

However

$$|\mathrm{Q}\{y_D[n]\} - y_D[n]|^2 = \left(\mathrm{Re}\{\mathrm{Q}\{y_D[n]\}\} - \mathrm{Re}\{y_D[n]\}\right)^2 + \\ + \left(\mathrm{Im}\{\mathrm{Q}\{y_D[n]\}\} - \mathrm{Im}\{y_D[n]\}\right)^2, \quad (2.74)$$

thus, Eqs. (2.69) and (2.74), as reference to Eq. (2.73) and solving the derivatives

$$\frac{\partial|\mathrm{Q}\{y_D[n]\}-y_D[n]|^2}{\partial\mathrm{Re}\{w_{D_i}[n]\}}=2\left[\mathrm{Re}\{\mathrm{Q}\{y_D[n]\}\}-\mathrm{Re}\{y_D[n]\}\right]\mathrm{Re}\{r[n-i]\}+$$

$$+2\left[\mathrm{Im}\{\mathrm{Q}\{y_D[n]\}\}-\mathrm{Im}\{y_D[n]\}\right]\mathrm{Im}\{r[n-i]\}, \quad (2.75)$$

$$\frac{\partial|\mathrm{Q}\{y_D[n]\}-y_D[n]|^2}{\partial\mathrm{Im}\{w_{D_i}[n]\}}=2\left[\mathrm{Im}\{\mathrm{Q}\{y_D[n]\}\}-\mathrm{Im}\{y_D[n]\}\right]\mathrm{Re}\{r[n-i]\}+$$

$$-2\left[\mathrm{Re}\{\mathrm{Q}\{y_D[n]\}\}-\mathrm{Re}\{y_D[n]\}\right]\mathrm{Im}\{r[n-i]\}, \quad (2.76)$$

being $e_D[n]$ the error function of the DD, given by

$$e_D[n]=\mathrm{Re}\{e_D[n]\}+j\mathrm{Im}\{e_D[n]\}, \quad (2.77)$$

where

$$\mathrm{Re}\{e_D[n]\}=\mathrm{Re}\{\mathrm{Q}\{y_D[n]\}\}-\mathrm{Re}\{y_D[n]\}, \quad (2.78)$$

$$\mathrm{Im}\{e_{MC}[n]\}=\mathrm{Im}\{\mathrm{Q}\{y_D[n]\}\}-\mathrm{Im}\{y_D[n]\}. \quad (2.79)$$

Therefore, substituting Eqs. (2.78) and (2.79) into Eqs. (2.75) and (2.76)

$$\frac{\partial|\mathrm{Q}\{y_D[n]\}-y_D[n]|^2}{\partial\mathrm{Re}\{w_{D_i}[n]\}}=-2[\mathrm{Re}\{e_D[n]\}\mathrm{Re}\{r[n-i]\}+\mathrm{Im}\{e_D[n]\}\mathrm{Im}\{r[n-i]\}], \quad (2.80)$$

$$\frac{\partial|\mathrm{Q}\{y_D[n]\}-y_D[n]|^2}{\partial\mathrm{Im}\{w_{D_i}[n]\}}=-2[\mathrm{Im}\{e_D[n]\}\mathrm{Re}\{r[n-i]\}-\mathrm{Re}\{e_D[n]\}\mathrm{Im}\{r[n-i]\}]. \quad (2.81)$$

Applying Eqs. (2.80) and (2.81) into Eq. (2.73)

$$-\nabla_i J_D[n]=[\mathrm{Re}\{e_D[n]\}\mathrm{Re}\{r[n-i]\}+\mathrm{Im}\{e_D[n]\}\mathrm{Im}\{r[n-i]\}]+$$

$$+j[\mathrm{Im}\{e_D[n]\}\mathrm{Re}\{r[n-i]\}-\mathrm{Re}\{e_D[n]\}\mathrm{Im}\{r[n-i]\}], \quad (2.82)$$

which results in

$$-\nabla_i J_D[n]=e_D[n]r[n-i]^*. \quad (2.83)$$

Finally, substituting Eq. (2.83) into (2.70)

$$\underline{w}_D[n+1]=\underline{w}_D[n]+\eta_D\, e_D[n]\underline{r}[n]^*. \quad (2.84)$$

2.5.5. SDD Equalizer

As the in the DD equalizer case, the SDD requires a pre-equalizer based on the CMA algorithm in order to minimize the CMA output error below a specified value

so that the SDD algorithm is able to achieve convergence. In this scenario, when the pre-equalization is accomplished, the CMA+SDD equalizer output can be represented by M Gaussian clusters around each symbol of the reference constellation, which can be modeled by *a posteriori* Probability Density Function (PDF) (CHEN, 2003). Differently from the DD hard decision scheme, expressed by $Q\{y_D[n]\} - y_D[n]$, the SDD works with *a posteriori* PDF $p\left(\underline{w_S}[n], y_S[n]\right)$. The domain of each PDF is each one of a total of $M/4$ decision regions ($\mathbb{S}_{i,l} = \{\mathcal{S}_{p,q}, p = 2i - 1, 2i, q = 2l - 1, 2l\}$) that are possible to obtain from the partitioning of the reference constellation in M/4 sub-regions, each one containing four adjacent reference symbols (CHEN, 2003; CHEN; CHNG, 2004), with the four symbol points having equal probability of occurrence. Figures 47 and 48 present the block diagram of the SDD equalizer and the 16 decision regions for a 64-QAM, respectively.

Figure 47 – Block diagram of the SDD equalizer.

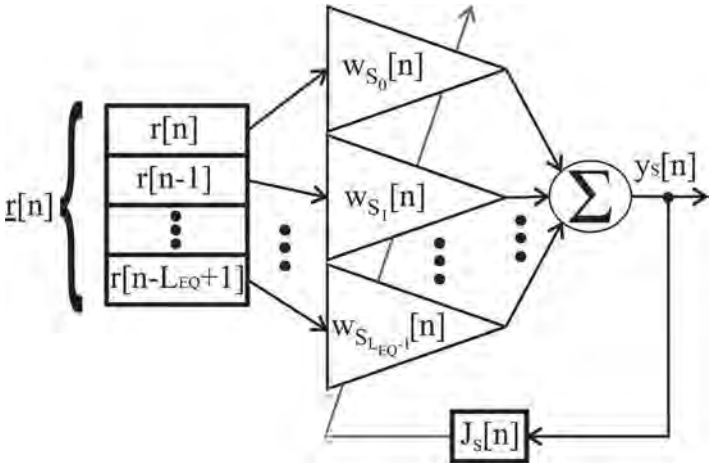

Source: Author (2018).

Figure 48 – SDD decision regions for a 64-QAM.

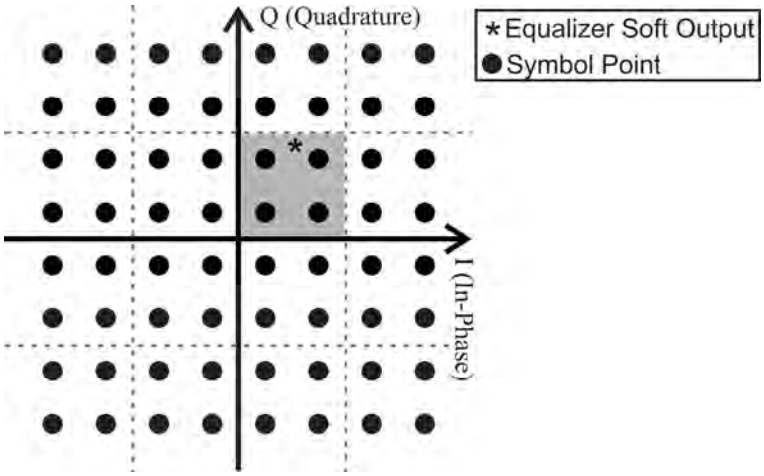

Source: Adapted of Chen (2003).

A posteriori PDF of the $M/4$ decision regions is

$$p\left(\underline{w}_S[n], y_S[n]\right) \approx \frac{p_{ql}}{2\pi\rho} \sum_{p=2i-1}^{2i} \sum_{q=2i-1}^{2l} \exp\left(-\frac{\left|y_S[n] - \mathcal{S}_{p,q}\right|^2}{2\rho}\right) = \frac{P_S[n] p_{ql}}{2\pi\rho}, \quad (2.85)$$

where p_{ql} is the symbol probability, $\underline{w}_S[n] = \left[w_{S_0}[n], w_{S_1}[n], \cdots, w_{S_{L_{EQ}-1}}[n]\right]^T$ is the coefficient vector of the SDD equalizer, $y_S[k]$ is the SDD output, ρ is the variance of the distorted input symbols, and $P_S[n] = \sum_{p=2i-1}^{2i} \sum_{q=2i-1}^{2l} \exp\left(-\frac{\left|y_S[n] - \mathcal{S}_{p,q}\right|^2}{2\rho}\right)$ is *a posteriori* PDF not normalized.

The SDD output is

$$y_S[n] = \sum_{i=0}^{L_{EQ}-1} w_{S_i}[n] r[n-i] = \underline{w}_S[n]^T \underline{r}[n], \quad (2.86)$$

and the SGD for the $\underline{w}_S[n]$ update is

$$\underline{w}_S[n+1] = \underline{w}_S[n] + \eta_S \nabla J_S[n], \quad (2.87)$$

where $\eta_S > 0$ is the SDD adaptive step, and $J_S[n]$ is the SDD cost function designed to maximize the log of *a posteriori* PDF as

$$J_S[n] = \rho \ln\left(p\left(\underline{w}_S[n], y_S[n]\right)\right). \quad (2.88)$$

Applying the gradient operator to Eq. (2.88), considering the i^{th} variation of the coefficient vector $\underline{w}_S[n]$:

$$\nabla_i J_S[n] = \nabla_i^R J_S[n] + j\nabla_i^I J_S[n] = \frac{\partial J_S[n]}{\partial \mathrm{Re}\{w_{S_i}[n]\}} + j\frac{\partial J_S[n]}{\partial \mathrm{Im}\{w_{S_i}[n]\}}, \quad (2.89)$$

Substituting Eq. (2.88) into Eq. (2.89)

$$\nabla_i J_S[n] = \rho\left[\frac{\partial \ln\left(p\left(\underline{w}_S[n], y_S[n]\right)\right)}{\partial \mathrm{Re}\{w_{S_i}[n]\}} + j\frac{\partial \ln\left(p\left(\underline{w}_S[n], y_S[n]\right)\right)}{\partial \mathrm{Im}\{w_{S_i}[n]\}}\right], \quad (2.90)$$

However,

$$\ln\left(p\left(\underline{w}_S[n], y_S[n]\right)\right) = \ln\left(\frac{P_S[n] p_{ql}}{2\pi\rho}\right) = \ln(P_S[n]) - \ln\left(\frac{2\pi\rho}{p_{ql}}\right), \quad (2.91)$$

thus, substituting Eq. (2.91) into (2.90)

$$\nabla_i J_S[n] = \rho\left[\frac{\partial\left\{\ln(P_S[n]) - \ln\left(\frac{2\pi\rho}{p_{ql}}\right)\right\}}{\partial\mathrm{Re}\{w_{S_i}[n]\}} + j\frac{\partial\left\{\ln(P_S[n]) - \ln\left(\frac{2\pi\rho}{p_{ql}}\right)\right\}}{\partial\mathrm{Im}\{w_{S_i}[n]\}}\right], \tag{2.92}$$

which results in

$$\nabla_i J_S[n] = \rho\left[\frac{\partial\ln(P_S[n])}{\partial\mathrm{Re}\{w_{S_i}[n]\}} + j\frac{\partial\ln(P_S[n])}{\partial\mathrm{Im}\{w_{S_i}[n]\}}\right]. \tag{2.93}$$

Solving the derivatives of Eq. (2.93), as reference to Eq. (2.85)

$$\frac{\partial\ln(P_S[n])}{\partial\mathrm{Re}\{w_{S_i}[n]\}} = -\frac{1}{2\rho P_S[n]}\sum_{p=2i-1}^{2i}\sum_{q=2i-1}^{2l}\left[\exp\left(-\frac{\left|y_S[n]-\mathcal{S}_{p,q}\right|^2}{2\rho}\right)\frac{\partial\left|y_S[n]-\mathcal{S}_{p,q}\right|^2}{\partial\mathrm{Re}\{w_{S_i}[n]\}}\right], \tag{2.94}$$

$$\frac{\partial\ln(P_S[n])}{\partial\mathrm{Im}\{w_{S_i}[n]\}} = -\frac{1}{2\rho P_S[n]}\sum_{p=2i-1}^{2i}\sum_{q=2i-1}^{2l}\left[\exp\left(-\frac{\left|y_S[n]-\mathcal{S}_{p,q}\right|^2}{2\rho}\right)\frac{\partial\left|y_S[n]-\mathcal{S}_{p,q}\right|^2}{\partial\mathrm{Im}\{w_{S_i}[n]\}}\right]. \tag{2.95}$$

However,

$$\left|y_S[n]-\mathcal{S}_{p,q}\right|^2 = \left[\mathrm{Re}\{w_{S_i}[n]\}\mathrm{Re}\{r[n-i]\} - \mathrm{Im}\{w_{S_i}[n]\}\mathrm{Im}\{r[n-i]\} - \mathrm{Re}\{\mathcal{S}_{p,q}\}\right]^2 + \\ +\left[\mathrm{Re}\{w_{S_i}[n]\}\mathrm{Im}\{r[n-i]\} + \mathrm{Im}\{w_{S_i}[n]\}\mathrm{Re}\{r[n-i]\} - \mathrm{Im}\{\mathcal{S}_{p,q}\}\right]^2. \tag{2.96}$$

Hence, substituting Eq. (2.96) as reference to Eqs. (2.94) and (2.95) and solving the derivatives

$$\frac{\partial\left|y_S[n]-\mathcal{S}_{p,q}\right|^2}{\partial\mathrm{Re}\{w_{S_i}[n]\}} = 2\left[\mathrm{Re}\{y_S[n]-\mathcal{S}_{p,q}\}\mathrm{Re}\{r[n-i]\} + \right. \\ \left. +\mathrm{Re}\{y_S[n]-\mathcal{S}_{p,q}\}\mathrm{Re}\{r[n-i]\}\right], \tag{2.97}$$

$$\frac{\partial\left|y_S[n]-\mathcal{S}_{p,q}\right|^2}{\partial\mathrm{Im}\{w_{S_i}[n]\}} = 2\left[\mathrm{Im}\{y_S[n]-\mathcal{S}_{p,q}\}\mathrm{Re}\{r[n-i]\} + \right. \\ \left. -\mathrm{Re}\{y_S[n]-\mathcal{S}_{p,q}\}\mathrm{Im}\{r[n-i]\}\right]. \tag{2.98}$$

Substituting Eqs. (2.94), (2.95), (2.97) and (2.98) into Eq. (2.93)

$$\nabla_i J_S[n] = -\left\{\sum_{p=2i-1}^{2i}\sum_{q=2i-1}^{2l}\left[\exp\left(-\frac{\left|y_S[n]-\mathcal{S}_{p,q}\right|^2}{2\rho}\right)\left(y_S[n]-\mathcal{S}_{p,q}\right)\right]\right\} r[n-i]^* \Big/ P_S[n], \tag{2.99}$$

being $e_S[n]$ the error function of the SDD equalizer, defined as

$$e_S[n] = \sum_{p=2i-1}^{2i} \sum_{q=2i-1}^{2l} \left[\exp\left(-\frac{\left| y_S[n] - \mathcal{S}_{p,q} \right|^2}{2\rho} \right) \left(\mathcal{S}_{p,q} - y_S[n] \right) \right], \tag{2.100}$$

substituting Eq. (2.100) into Eq. (2.99)

$$\nabla_i J_S[n] = \frac{e_S[n] r[n-i]^*}{P_S[n]}, \tag{2.101}$$

and finally, applying Eq. (2.101) into Eq. (2.87)

$$\underline{w_S}[n+1] = \underline{w_S}[n] + \eta_S \frac{e_S[n] \underline{r}[n]^*}{P_S[n]}. \tag{2.102}$$

2.5.6. CMA-DD Concurrent Equalizer

The concurrent architecture of equalization, proposed by De Castro F. C. C., De Castro M. C. F. and Arantes (2001), uses two equalizers, one CMA and one DD, as presented in the block diagram of the Figure 49.

Figure 49 – Block diagram of the CMA-DD concurrent equalizer.

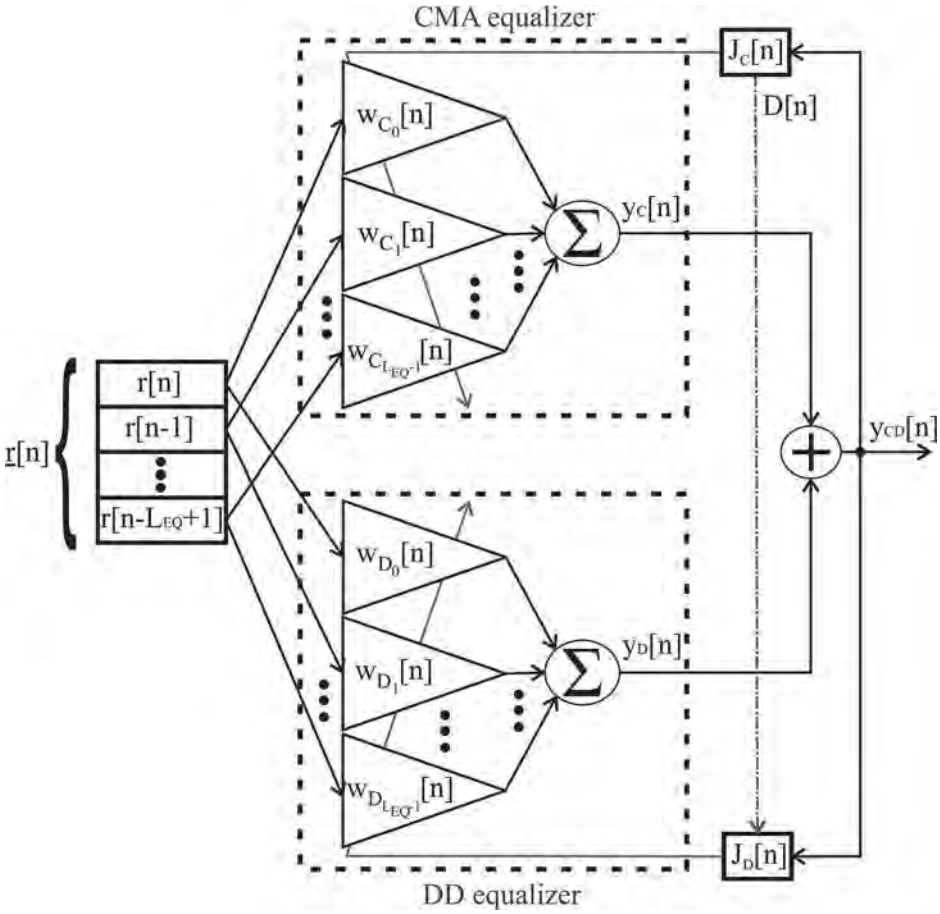

Source: Author (2018).

In the concurrent architecture, the CMA equalizer and the DD equalizer operate simultaneously in a cooperative mode, but controlled by a nonlinear link $D[n]$ between the two equalizers that enables or disables the DD at instant n according to the instantaneous minimization of the CMA cost function. This approach drastically improves the convergence rate.

The CMA-DD concurrent equalizer output $y_{CD}[n]$ is given by

$$y_{CD}[n] = \sum_{i=0}^{L_{EQ}-1} w_{C_i}[n]r[n-i] + \sum_{i=0}^{L_{EQ}-1} w_{D_i}[n]r[n-i] = y_C[n] + y_D[n]. \quad (2.103)$$

In order to update the CMA coefficient vector $\underline{w_C}[n]$, Eq. (2.18) is used as

$$\underline{w_C}[n+1] = \underline{w_C}[n] + \eta_C y_{CD}[n](\gamma - |y_{CD}[n]^2|)\underline{r}[n]^*. \quad (2.104)$$

The update of the DD coefficient vector $\underline{w_D}[n]$ is controlled by the nonlinear link $D[n]$, as follows

$$D[n] = \begin{cases} 1, & \mathrm{Q}\{y_{CD}[n]\} = \mathrm{Q}\{\hat{y}_{CD}[n]\}, \\ 0, & \mathrm{Q}\{y_{CD}[n]\} \neq \mathrm{Q}\{\hat{y}_{CD}[n]\}, \end{cases} \quad (2.105)$$

where $\hat{y}_{CD}[n]$ is the CMA-DD concurrent equalizer output after the update of the CMA coefficient vector $\underline{w_C}[n]$, by Eq. (2.104). Thus, $\hat{y}_{CD}[n]$ is obtained by:

$$\hat{y}_{CD}[n] = \sum_{i=0}^{L_{EQ}-1} w_{C_i}[n+1]r[n-i] + \sum_{i=0}^{L_{EQ}-1} w_{D_i}[n]r[n-i]. \quad (2.106)$$

According to Eq. (2.105), if $D[n] = 1$, it means that the CMA-DD equalizer output $y_{CD}[n]$ and its updated version $\hat{y}_{CD}[n]$ resulted in the same IQ symbol. In this case, the DD coefficients are updated. Nevertheless, if $D[n] = 0$, the DD coefficients are not updated.

The DD coefficient vector update is given by

$$\underline{w_D}[n+1] = \underline{w_D}[n] + \eta_D D[n](\mathrm{Q}\{y_{CD}[n]\} - y_{CD}[n])\underline{r}[n]^*. \quad (2.107)$$

2.5.7. CMA-SDD Concurrent Equalizer

Using the architecture proposed by De Castro F. C. C., De Castro M. C. F. and Arantes (2001), Chen (2003) substituted the DD equalizer for a SDD equalizer,

replacing the direct hard decision for a soft decision (CHEN, 2003). Figure 50 depicts the block diagram of the CMA-SDD concurrent equalizer.

Figure 50 – Block diagram of the CMA-SDD concurrent equalizer.

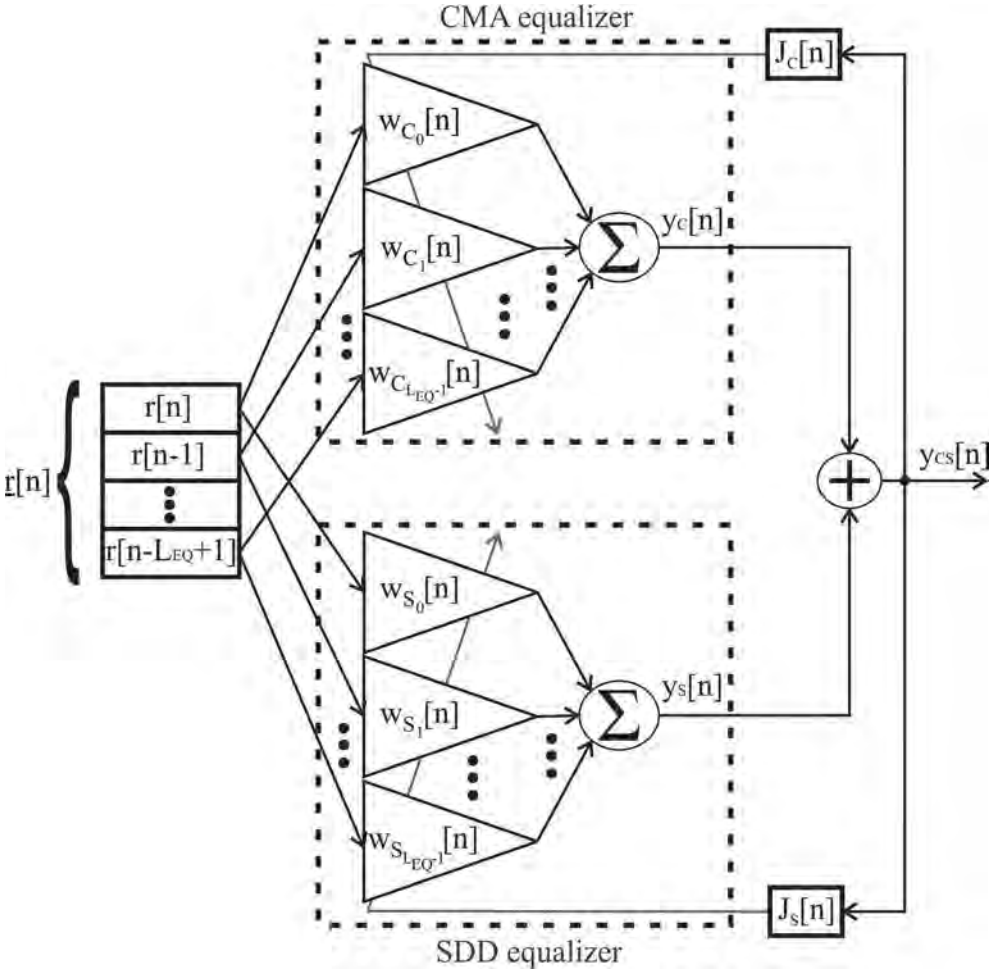

Source: Author (2018).

As addressed by Chen (2003), for the CMA-DD concurrent equalizer, if the hard decision is wrong, the coefficients update degrades the system performance. Otherwise, if the hard decision is correct, it increases the convergence rate and it is capable of lowering the residual MSE (CHEN, 2003). Differently, the CMA-SDD concurrent equalizer does not have the hard decision issue, due to the soft decision characteristic of the SDD. CMA-SDD concurrent equalizer output $y_{CS}[n]$ is given by

$$y_{CS}[n] = \sum_{i=0}^{L_{EQ}-1} w_{C_i}[n]r[n-i] + \sum_{i=0}^{L_{EQ}-1} w_{S_i}[n]r[n-i] = y_C[n] + y_S[n]. \quad (2.108)$$

In order to update the CMA coefficient vector $\underline{w_C}[n]$, Eq. (2.18) is used as

$$\underline{w_C}[n+1] = \underline{w_C}[n] + \eta_C y_{CS}[n](\gamma - |y_{CS}[n]^2|)\underline{r}[n]^*, \quad (2.109)$$

and to update the SDD coefficient vector $\underline{w_S}[n]$, Eq. (2.102) is used as follows

$$\underline{w_S}[n+1] = \underline{w_S}[n] + \eta_S \frac{e_{CS}[n]\underline{r}[n]^*}{P_{CS}[n]}, \tag{2.110}$$

where

$$P_{CS}[n] = \sum_{p=2i-1}^{2i} \sum_{q=2i-1}^{2l} \exp\left(-\frac{\left|y_{CS}[n] - \mathcal{S}_{p,q}\right|^2}{2\rho}\right), \tag{2.111}$$

$$e_{CS}[n] = \sum_{p=2i-1}^{2i} \sum_{q=2i-1}^{2l} \left[\exp\left(-\frac{\left|y_{CS}[n] - \mathcal{S}_{p,q}\right|^2}{2\rho}\right)\left(\mathcal{S}_{p,q} - y_{CS}[n]\right)\right]. \tag{2.112}$$

The CMA-SDD concurrent equalizer architecture presents better results for multipath scenarios, being the state of the art in single carrier channel equalization.

3. NMCMA-SDD CONCURRENT EQUALIZER

In this chapter, the proposed NMCMA-SDD concurrent equalizer architecture is presented to the reader.

The proposed approach is based on the concurrent equalizer proposed by De Castro F. C. C., De Castro M. C. F. and Arantes (2001), with the replacement of the CMA for the NMCMA algorithm and with the replacement of the DD for the SDD algorithm. The structure of the NMCMA-SDD concurrent equalizer is presented in Figure 51.

Figure 51 – Block diagram of the NMCMA-SDD concurrent equalizer.

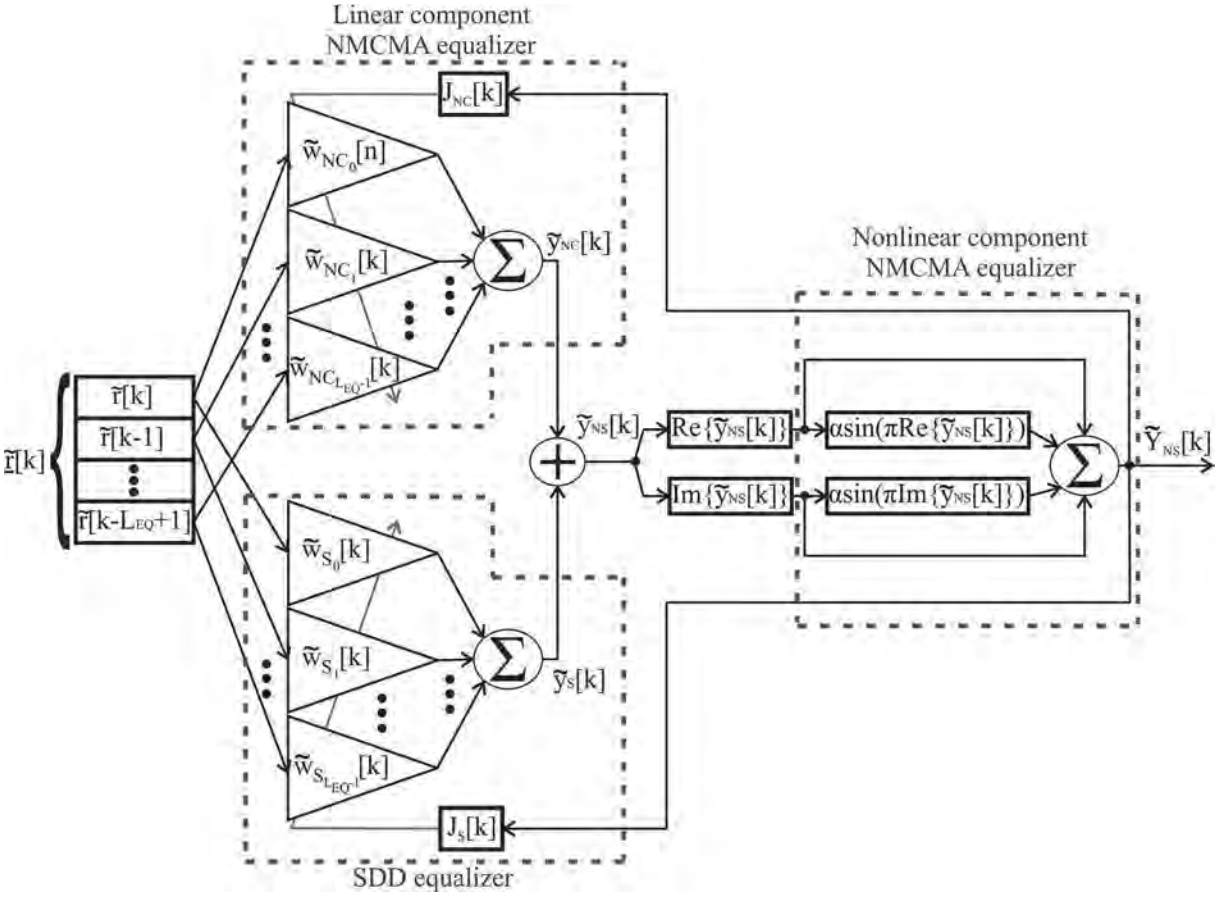

Source: Author (2018).

Considering only the NMCMA algorithm, the linear component $\tilde{y}_{NC}[k]$ is responsible for the convergence rate and the constellation phase recovery, as in the MCMA equalizer structure. On the other hand, the NMCMA nonlinear component $\tilde{Y}_{NS}[k]$ is responsible for the minimization of the output error, by establishing sharper decision regions. In this context, the proposed concurrent architecture adds the SDD decision scheme to the linear component of the NMCMA algorithm, in concurrent

operation, so that the SDD is able to increase the convergence rate, without decreasing the nonlinear operation effect.

The NMCMA-SDD concurrent equalizer output $\tilde{Y}_{NS}[k]$ is

$$\tilde{Y}_{NS}[k] = [\mathrm{Re}\{\tilde{y}_{NS}[k]\} + \alpha \sin(\pi \mathrm{Re}\{\tilde{y}_{NS}[k]\})] + \\ + j[\mathrm{Im}\{\tilde{y}_{NS}[k]\} + \alpha \sin(\pi \mathrm{Im}\{\tilde{y}_{NS}[k]\})], \quad (3.1)$$

where $\tilde{y}_{NS}[k]$ is the liner component output of the NMCMA-SDD concurrent equalizer, presented in Figure 51, obtained as

$$\tilde{y}_{NS}[k] = \sum_{i=0}^{\tilde{L}_{EQ}-1} \widetilde{w}_{NC_i}[k]\tilde{r}[k-i] + \sum_{i=0}^{\tilde{L}_{EQ}-1} \widetilde{w}_{S_i}[k]\tilde{r}[k-i] = \tilde{y}_{NC}[k] + \tilde{y}_S[k], \quad (3.2)$$

where $\tilde{L}_{EQ} \geq 2\, L_{CH} - 1$ is the number of coefficients of the upsampled equalizer, $\widetilde{w}_{NC}[k] = \left[\widetilde{w}_{NC_0}[k], \widetilde{w}_{NC_1}[k], \cdots, \widetilde{w}_{NC_{\tilde{L}_{EQ}-1}}[k]\right]^T$ is the upsampled NMCMA coefficient vector, $\widetilde{w}_S[k] = \left[\widetilde{w}_{S_0}[k], \widetilde{w}_{S_1}[k], \cdots, \widetilde{w}_{S_{\tilde{L}_{EQ}-1}}[k]\right]^T$ is the upsampled SDD coefficient vector, $\tilde{y}_{NC}[k]$ is the NMCMA upsampled output, and $\tilde{y}_S[k]$ is the DD upsampled output.

In order to update the upsampled NMCMA coefficient vector $\underline{\widetilde{w}}_{NC}[k]$, the Eq. (2.18) is used as

$$\underline{\widetilde{w}}_{NC}[k+1] = \begin{cases} \underline{\widetilde{w}}_{NC}[k] - \eta_{NC}\, \tilde{e}_{NS}[k]\underline{\tilde{r}}[k]^*, & \text{for even } k, \\ \underline{\widetilde{w}}_{NC}[k], & \text{for odd } k, \end{cases} \quad (3.3)$$

being $\tilde{e}_{NS}[k]$ the upsampled error function of the NMCMA-SDD concurrent equalizer, given by

$$\tilde{e}_{NS}[k] = \mathrm{Re}\{\tilde{e}_{NS}[k]\} + j\mathrm{Im}\{\tilde{e}_{NS}[k]\}, \quad (3.4)$$

where

$$\mathrm{Re}\{\tilde{e}_{NS}[k]\} = \mathrm{Re}\{\tilde{Y}_{NS}[k]\}\left(\mathrm{Re}\{\tilde{Y}_{NS}[k]\}^2 - \gamma_R\right)[1 + \alpha\pi \cos(\pi \mathrm{Re}\{\tilde{y}_{NS}[k]\})], \quad (3.5)$$

$$\mathrm{Im}\{\tilde{e}_{NS}[k]\} = \mathrm{Im}\{\tilde{Y}_{NS}[k]\}\left(\mathrm{Im}\{\tilde{Y}_{NS}[k]\}^2 - \gamma_I\right)[1 + \alpha\pi \cos(\pi \mathrm{Im}\{\tilde{y}_{NS}[k]\})]. \quad (3.6)$$

The upsampled SDD coefficients update follows the Eq. (2.102) as

$$\underline{\widetilde{w}}_S[k+1] = \begin{cases} \underline{\widetilde{w}}_S[k] + \eta_S \dfrac{\tilde{e}_S[k]\underline{\tilde{r}}[k]^*}{\tilde{P}_{NS}[k]}, & \text{for even } k, \\ \underline{\widetilde{w}}_S[k], & \text{for odd } k, \end{cases} \tag{3.7}$$

where the $\tilde{P}_{NS}[k]$ is *a posteriori* PDF not normalized of the NMCMA-SDD concurrent equalizer, given by

$$\tilde{P}_{NS}[k] = \sum_{p=2i-1}^{2i} \sum_{q=2i-1}^{2l} \exp\left(-\frac{\left|\tilde{Y}_{NS}[k] - \mathcal{S}_{p,q}\right|^2}{2\rho}\right), \tag{3.8}$$

and $\tilde{e}_S[k]$ is the error function of the upsampled SDD

$$\tilde{e}_S[k] = \sum_{p=2i-1}^{2i} \sum_{q=2i-1}^{2l} \left[\exp\left(-\frac{\left|\tilde{Y}_{NS}[k] - \mathcal{S}_{p,q}\right|^2}{2\rho}\right)\left(\mathcal{S}_{p,q} - \tilde{Y}_{NS}[k]\right)\right]. \tag{3.9}$$

The NMCMA-SDD concurrent equalizer output $Y_{NS}[n]$, presented in Figure 51, is a downsampled version of the $\tilde{Y}_{NS}[k]$ given by

$$Y_{NS}[n] = \tilde{Y}_{NS}[2n]. \tag{3.10}$$

4. RESULTS

In this chapter, simulation results of the proposed equalizer are presented, considering single carrier *M*-QAM constellations, for $M = 16$, 64, and 256. The computational simulation of the proposed NMCMA-SDD are compared with the state of the art CMA-SDD concurrent equalizer.

The evaluated concurrent equalizers (the proposed NMCMA-SDD and the CMA-SDD) have been implemented in C programming language with double precision variables. In the simulated system, it is assumed perfect synchronism between transmitter and receiver. Besides, the simulation was restricted to baseband symbol generation, baseband symbol transmission (AWGN, multipath, and Doppler shift), and baseband symbol reception (channel equalizer). Digital communication system blocks source coding, channel coding, up/downconversion and others (HAYKIN, 2013; PROAKIS; SALEHI, 2008) were not implemented since these blocks do not directly interfere in the proposed channel equalization algorithm.

In a real world system, the upsampling process occurs at the receiver. However, for the sake of simulation of a FSE with $\Upsilon = 2$, the communication channel requires an upsampling process (CHEN; CHNG, 2004), as presented in Figure 52.

Figure 52 – Proposed approach with FSE scheme for $\Upsilon = 2$.

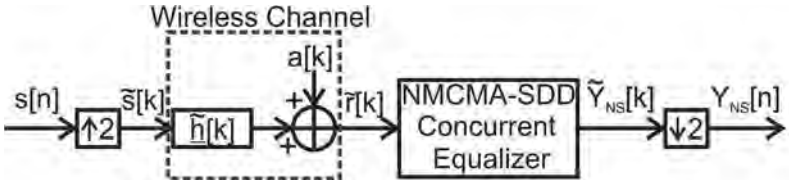

Source: Author (2018).

In order to generate the FSE architecture, the upsampled transmitted symbols $\tilde{s}[k]$ are defined by

$$\tilde{s}[k] = \begin{cases} s[k/2], & \text{for even } k, \\ 0, & \text{for odd } k, \end{cases} \tag{4.1}$$

where $k = 0, 1, \ldots, k \to \infty$ is the index used to describe the FSE architecture.

The stream of M-QAM symbols $s[n]$ at the transmitter is generated by a pseudorandom generator with uniform distribution and symbol rate $S_R =$ 10.7622377622 MHz (ATSC, 2006). Next, the stream of M-QAM symbols is upsampled by $\Upsilon = 2$, as presented in Eq. (4.1), to implement the FSE architecture.

After that, the upsampled symbols are applied to the communication channel, where AWGN, multipath, and Doppler shift effects are introduced. The dynamic Brazil channels adopt Doppler frequency of 20 Hz and 50 Hz. The channel output $\tilde{r}[k]$ is given by

$$\tilde{r}[k] = \sum_{i=0}^{2L_{CH}-1} \tilde{h}_i[k]\tilde{s}[k-i] + a[k], \tag{4.2}$$

where $\tilde{h}_i[k]$ is the i^{th} path of the upsampled dynamic CIR vector $\underline{\tilde{h}}[k] = \left[\tilde{h}_0[k], \tilde{h}_1[k], \cdots, \tilde{h}_{2L_{CH}-1}[k]\right]^T$. Then, the distorted symbols $\tilde{r}[k]$ are applied to the channel equalizer under test. Notice that both NMCMA-SDD and CMA-SDD equalizers have their outputs downsampled by 2. Finally, the complex symbols of the equalizer outputs and the original transmitted symbols are used to calculate the SER and the MSE.

In order to assess the proposed algorithm performance, the Symbol Error Rate (SER) and the MSE were computed and graphically represented for different values of SNR, Doppler frequency and for different multipath channel profiles. The proposed NMCMA-SDD and the CMA-SDD (CHEN; CHNG, 2004) concurrent equalizers have been compared operating with 16-QAM, 64-QAM and 256-QAM modulations, over AWGN and dynamic multipath scenarios. Figure 53 illustrates the block diagram of the implemented system.

Figure 53 – Block diagram of the implemented system.

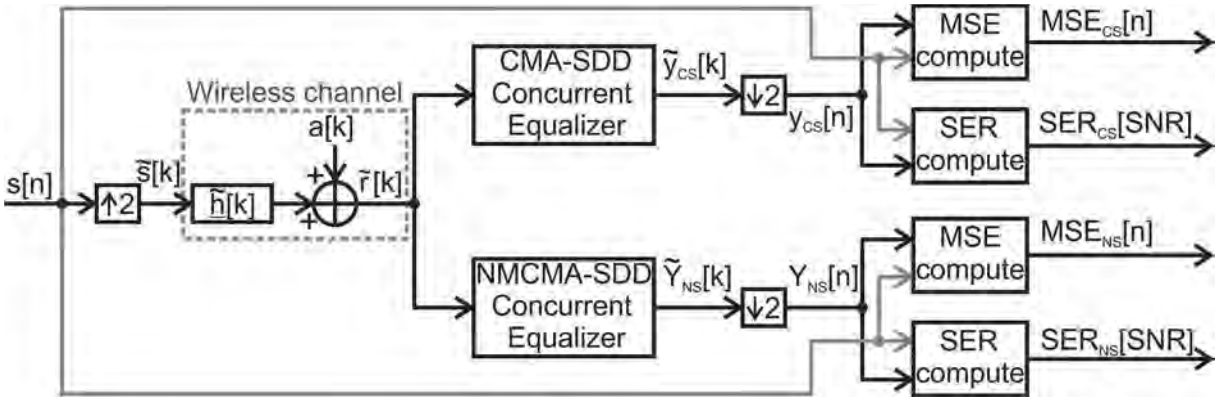

Source: Author (2018).

The MSE is useful to assess the equalizer dynamics, since the MSE curve shows the convergence rate during the convergence process and shoes the steady-

state value after convergence. The MSE of the CMA-SDD ($\mathrm{MSE}_{CS}[n]$) and NMCMA-SDD ($\mathrm{MSE}_{NS}[n]$) concurrent equalizers are given by

$$\mathrm{MSE}_{CS}[n](\mathrm{dB}) = 10\log_{10}\left(\frac{1}{L_{MSE}}\sum_{b=0}^{L_{MSE}-1}|s[n-b]-y_{CS}[n-b]|^2\right), \tag{4.3}$$

$$\mathrm{MSE}_{NS}[n](\mathrm{dB}) = 10\log_{10}\left(\frac{1}{L_{MSE}}\sum_{b=0}^{L_{MSE}-1}|s[n-b]-Y_{NS}[n-b]|^2\right), \tag{4.4}$$

where $L_{MSE} = 500$ is number of samples used to calculate the MSE.

The SER of the CMA-SDD (SER_{CS}) and NMCMA-SDD (SER_{NS}) concurrent equalizers are given by the comparison between the transmitted symbols and the downsampled equalizers output as

$$\mathrm{SER}_{CS}[\mathrm{SNR(dB)}] = \frac{1}{L_{SER}}\sum_{n=0}^{L_{SER}-1}\varepsilon_{CS}[n], \tag{4.5}$$

$$\mathrm{SER}_{NS}[\mathrm{SNR(dB)}] = \frac{1}{L_{SER}}\sum_{n=0}^{L_{SER}-1}\varepsilon_{NS}[n], \tag{4.6}$$

where L_{SER} is the number of symbols used to calculate the SER, $\varepsilon_{CS}[n]$ and $\varepsilon_{NS}[n]$ are the instantaneous errors of the CMA-SDD and the NMCMA-SDD concurrent equalizers, respectively, given by

$$\varepsilon_{CS}[n] = \begin{cases} 1, & s[n] = y_{CS}[n], \\ 0, & s[n] \neq y_{CS}[n], \end{cases} \tag{4.7}$$

$$\varepsilon_{NS}[n] = \begin{cases} 1, & s[n] = Y_{NS}[n], \\ 0, & s[n] \neq Y_{NS}[n]. \end{cases} \tag{4.8}$$

Same operation conditions have been applied to both CMA-SDD and NMCMA-SDD concurrent equalizers. For both equalizers, the initialization scheme is as follows:

- The initialization of the CMA and NMCMA filter coefficients follow the single spike method (ENDRES, 1997);
- The SDD coefficient vector is initialized with $\underline{\widetilde{w}_S}[k] = \underline{0 + j0}$.

The following sections presents the results of the NMCMA-SDD and the CMA-SDD concurrent equalizers.

4.1. 16-QAM SIMULATION

In this section, the 16-QAM simulations for the NMCMA-SDD and the CMA-SDD concurrent equalizers operating under the Brazil Channels (ITU, 2008) are presented. The results for the static and dynamic Brazil channels with $f_D = 20$ Hz are presented in the Appendix A. For both equalizers, the parameters are as follows:

The dispersion constants of the NMCMA and of the CMA are $\gamma_R = \gamma_I = 13.2$ and $\gamma = 8.2$;

- The nonlinear constant of the NMCMA is $\alpha = 0.2$;
- The SDD variance is $\rho = 0.6$;
- SNR = 30 dB to evaluate the MSE;
- 200,000 symbols have been used to evaluate the SER.

4.1.1. Dynamic Brazil A - 16-QAM Simulation

For both equalizers, the number of coefficients of the filter is $L_{EQ} = 192$, which is a value fifty percent greater than the delay spread of the dynamic Brazil A. The SER is evaluated for SNR ranging from 15 dB to 25 dB. The adaptive steps of the CMA-SDD are η_C =1x10^{-6}, η_S =5x10^{-4}, and the NMCMA-SDD are η_{NC} =2x10^{-6}, η_S =5x10^{-4}.

Figure 54 depicts the MSE comparison of the CMA-SDD and NMCMA-SDD concurrent equalizers for the dynamic Brazil A with $f_D = 50$ Hz. Convergence of both equalizers is established after 80,000 symbols, with equalizer output fluctuation of 2 dB caused by the Doppler shift $f_D = 50$ Hz. The NMCMA-SDD presents a better performance than the CMA-SDD, achieving 5 dB lower in the MSE steady-state, and a minimum MSE = -20 dB.

Figure 55 depicts the SER comparison of the CMA-SDD and NMCMA-SDD concurrent equalizers for the dynamic Brazil A with $f_D = 50$ Hz. The NMCMA-SDD presents a better performance than the CMA-SDD, obtaining a SER 1/5 order of

magnitude lower up to a SNR = 22 dB, and for a SNR > 22dB, the performance is increased to a SER 1/2 order of magnitude lower.

Figure 54 – 16-QAM - MSE comparison of the CMA-SDD and NMCMA-SDD concurrent equalizers to the dynamic Brazil A for $f_D = 50$ Hz.

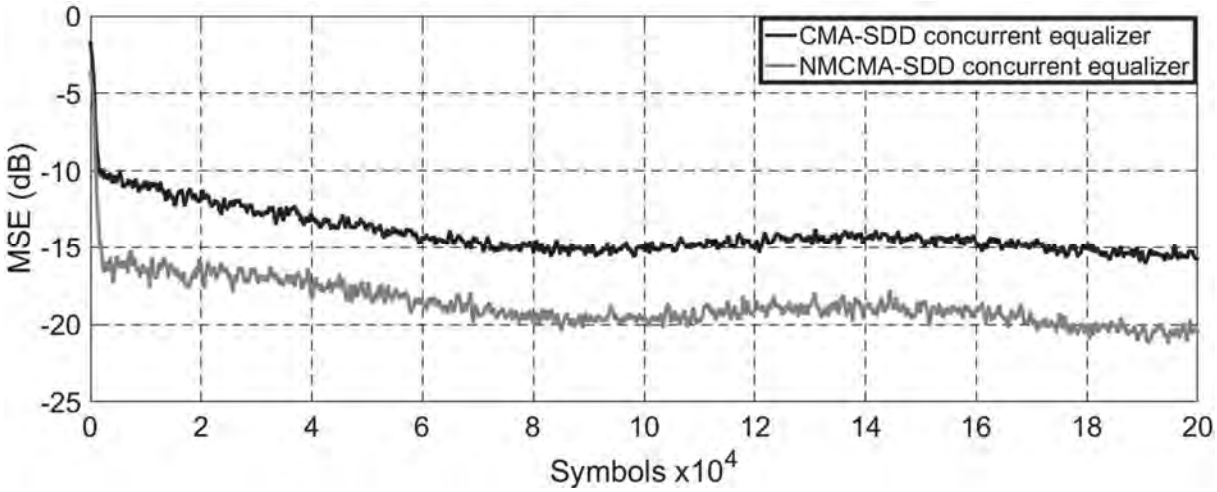

Source: Author (2018).

Figure 55 – 16-QAM - SER comparison of the CMA-SDD and NMCMA-SDD concurrent equalizers to the dynamic Brazil A for $f_D = 50$ Hz.

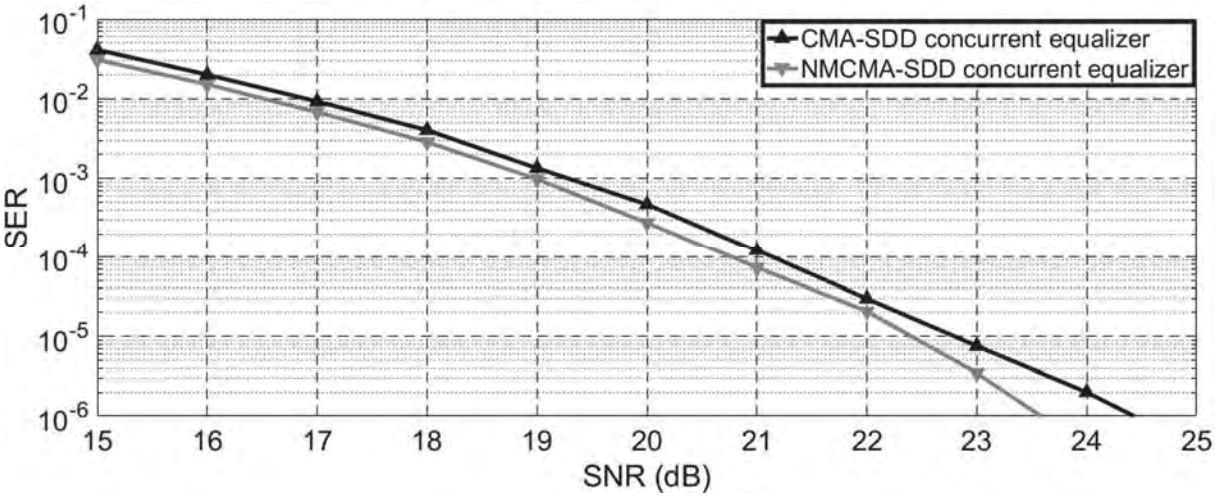

Source: Author (2018).

4.1.2. Dynamic Brazil B - 16-QAM Simulation

For both equalizers, the number of coefficients of the filter is $L_{EQ} = 411$, which is a value fifty percent greater than the delay spread of the dynamic Brazil B. The SER is evaluated for SNR ranging from 15 dB to 23 dB. The adaptive steps of the CMA-SDD are η_C =2x10^{-6}, η_S =4x10^{-4}, and the NMCMA-SDD are η_{NC} =2x10^{-6}, η_S =4x10^{-4}.

Figure 56 depicts the MSE comparison of the CMA-SDD and NMCMA-SDD concurrent equalizers for the dynamic Brazil B with $f_D = 50$ Hz. Convergence of both equalizers is established after 5,000 symbols, with equalizer output fluctuation of 2 dB caused by the Doppler shift $f_D = 50$ Hz. The NMCMA-SDD presents a better performance than the CMA-SDD, achieving 5 dB lower in the MSE steady-state, and a minimum MSE = -20 dB.

Figure 56 – 16-QAM - MSE comparison of the CMA-SDD and NMCMA-SDD concurrent equalizers to the dynamic Brazil B for $f_D = 50$ Hz.

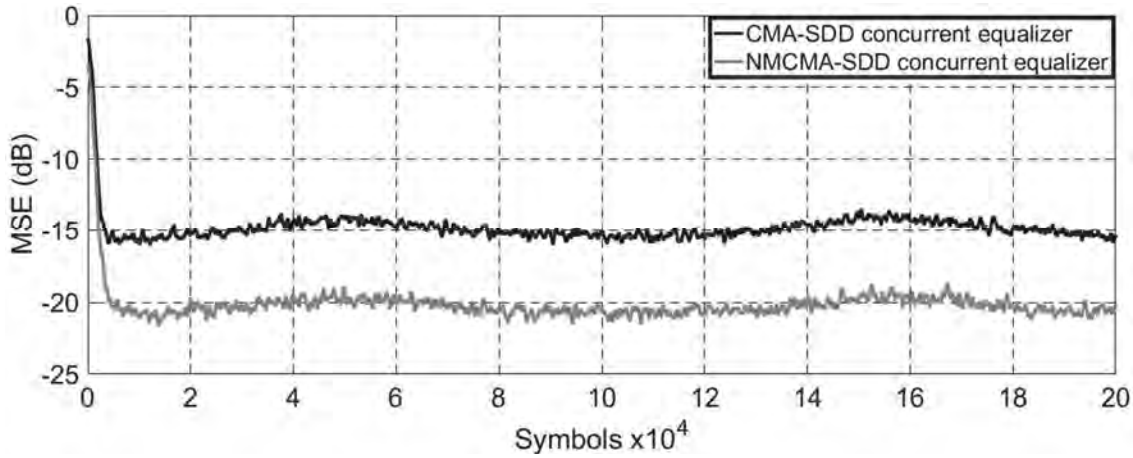

Source: Author (2018).

Figure 57 depicts the SER comparison of the CMA-SDD and NMCMA-SDD concurrent equalizers for the dynamic Brazil B with $f_D = 50$ Hz. The NMCMA-SDD presents a better performance than the CMA-SDD, obtaining a SER 1/3 order of magnitude lower up to a SNR = 20 dB, and for a SNR > 20dB, the performance is increased to a SER of 1 order of magnitude lower.

Figure 57 – 16-QAM - SER comparison of the CMA-SDD and NMCMA-SDD concurrent equalizers to the dynamic Brazil B for $f_D = 50$ Hz.

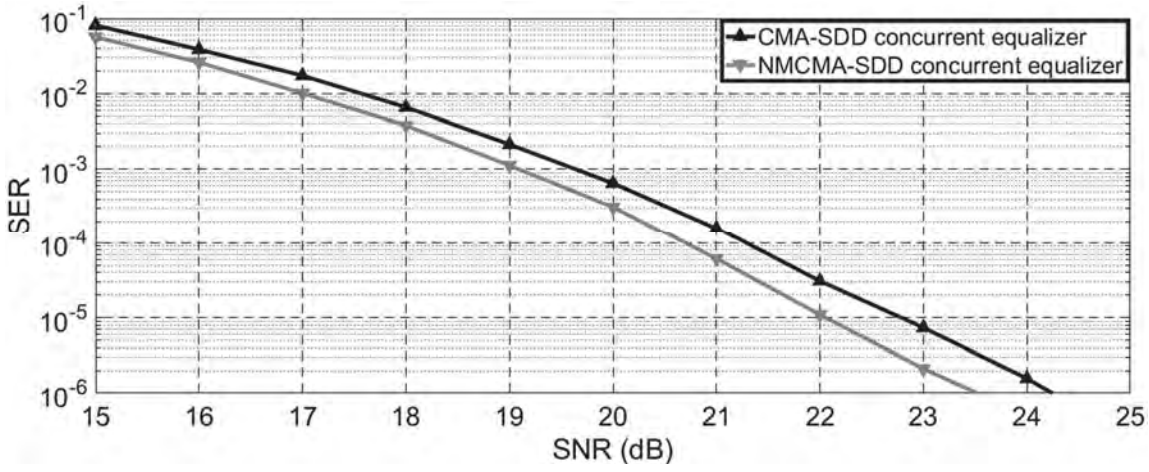

Source: Author (2018).

4.1.3. Dynamic Brazil C - 16-QAM Simulation

For both equalizers, the number of coefficients of the filter is $L_{EQ} = 92$, which is a value fifty percent greater than the delay spread of the dynamic Brazil C. The SER is evaluated for SNR ranging from 15 dB to 29 dB. The adaptive steps of the CMA-SDD are η_C =6x10^{-7}, η_S =2x10^{-4}, and the NMCMA-SDD are η_{NC} =6x10^{-7}, η_S =2x10^{-4}.

Figure 58 depicts the MSE comparison of the CMA-SDD and NMCMA-SDD concurrent equalizers for the dynamic Brazil C with $f_D = 50$ Hz. Convergence of both equalizers is established after 15,000 symbols, without equalizer output fluctuations. The NMCMA-SDD presents a better performance than the CMA-SDD, achieving 5 dB lower in the MSE steady-state, and a minimum MSE = -19 dB.

Figure 58 – 16-QAM - MSE comparison of the CMA-SDD and NMCMA-SDD concurrent equalizers to the dynamic Brazil C for $f_D = 50$ Hz.

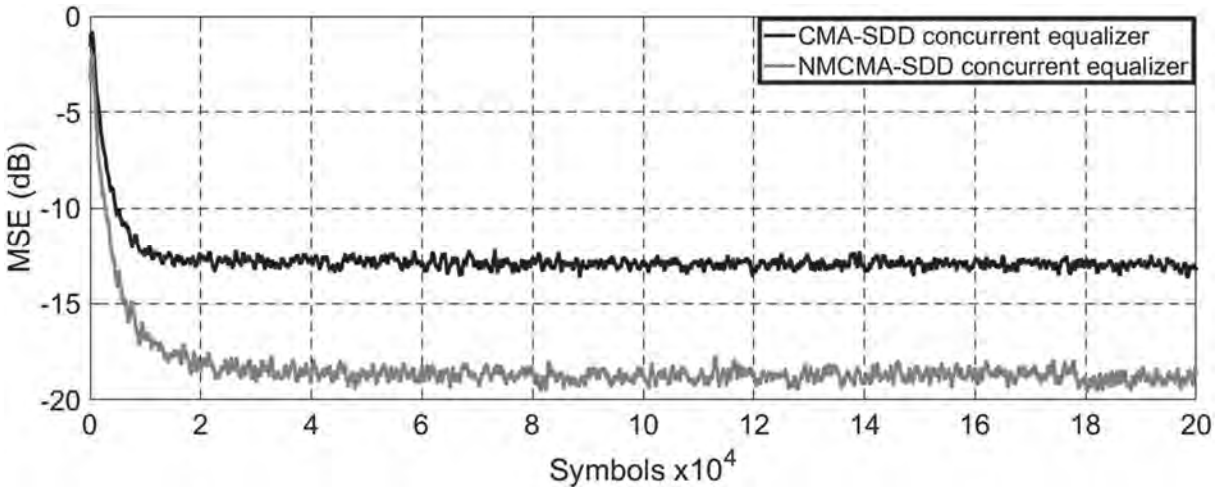

Source: Author (2018).

Figure 59 depicts the SER comparison of the CMA-SDD and NMCMA-SDD concurrent equalizers for the dynamic Brazil C with $f_D = 50$ Hz. Both equalizers present equal result from SNR = 15 dB to SNR = 25 dB, and for a SNR > 25 dB, the performance is increased to a SER of 1 order of magnitude lower.

Figure 59 – 16-QAM - SER comparison of the CMA-SDD and NMCMA-SDD concurrent equalizers to the dynamic Brazil C for $f_D = 50$ Hz.

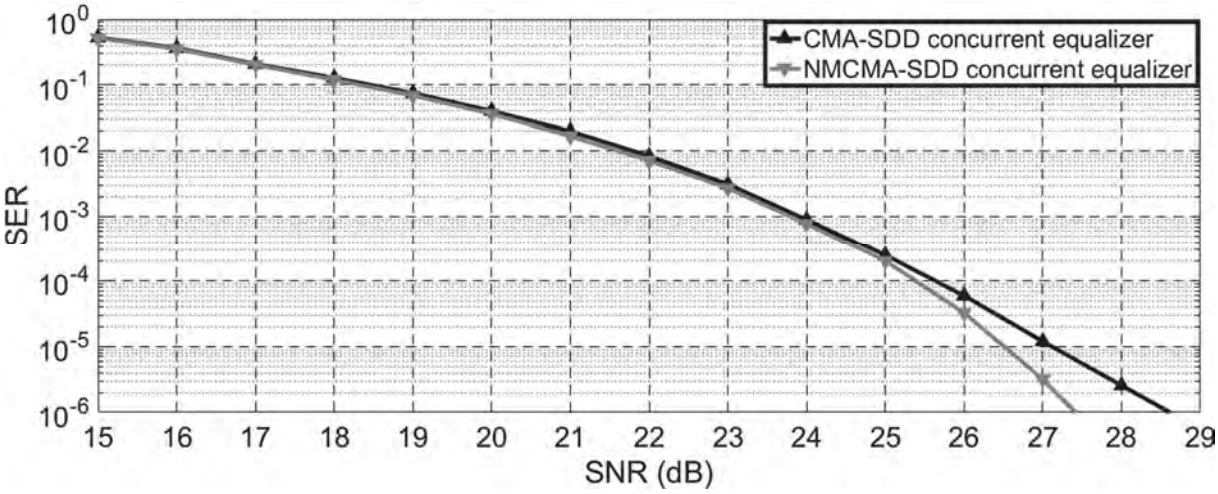

Source: Author (2018).

4.1.4. Dynamic Brazil D - 16-QAM Simulation

For both equalizers, the number of coefficients of the filter is $L_{EQ} = 192$, which is a value fifty percent greater than the delay spread of the dynamic Brazil D. The SER is evaluated for SNR ranging from 15 dB to 26 dB. The adaptive steps of the CMA-SDD are η_C =5x10^{-7}, η_S =1x10^{-4}, and the NMCMA-SDD are η_{NC} =5x10^{-7}, η_S =1x10^{-4}.

Figure 60 depicts the MSE comparison of the CMA-SDD and NMCMA-SDD concurrent equalizers for the dynamic Brazil D with $f_D = 50$ Hz. Convergence of both equalizers is established after few symbols, without equalizer output fluctuations. The NMCMA-SDD presents a better performance than the CMA-SDD, achieving 6 dB lower in the MSE steady-state, and a minimum MSE = -21 dB.

Figure 61 depicts the SER comparison of the CMA-SDD and NMCMA-SDD concurrent equalizers for the dynamic Brazil D with $f_D = 50$ Hz. Both equalizers present equal result from SNR = 15 dB to SNR = 23 dB, and for a SNR > 23 dB, the performance is increased to a SER of 1/3 order of magnitude lower.

Figure 60 – 16-QAM - MSE comparison of the CMA-SDD and NMCMA-SDD concurrent equalizers to the dynamic Brazil D for $f_D = 50$ Hz.

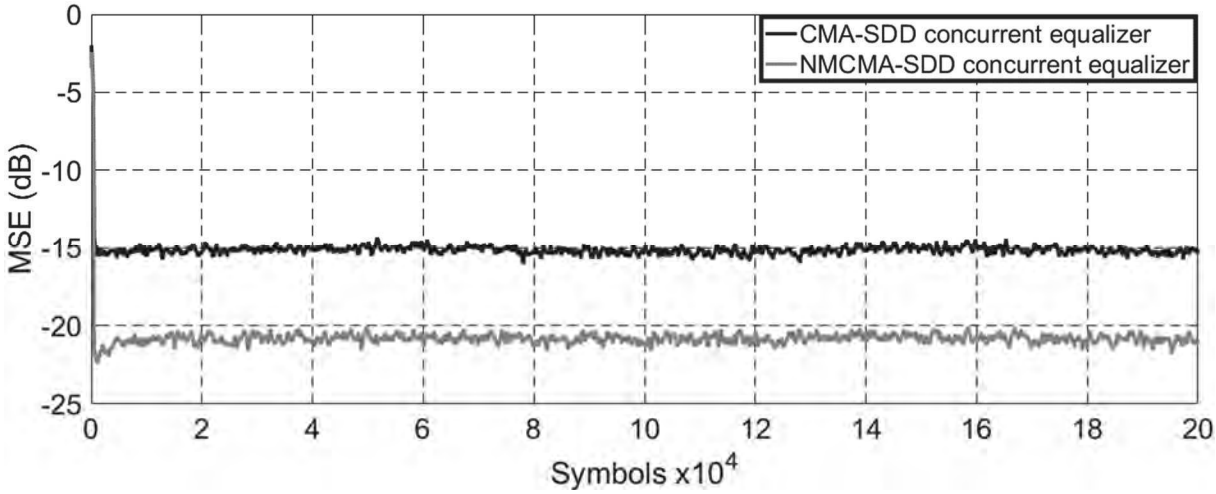

Source: Author (2018).

Figure 61 – 16-QAM - SER comparison of the CMA-SDD and NMCMA-SDD concurrent equalizers to the dynamic Brazil D for $f_D = 50$ Hz.

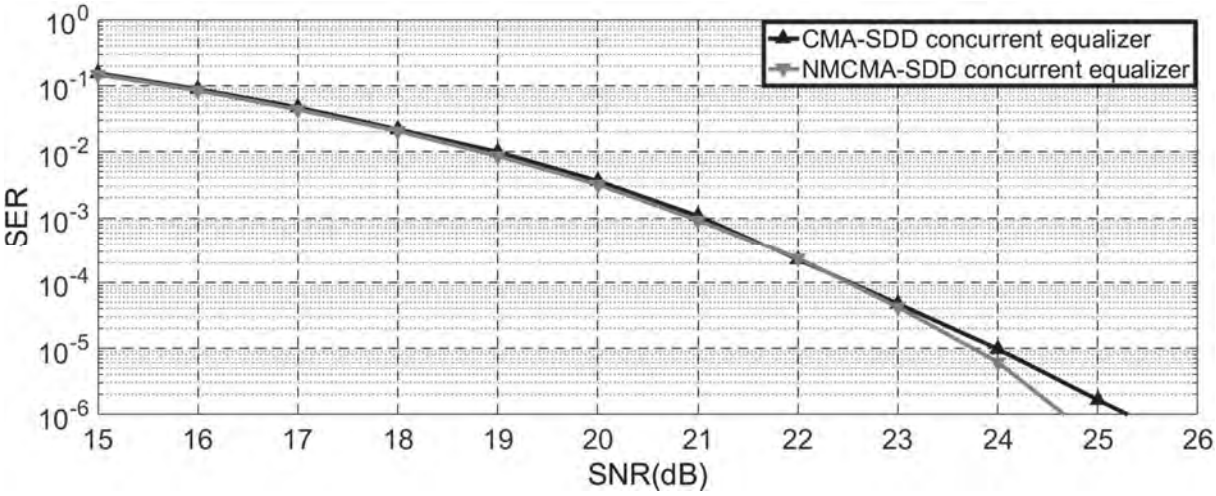

Source: Author (2018).

4.1.5. Dynamic Brazil E - 16-QAM Simulation

For both equalizers, the number of coefficients of the filter is $L_{EQ} = 66$, which is a value fifty percent greater than the delay spread of the dynamic Brazil E. The SER is evaluated for SNR ranging from 15 dB to 23 dB. The adaptive steps of the CMA-SDD are η_C =5x10^{-7}, η_S =1x10^{-4}, and the NMCMA-SDD are η_{NC} =5x10^{-7}, η_S =1x10^{-4}.

Figure 62 depicts the MSE comparison of the CMA-SDD and NMCMA-SDD concurrent equalizers for the dynamic Brazil E with $f_D = 50$ Hz. Convergence of both

equalizers is established after few symbols, without equalizer output fluctuations. The NMCMA-SDD presents a better performance than the CMA-SDD, achieving 5 dB lower in the MSE steady-state, and a minimum MSE = -22.5 dB.

Figure 62 – 16-QAM - MSE comparison of the CMA-SDD and NMCMA-SDD concurrent equalizers to the dynamic Brazil E for $f_D = 50$ Hz.

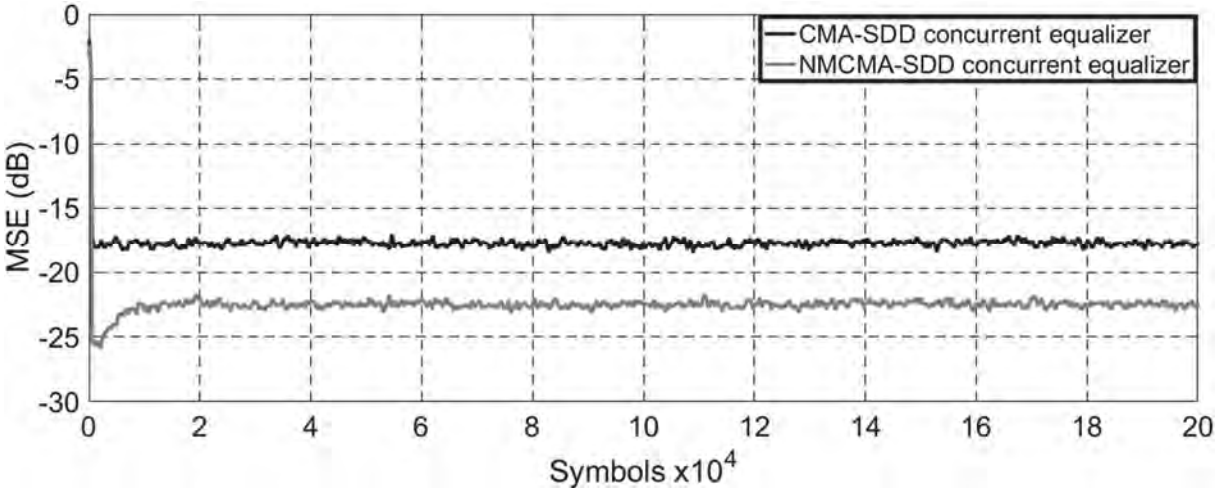

Source: Author (2018).

Figure 63 depicts the SER comparison of the CMA-SDD and NMCMA-SDD concurrent equalizers for the dynamic Brazil E with $f_D = 50$ Hz. Both equalizers present equal result from SNR = 15 dB to SNR = 21 dB, and for a SNR > 21 dB, the performance is increased to a SER of 1/10 order of magnitude lower.

Figure 63 – 16-QAM - SER comparison of the CMA-SDD and NMCMA-SDD concurrent equalizers to the dynamic Brazil E for $f_D = 50$ Hz.

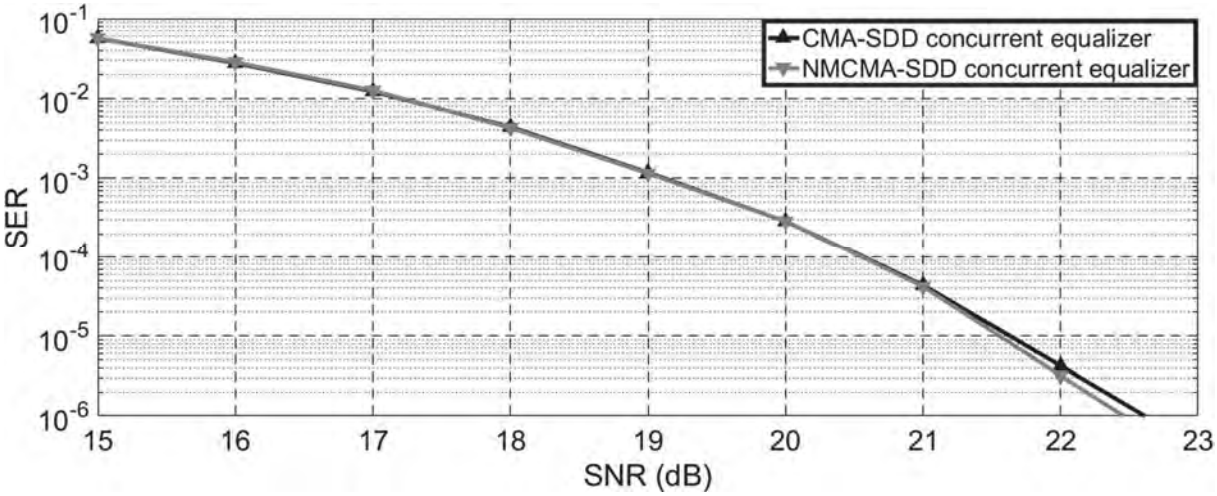

Source: Author (2018).

4.2. 64-QAM SIMULATION

In this section, the 64-QAM simulations for the NMCMA-SDD and the CMA-SDD concurrent equalizers operating under the Brazil Channels (ITU, 2008) are presented. The results for the static and dynamic Brazil channels with $f_D = 20$ Hz are presented in the Appendix B. For both equalizers, the parameters are as follows:

- The dispersion constants of the NMCMA and of the CMA are $\gamma_R = \gamma_I = 37$ and $\gamma = 58$;
- The nonlinear constant of the NMCMA is $\alpha = 0.3$;
- The SDD variance is $\rho = 0.5$;
- SNR = 40 dB to evaluate the MSE;
- 1,000,000 symbols have been used to evaluate the SER.

4.2.1. Dynamic Brazil A - 64-QAM Simulation

For both equalizers, the number of coefficients of the filter is $L_{EQ} = 192$, which is a value fifty percent greater than the delay spread of the dynamic Brazil A. The SER is evaluated for SNR ranging from 20 dB to 32 dB. The adaptive steps of the CMA-SDD are $\eta_C = 1\text{x}10^{-7}$, $\eta_S = 7\text{x}10^{-5}$, and the NMCMA-SDD are $\eta_{NC} = 2\text{x}10^{-7}$, $\eta_S = 9\text{x}10^{-5}$.

Figure 64 depicts the MSE comparison of the CMA-SDD and NMCMA-SDD concurrent equalizers for the dynamic Brazil A with $f_D = 50$ Hz. Convergence of both equalizers is established after 80,000 symbols, with equalizer output fluctuation of 7 dB caused by the Doppler shift $f_D = 50$ Hz. The NMCMA-SDD presents a better performance than the CMA-SDD, achieving 8 dB lower in the MSE steady-state, and a minimum MSE = -31 dB.

Figure 65 depicts the SER comparison of the CMA-SDD and NMCMA-SDD concurrent equalizers for the dynamic Brazil A with $f_D = 50$ Hz. The NMCMA-SDD presents a better performance than the CMA-SDD, obtaining a SER 1/2 order of magnitude lower for a SNR > 20dB.

Figure 64 – 64-QAM - MSE comparison of the CMA-SDD and NMCMA-SDD concurrent equalizers to the dynamic Brazil A for $f_D = 50$ Hz.

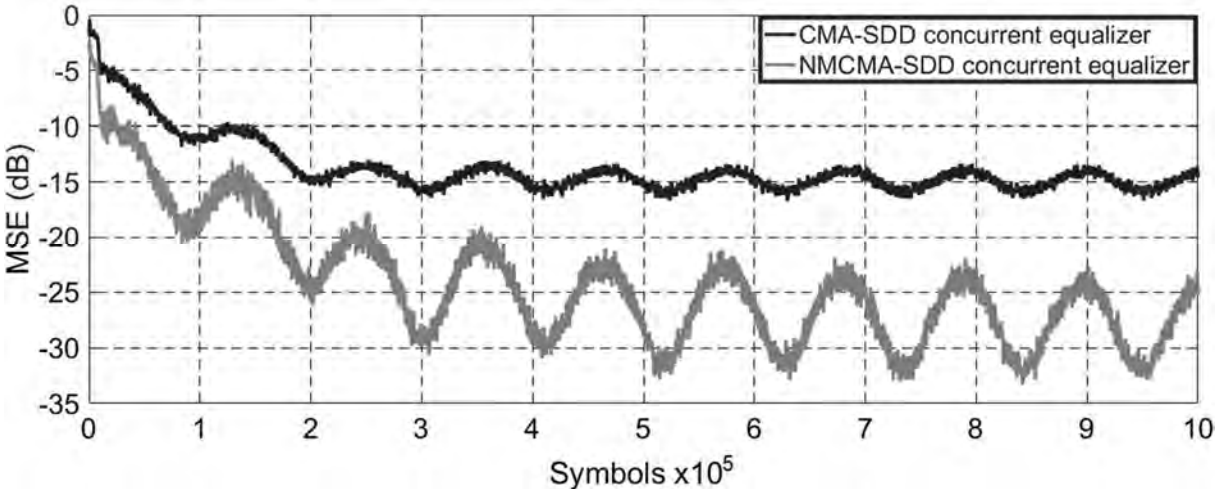

Source: Author (2018).

Figure 65 – 64-QAM - SER comparison of the CMA-SDD and NMCMA-SDD concurrent equalizers to the dynamic Brazil A for $f_D = 50$ Hz.

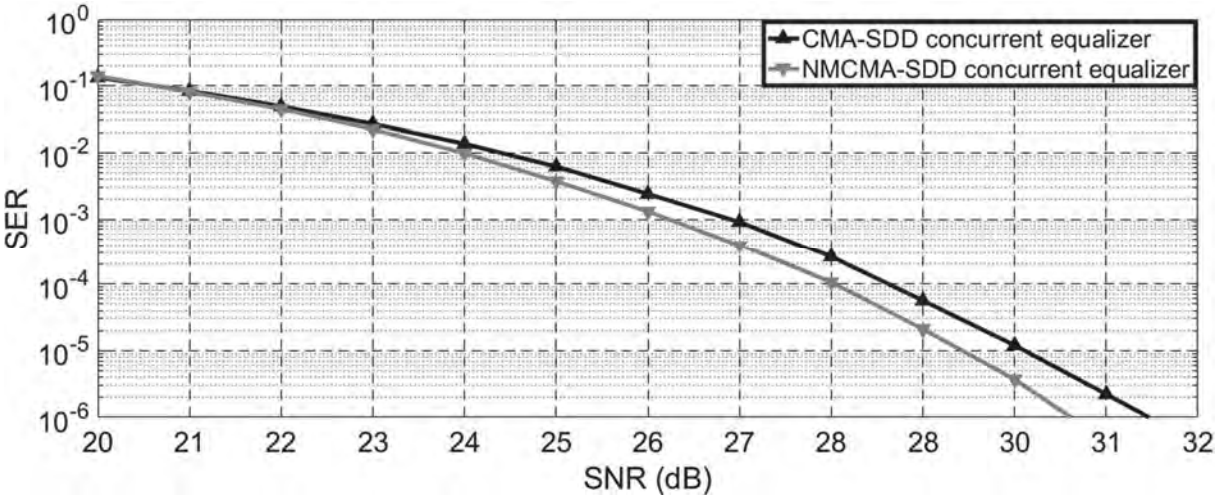

Source: Author (2018).

4.2.2. Dynamic Brazil B - 64-QAM Simulation

For both equalizers, the number of coefficients of the filter is $L_{EQ} = 411$, which is a value fifty percent greater than the delay spread of the dynamic Brazil B. The SER is evaluated for SNR ranging from 20 dB to 31 dB. The adaptive steps of the CMA-SDD are η_C =7x10^{-8}, η_S =3x10^{-5}, and the NMCMA-SDD are η_{NC} =7x10^{-8}, η_S =3x10^{-5}.

Figure 66 depicts the MSE comparison of the CMA-SDD and NMCMA-SDD concurrent equalizers for the dynamic Brazil B with $f_D = 50$ Hz. Convergence of both

equalizers is established after 30,000 symbols, without equalizer output fluctuation. The NMCMA-SDD presents a better performance than the CMA-SDD, achieving 17 dB lower in the MSE steady-state, and a minimum MSE = -35 dB.

Figure 66 – 64-QAM - MSE comparison of the CMA-SDD and NMCMA-SDD concurrent equalizers to the dynamic Brazil B for $f_D = 50$ Hz.

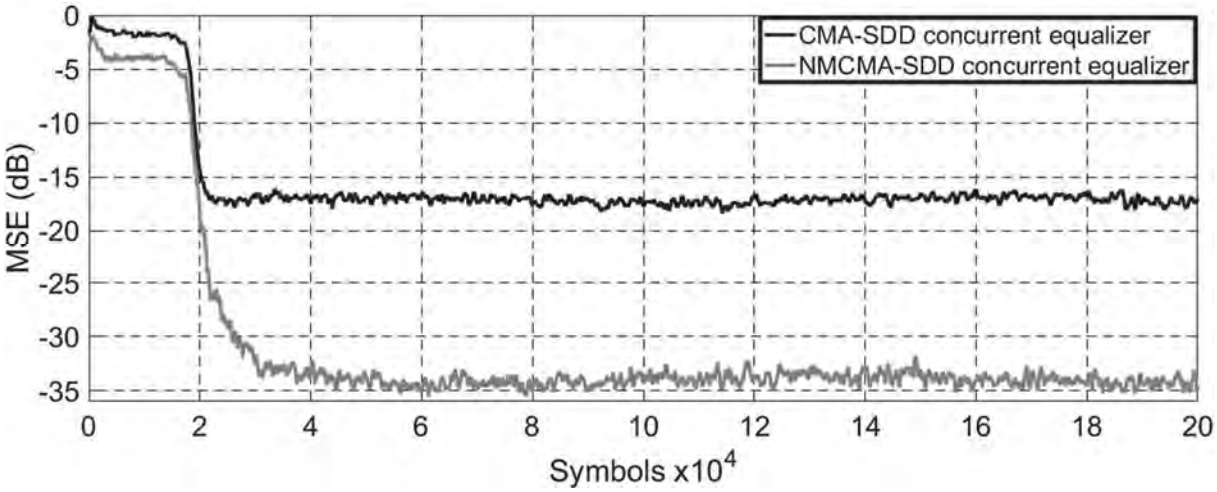

Source: Author (2018).

Figure 67 depicts the SER comparison of the CMA-SDD and NMCMA-SDD concurrent equalizers for the dynamic Brazil B with $f_D = 50$ Hz. The NMCMA-SDD presents a better performance than the CMA-SDD, obtaining a SER 2 orders of magnitude lower for a SNR > 27 dB.

Figure 67 – 64-QAM - SER comparison of the CMA-SDD and NMCMA-SDD concurrent equalizers to the dynamic Brazil B for $f_D = 50$ Hz.

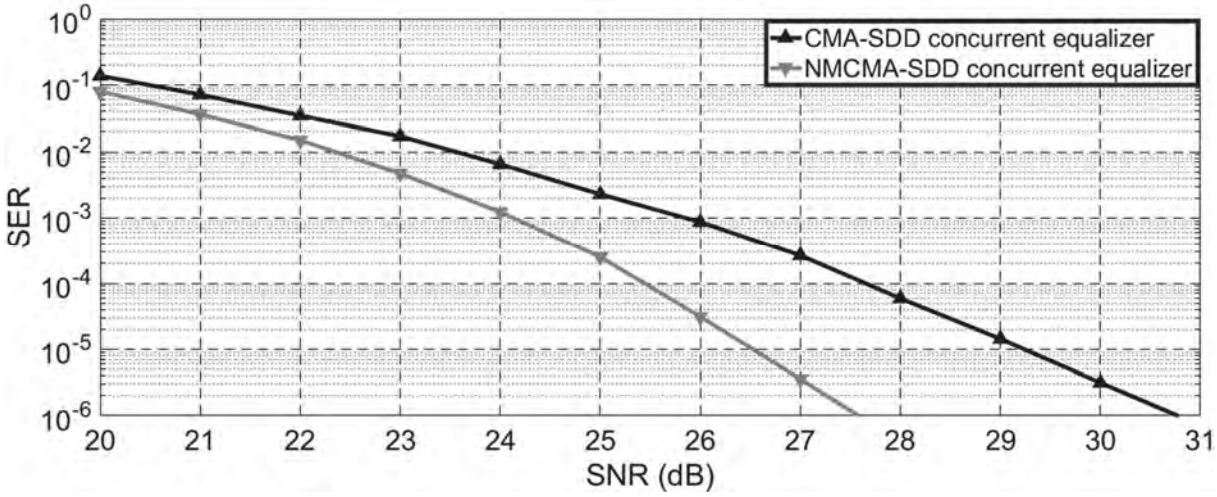

Source: Author (2018).

4.2.3. Dynamic Brazil C - 64-QAM Simulation

For both equalizers, the number of coefficients of the filter is $L_{EQ} = 92$, which is a value fifty percent greater than the delay spread of the dynamic Brazil C. The SER is evaluated for SNR ranging from 20 dB to 35 dB. The adaptive steps of the CMA-SDD are η_C =4x10^{-8}, η_S =3x10^{-5}, and the NMCMA-SDD are η_{NC} =9x10^{-8}, η_S =5x10^{-5}.

Figure 68 depicts the MSE comparison of the CMA-SDD and NMCMA-SDD concurrent equalizers for the dynamic Brazil C with $f_D = 50$ Hz. Convergence of both equalizers is established after 60,000 symbols, without CMA-DD equalizer output fluctuations, and with NMCMA-SDD equalizer output fluctuations of 1 dB. The NMCMA-SDD presents a better performance than the CMA-SDD, achieving 15 dB lower in the MSE steady-state, and a minimum MSE = -30 dB.

Figure 68 – 64-QAM - MSE comparison of the CMA-SDD and NMCMA-SDD concurrent equalizers to the dynamic Brazil C for $f_D = 50$ Hz.

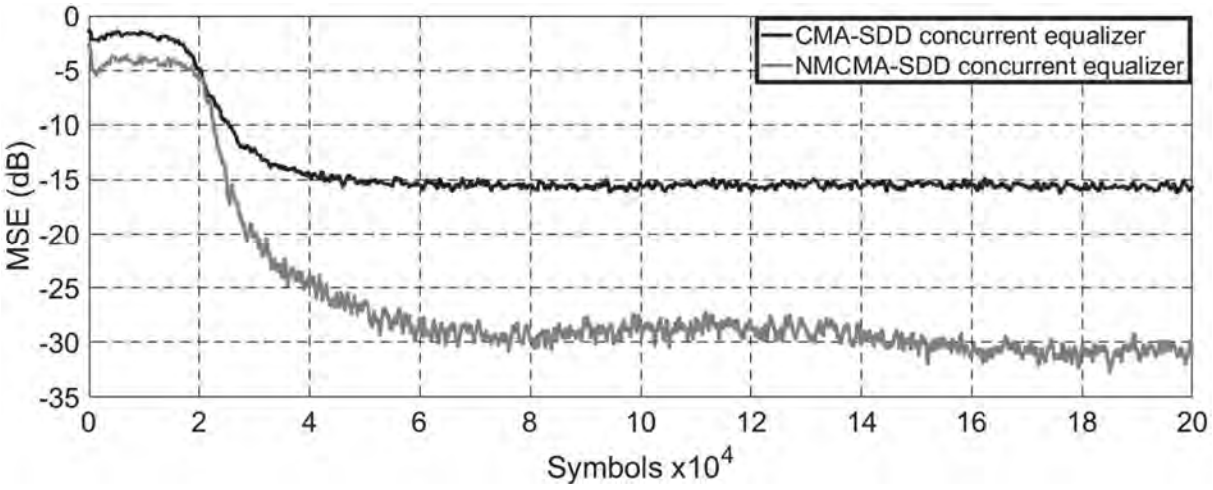

Source: Author (2018).

Figure 69 depicts the SER comparison of the CMA-SDD and NMCMA-SDD concurrent equalizers for the dynamic Brazil C with $f_D = 50$ Hz. The CMA-SDD achieves a SER 1/10 order of magnitude better performance than the NMCMA-SDD up to a SNR = 25 dB, from SNR = 26 dB to SNR = 30 dB both equalizers present equal result, and for a SNR > 30 dB, the NMCMA-SDD performance is increased to a SER 1/2 order of magnitude lower.

Figure 69 – 64-QAM - SER comparison of the CMA-SDD and NMCMA-SDD concurrent equalizers to the dynamic Brazil C for $f_D = 50$ Hz.

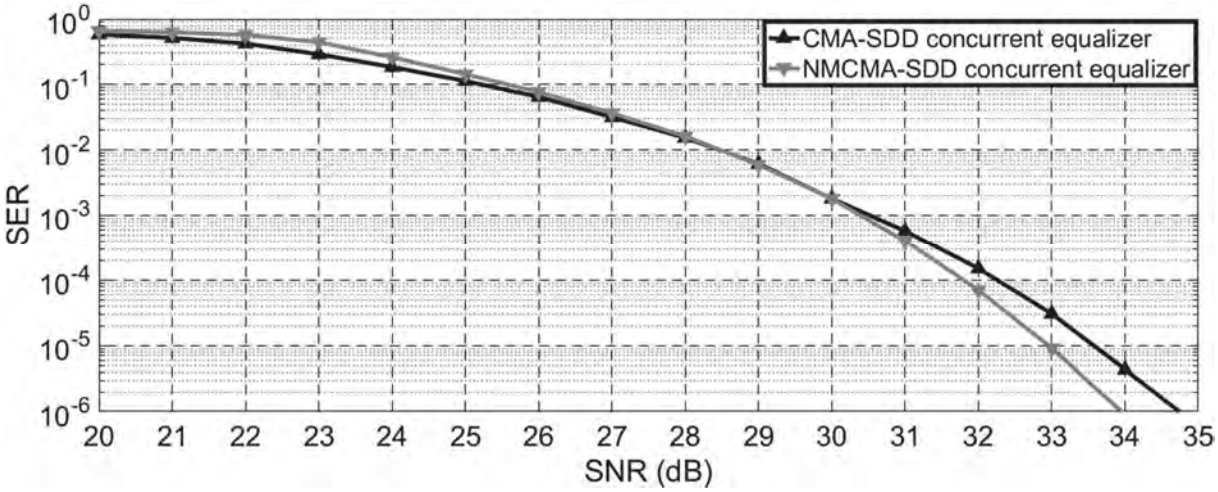

Source: Author (2018).

4.2.4. Dynamic Brazil D - 64-QAM Simulation

For both equalizers, the number of coefficients of the filter is $L_{EQ} = 192$, which is a value fifty percent greater than the delay spread of the dynamic Brazil D. The SER is evaluated for SNR ranging from 20 dB to 31 dB. The adaptive steps of the CMA-SDD are η_C =1x10^{-8}, η_S =1x10^{-5}, and the NMCMA-SDD are η_{NC} =9x10^{-8}, η_S =1x10^{-5}.

Figure 70 depicts the MSE comparison of the CMA-SDD and NMCMA-SDD concurrent equalizers for the dynamic Brazil D with $f_D = 50$ Hz. Convergence of both equalizers is established after few symbols, without equalizer output fluctuations. The NMCMA-SDD presents a better performance than the CMA-SDD, achieving 15 dB lower in the MSE steady-state, and a minimum MSE = -35 dB.

Figure 71 depicts the SER comparison of the CMA-SDD and NMCMA-SDD concurrent equalizers for the dynamic Brazil D with $f_D = 50$ Hz. The CMA-SDD achieves a SER 1/10 order of magnitude better performance than the NMCMA-SDD up to a SNR = 26 dB, from SNR = 27 dB to SNR = 29 dB both equalizers present equal result, and for a SNR > 29 dB, the NMCMA-SDD performance is increased to a SER 1/3 order of magnitude lower.

Figure 70 – 64-QAM - MSE comparison of the CMA-SDD and NMCMA-SDD concurrent equalizers to the dynamic Brazil D for $f_D = 50$ Hz.

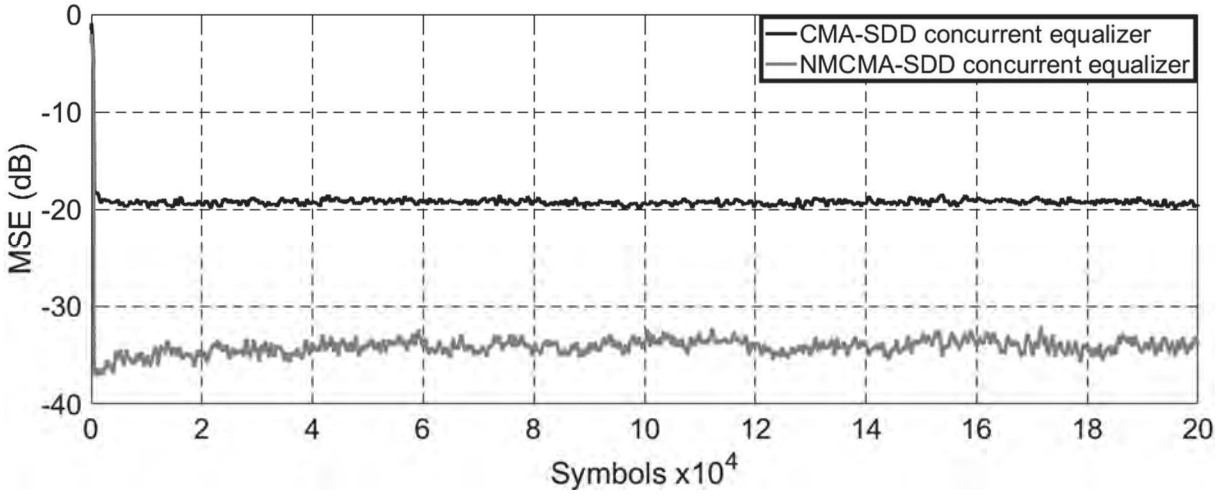

Source: Author (2018).

Figure 71 – 64-QAM - SER comparison of the CMA-SDD and NMCMA-SDD concurrent equalizers to the dynamic Brazil D for $f_D = 50$ Hz.

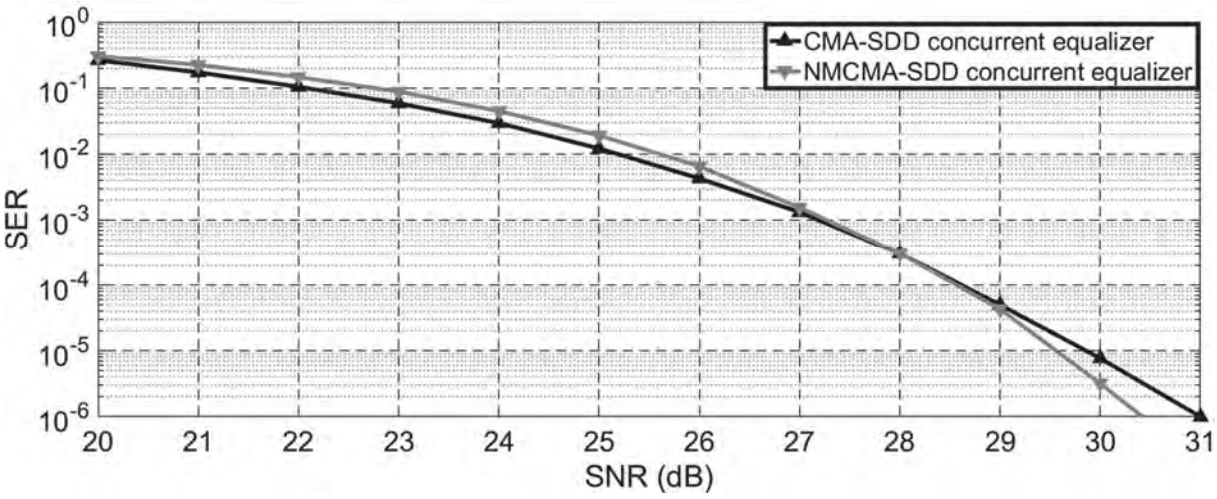

Source: Author (2018).

4.2.5. Dynamic Brazil E - 64-QAM Simulation

For both equalizers, the number of coefficients of the filter is $L_{EQ} = 66$, which is a value fifty percent greater than the delay spread of the dynamic Brazil E. The SER is evaluated for SNR ranging from 20 dB to 29 dB. The adaptive steps of the CMA-SDD are η_C =1x10^{-8}, η_S =1x10^{-5}, and the NMCMA-SDD are η_{NC} =9x10^{-8}, η_S =3x10^{-5}.

Figure 72 depicts the MSE comparison of the CMA-SDD and NMCMA-SDD concurrent equalizers for the dynamic Brazil E with $f_D = 50$ Hz. Convergence of both

equalizers is established after few symbols, without equalizer output fluctuations. The NMCMA-SDD presents a better performance than the CMA-SDD, achieving 14 dB lower in the MSE steady-state, and a minimum MSE = -36 dB.

Figure 72 – 64-QAM - MSE comparison of the CMA-SDD and NMCMA-SDD concurrent equalizers to the dynamic Brazil E for $f_D = 50$ Hz.

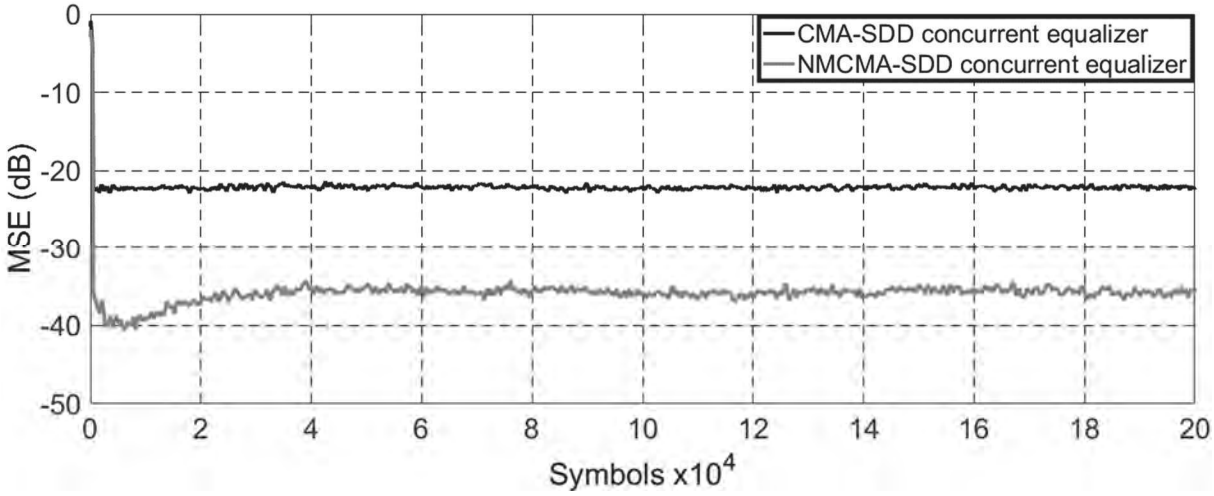

Source: Author (2018).

Figure 73 depicts the SER comparison of the CMA-SDD and NMCMA-SDD concurrent equalizers for the dynamic Brazil E with $f_D = 50$ Hz. Both equalizers present equal result from SNR = 20 dB to SNR = 27 dB, and for a SNR > 27 dB, the NMCMA-SDD performance is increased to a SER 1/5 order of magnitude lower.

Figure 73 – 64-QAM - SER comparison of the CMA-SDD and NMCMA-SDD concurrent equalizers to the dynamic Brazil E for $f_D = 50$ Hz.

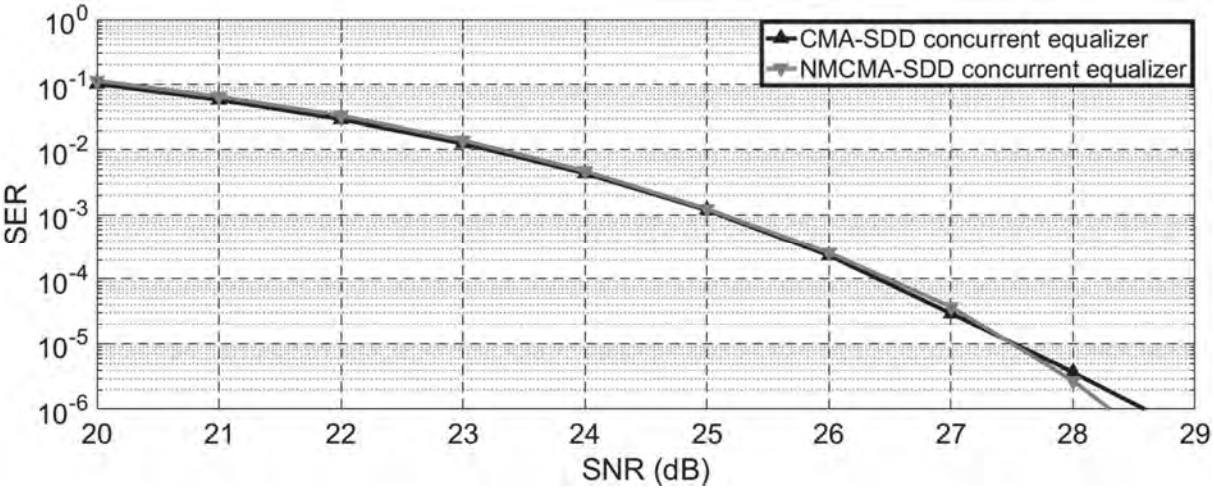

Source: Author (2018).

4.3. 256-QAM SIMULATION

In this section, the 256-QAM simulations for the NMCMA-SDD and the CMA-SDD concurrent equalizers operating under the Brazil Channels (ITU, 2008) are presented. The results for the static and dynamic Brazil channels with $f_D = 20$ Hz are presented in the Appendix C. For both equalizers, the parameters are as follows:

- The dispersion constants of the NMCMA and of the CMA are $\gamma_R = \gamma_I = 152.2$ and $\gamma = 237.2$;
- The nonlinear constant of the NMCMA is $\alpha = 0.15$;
- The SDD variance is $\rho = 0.15$;
- SNR = 50 dB to evaluate the MSE;
- 1,500,000 symbols have been used to evaluate the SER.

4.3.1. Dynamic Brazil A - 256-QAM Simulation

For both equalizers, the number of coefficients of the filter is $L_{EQ} = 192$, which is a value fifty percent greater than the delay spread of the dynamic Brazil A. The SER is evaluated for SNR ranging from 30 dB to 45 dB. The adaptive steps of the CMA-SDD are $\eta_C = 1\text{x}10^{-8}$, $\eta_S = 1\text{x}10^{-5}$, and the NMCMA-SDD are $\eta_{NC} = 1\text{x}10^{-8}$, $\eta_S = 1\text{x}10^{-5}$.

Figure 74 depicts the MSE comparison of the CMA-SDD and NMCMA-SDD concurrent equalizers for the dynamic Brazil A with $f_D = 50$ Hz. Convergence of both equalizers is established after 1,005,000 symbols, with NMCMA-SDD equalizer output fluctuations of 5 dB, and CMA-SDD equalizer output fluctuations of 2.5 dB, caused by the Doppler shift $f_D = 50$ Hz. The NMCMA-SDD presents a better performance than the CMA-SDD, achieving 10 dB lower in the MSE steady-state, and a minimum MSE = -15 dB.

Figure 75 depicts the SER comparison of the CMA-SDD and NMCMA-SDD concurrent equalizers for the dynamic Brazil A with $f_D = 50$ Hz. The NMCMA-SDD achieves a SER 1/10 order of magnitude better performance than the CMA-SDD up to a SNR = 34 dB, and for a SNR > 34 dB, the NMCMA-SDD performance is increased to a SER 2 orders of magnitude lower.

Figure 74 – 256-QAM - MSE comparison of the CMA-SDD and NMCMA-SDD concurrent equalizers to the dynamic Brazil A for $f_D = 50$ Hz.

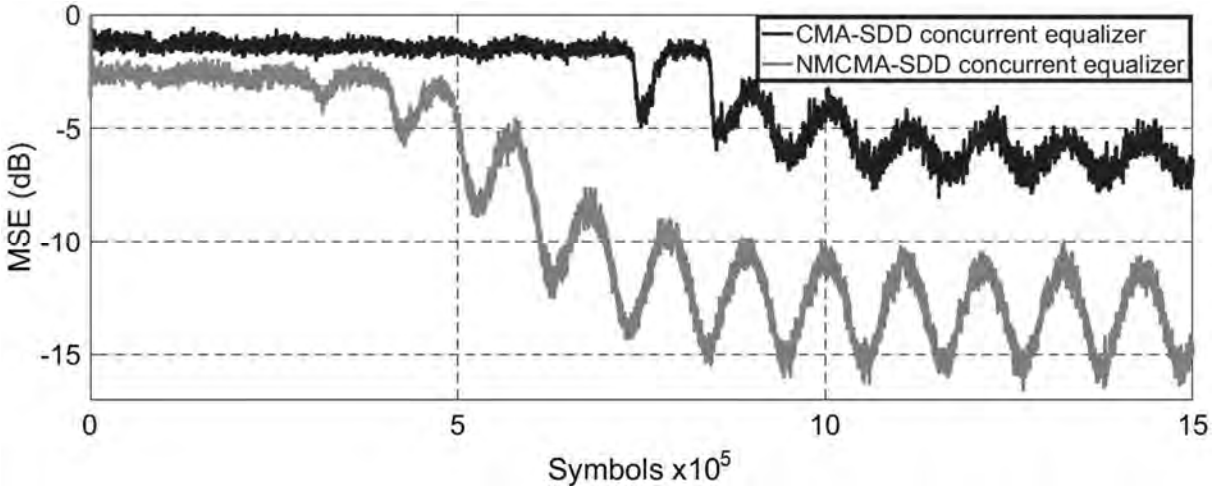

Source: Author (2018).

Figure 75 – 256-QAM - SER comparison of the CMA-SDD and NMCMA-SDD concurrent equalizers to the dynamic Brazil A for $f_D = 50$ Hz.

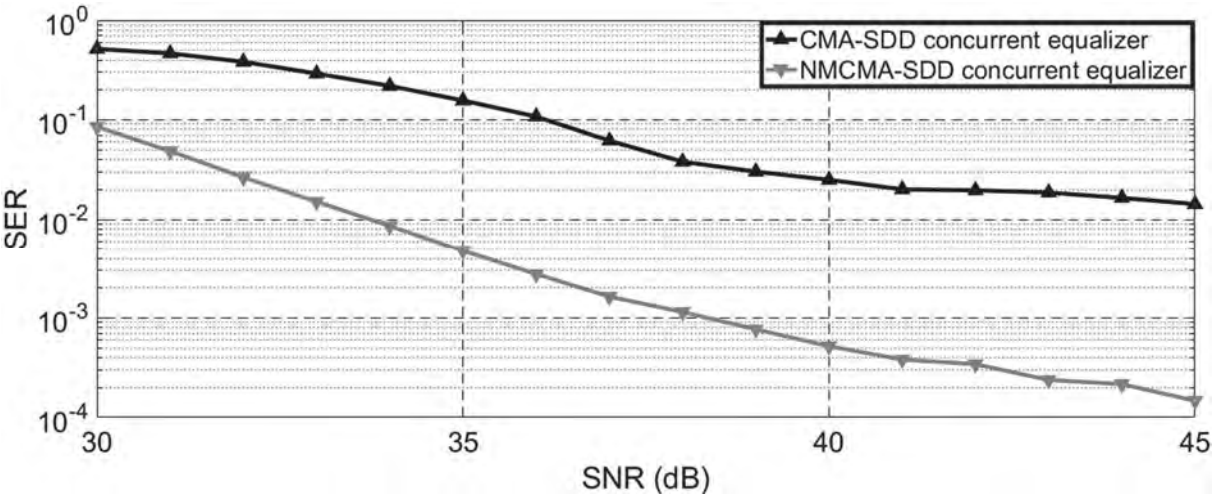

Source: Author (2018).

4.3.2. Dynamic Brazil B - 256-QAM Simulation

For both equalizers, the number of coefficients of the filter is $L_{EQ} = 411$, which is a value fifty percent greater than the delay spread of the dynamic Brazil B. The SER is evaluated for SNR ranging from 25 dB to 37 dB. The adaptive steps of the CMA-SDD are $\eta_C = 1\text{x}10^{-9}$, $\eta_S = 1\text{x}10^{-6}$, and the NMCMA-SDD are $\eta_{NC} = 1\text{x}10^{-9}$, $\eta_S = 3.5\text{x}10^{-6}$.

Figure 76 depicts the MSE comparison of the CMA-SDD and NMCMA-SDD concurrent equalizers for the dynamic Brazil B with $f_D = 50$ Hz. Convergence of both

equalizers is established after 100,000 symbols, with NMCMA-SDD equalizer output fluctuations of 2 dB, and CMA-SDD equalizer output fluctuations of 1 dB, caused by the Doppler shift $f_D = 50$ Hz. The NMCMA-SDD presents a better performance than the CMA-SDD, achieving 12 dB lower in the MSE steady-state, and a minimum MSE = -26 dB.

Figure 76 – 256-QAM - MSE comparison of the CMA-SDD and NMCMA-SDD concurrent equalizers to the dynamic Brazil B for $f_D = 50$ Hz.

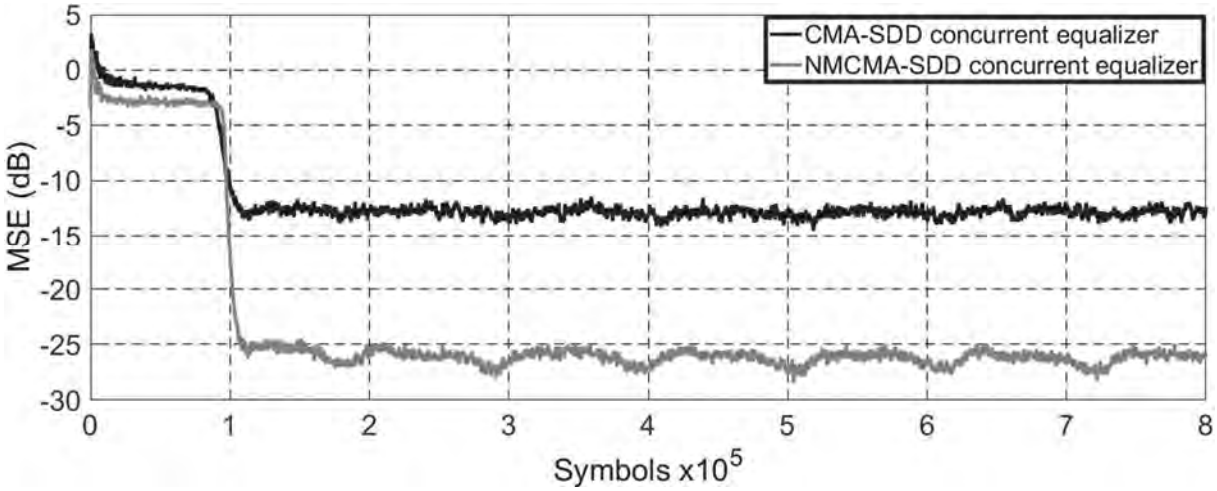

Source: Author (2018).

Figure 77 depicts the SER comparison of the CMA-SDD and NMCMA-SDD concurrent equalizers for the dynamic Brazil B with $f_D = 50$ Hz. The NMCMA-SDD presents a better performance than the CMA-SDD, obtaining a SER 2 orders of magnitude lower for a SNR > 33 dB.

Figure 77 – 256-QAM - SER comparison of the CMA-SDD and NMCMA-SDD concurrent equalizers to the dynamic Brazil B for $f_D = 50$ Hz.

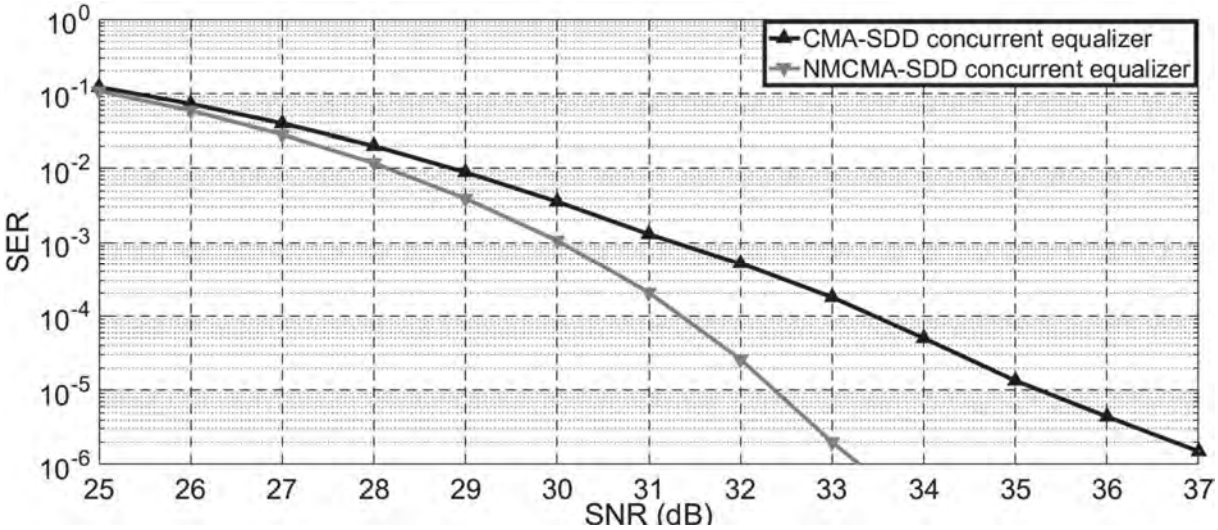

Source: Author (2018).

4.3.3. Dynamic Brazil C - 256-QAM Simulation

For both equalizers, the number of coefficients of the filter is $L_{EQ} = 92$, which is a value fifty percent greater than the delay spread of the dynamic Brazil C. The SER is evaluated for SNR ranging from 30 dB to 43 dB. The adaptive steps of the CMA-SDD are η_C =3x10^{-9}, η_S =7x10^{-6}, and the NMCMA-SDD are η_{NC} =3x10^{-9}, η_S =7x10^{-6}.

Figure 78 depicts the MSE comparison of the CMA-SDD and NMCMA-SDD concurrent equalizers for the dynamic Brazil C with $f_D = 50$ Hz. Convergence of both equalizers is established after 200,000 symbols, with NMCMA-SDD equalizer output fluctuations of 2 dB, and CMA-SDD equalizer output fluctuations of 1 dB, caused by the Doppler shift $f_D = 50$ Hz. The NMCMA-SDD presents a better performance than the CMA-SDD, achieving 8 dB lower in the MSE steady-state, and a minimum MSE = -23 dB.

Figure 78 – 256-QAM - MSE comparison of the CMA-SDD and NMCMA-SDD concurrent equalizers to the dynamic Brazil C for $f_D = 50$ Hz.

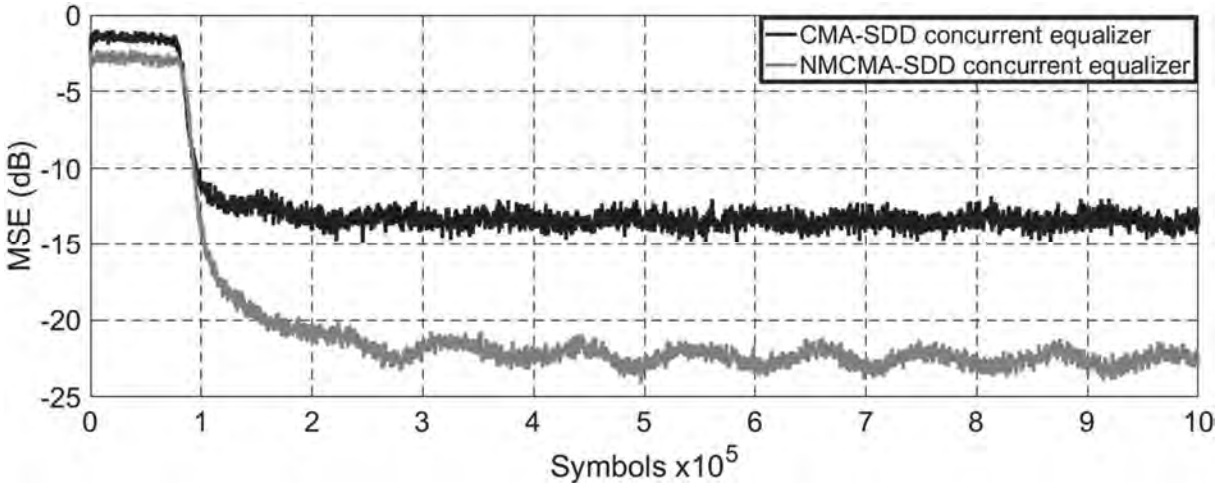

Source: Author (2018).

Figure 79 depicts the SER comparison of the CMA-SDD and NMCMA-SDD concurrent equalizers for the dynamic Brazil C with $f_D = 50$ Hz. The NMCMA-SDD presents a better performance than the CMA-SDD, obtaining a SER 2 orders of magnitude lower for a SNR > 39 dB.

Figure 79 – 256-QAM - SER comparison of the CMA-SDD and NMCMA-SDD concurrent equalizers to the dynamic Brazil C for $f_D = 50$ Hz.

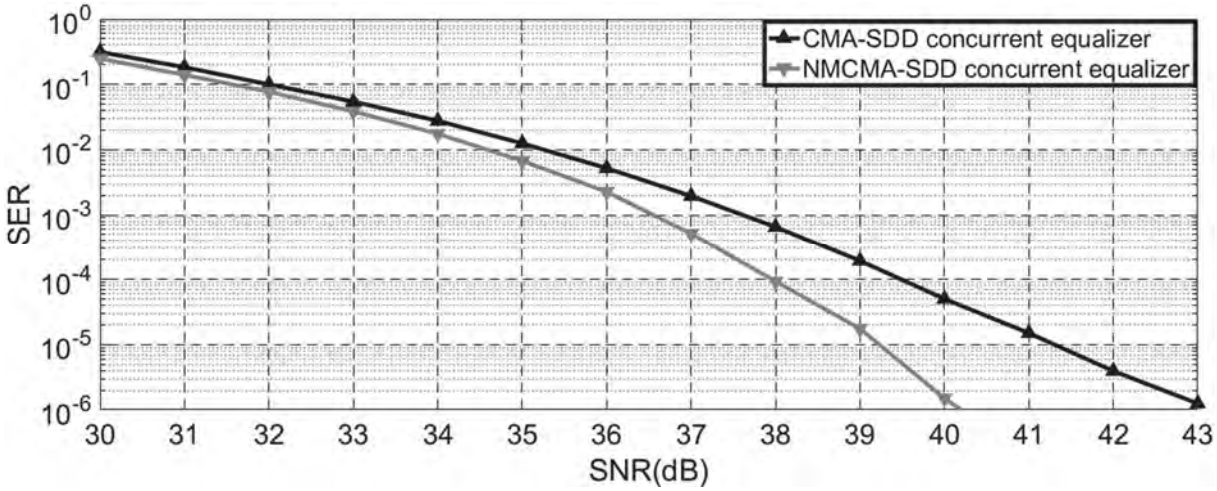

Source: Author (2018).

4.3.4. Dynamic Brazil D - 256-QAM Simulation

For both equalizers, the number of coefficients of the filter is $L_{EQ} = 192$, which is a value fifty percent greater than the delay spread of the dynamic Brazil D. The SER is evaluated for SNR ranging from 25 dB to 38 dB. The adaptive steps of the CMA-SDD are $\eta_C = 1\text{x}10^{-10}$, $\eta_S = 3\text{x}10^{-6}$, and the NMCMA-SDD are $\eta_{NC} = 1\text{x}10^{-10}$, $\eta_S = 3\text{x}10^{-6}$.

Figure 80 depicts the MSE comparison of the CMA-SDD and NMCMA-SDD concurrent equalizers for the dynamic Brazil D with $f_D = 50$ Hz. Convergence of both equalizers is established after few symbols, without equalizer output fluctuations. The NMCMA-SDD presents a better performance than the CMA-SDD, achieving 6 dB lower in the MSE steady-state, and a minimum MSE = -30 dB.

Figure 81 depicts the SER comparison of the CMA-SDD and NMCMA-SDD concurrent equalizers for the dynamic Brazil D with $f_D = 50$ Hz. Both equalizers present equal result from SNR = 25 dB to SNR = 34 dB, and for a SNR > 27 dB, the NMCMA-SDD performance is increased to a SER 1/2 order of magnitude lower.

Figure 80 – 256-QAM - MSE comparison of the CMA-SDD and NMCMA-SDD concurrent equalizers to the dynamic Brazil D for $f_D = 50$ Hz.

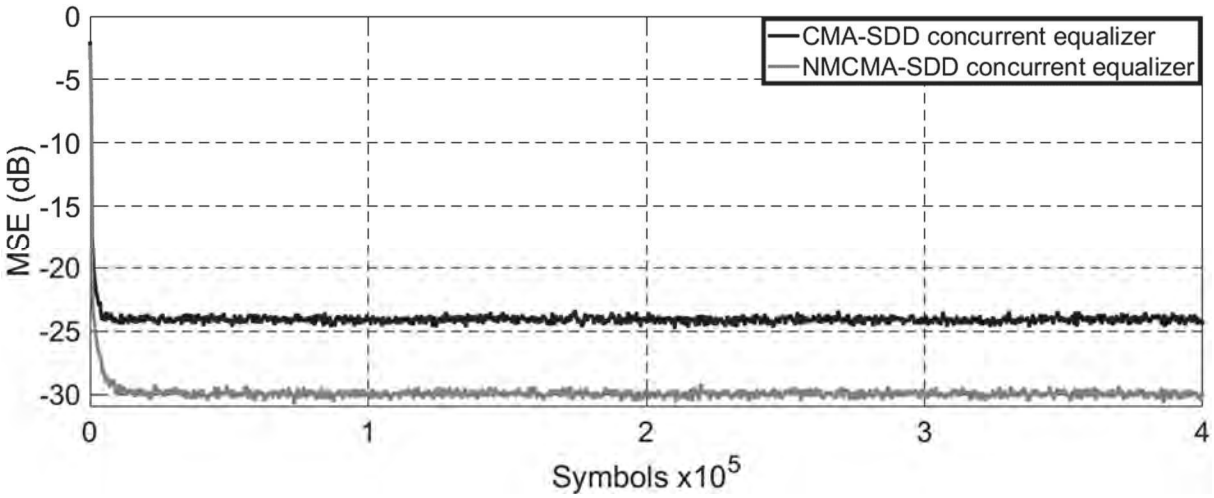

Source: Author (2018).

Figure 81 – 256-QAM - SER comparison of the CMA-SDD and NMCMA-SDD concurrent equalizers to the dynamic Brazil D for $f_D = 50$ Hz.

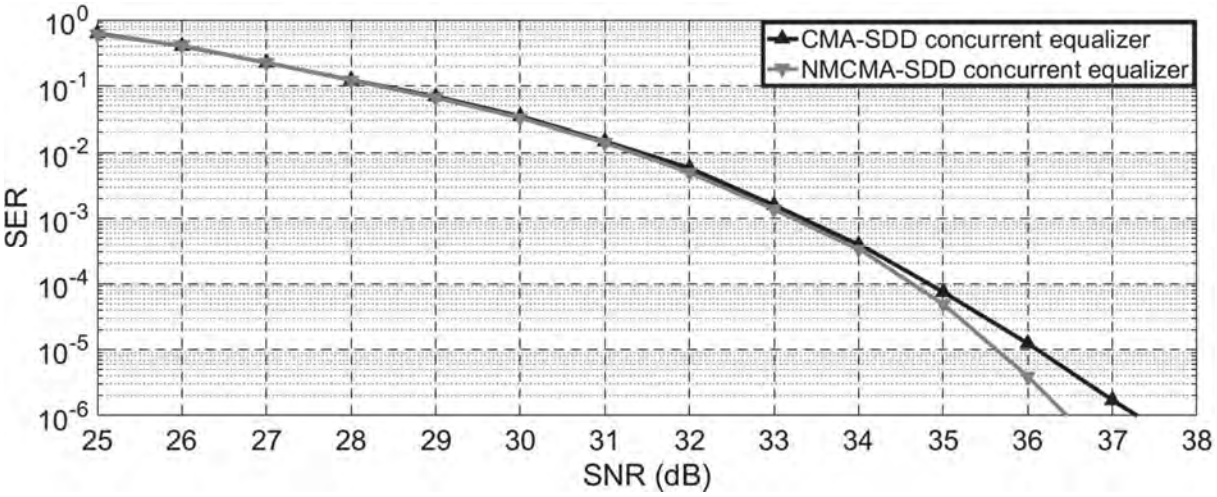

Source: Author (2018).

4.3.5. Dynamic Brazil E - 256-QAM Simulation

For both equalizers, the number of coefficients of the filter is $L_{EQ} = 66$, which is a value fifty percent greater than the delay spread of the dynamic Brazil E. The SER is evaluated for SNR ranging from 25 dB to 35 dB. The adaptive steps of the CMA-SDD are $\eta_C = 1\text{x}10^{-10}$, $\eta_S = 3\text{x}10^{-6}$, and the NMCMA-SDD are $\eta_{NC} = 1\text{x}10^{-10}$, $\eta_S = 3\text{x}10^{-6}$.

Figure 82 depicts the MSE comparison of the CMA-SDD and NMCMA-SDD concurrent equalizers for the dynamic Brazil E with $f_D = 50$ Hz. Convergence of both

equalizers is established after few symbols, without equalizer output fluctuations. The NMCMA-SDD presents a better performance than the CMA-SDD, achieving 6 dB lower in the MSE steady-state, and a minimum MSE = -32 dB.

Figure 82 – 256-QAM - MSE comparison of the CMA-SDD and NMCMA-SDD concurrent equalizers to the dynamic Brazil E for $f_D = 50$ Hz.

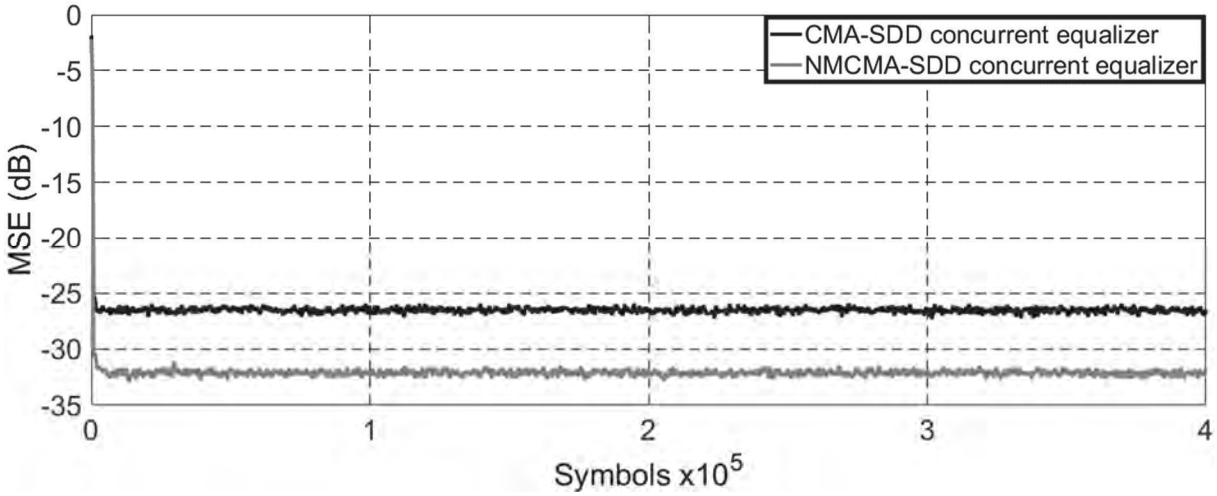

Source: Author (2018).

Figure 83 depicts the SER comparison of the CMA-SDD and NMCMA-SDD concurrent equalizers for the dynamic Brazil E with $f_D = 50$ Hz. Both equalizers present equal result from SNR = 25 dB to SNR = 32 dB, and for a SNR > 32 dB, the NMCMA-SDD performance is increased to a SER 1/5 order of magnitude lower.

Figure 83 – 256-QAM - SER comparison of the CMA-SDD and NMCMA-SDD concurrent equalizers to the dynamic Brazil E for $f_D = 50$ Hz.

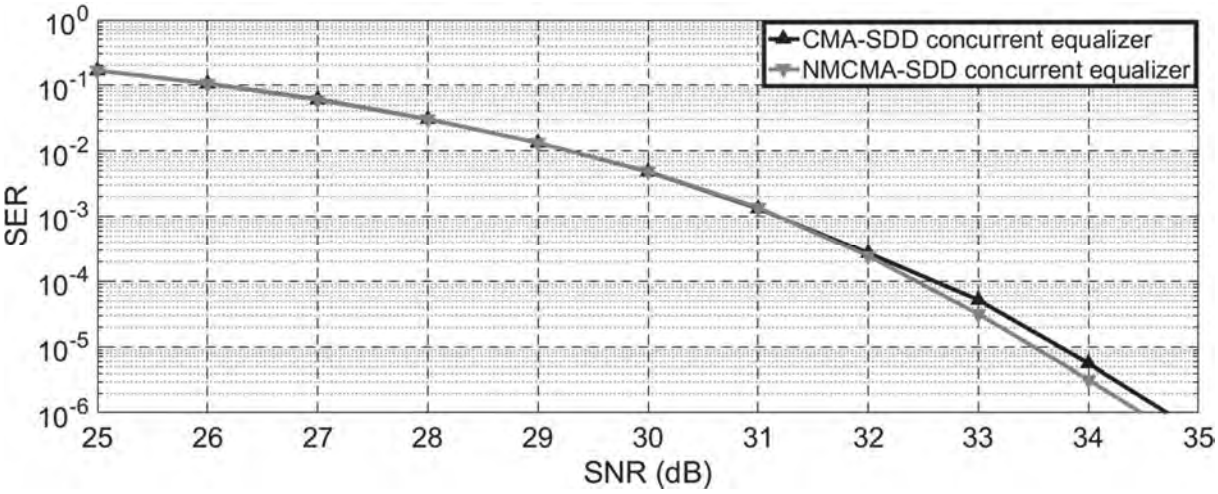

Source: Author (2018).

5. CONCLUSIONS

This work proposed a novel blind equalization scheme for *M*-QAM single carrier systems that aims at mitigating dynamic multipath channel distortion, which may adversely affect the communication system performance. The presented equalizer architecture is based on the NMCMA and SDD equalizers, and more importantly, on the concurrent architecture. In addition, multipath profiles of typical VHF (Very High Frequency) and UHF (Ultra High Frequency) wireless channel distortions were presented and the state of the art (CMA-SDD concurrent equalizer) and the proposed approach (NMCMA-SDD concurrent equalizer) were simulated in order to measure their performance against such multipath scenarios.

Based on the synergistic combination of the equalization algorithms described in Chapter 2, the proposed NMCMA-SDD concurrent equalizer is presented in Chapter 3. The main functional features of the NMCMA-SDD concurrent equalizer can be summarized as follows: (1) The concurrent architecture overall improves the convergence rate and lowers the steady-state MSE of the equalizer system, (2) the NMCMA algorithm lowers the steady state MSE due to the nonlinear operation at its output, and (3) the SDD equalizer increase the overall convergence rate due to the soft decision approach.

Chapter 3 also addressed the fractionally spaced equalizer architecture for the proposed NMCMA-SDD concurrent equalizer. The upsampling factor of 2 was suggested in Chapter 2 in order to improve the overall system performance without drastically increasing the computational complexity, particularly when the channel has zeros over the unitary circle in the z-plane.

The proposed approach is robust over dynamic channels, in the sense that the equalizer architecture presents a fast convergence rate, given by the SDD equalizer and the concurrent architecture, also presenting a low steady-state MSE, given by the NMCMA and the concurrent architecture.

Next, Chapter 4 presents the main results of this dissertation. The first simulation set-up uses 16-QAM modulation over dynamic Brazil channels. The CMA-SDD and the NMCMA-SDD concurrent equalizers were simulated with the NMCMA-SDD achieving better results, particularly for dynamic Brazil B channel, for which the NMCMA-SDD output SER resulted one order of magnitude lower than the CMA-SDD

output SER. Also, a set-up using 64-QAM modulation over dynamic Brazil channels was simulated as well. Again, the NMCMA-SDD concurrent equalizer achieved better results than the CMA-SDD concurrent equalizer, particularly for dynamic Brazil B, with a SER two orders of magnitude lower. For the set-up using 256-QAM over dynamic Brazil channels, dynamic brazil B simulation presented the best result again, with the NMCMA-SDD achieving a SER two orders of magnitude lower than the state of the art CMA-SDD.

For channels with short dispersion (Brazil E), the proposed NMCMA-SDD and the state of the art CMA-SDD presented similar results. On the other hand, for channels with large dispersion the NMCMA-SDD presented significant better result compared with the CMA-SDD. This is due to the sharper decision region established by the nonlinear transmittance of the NMCMA equalizer, which behaves similarly to the activation function of a neuron in an artificial neural network.

The nonlinear transmittance of the NMCMA equalizer is also responsible for the better NMCMA-SDD performance for higher modulation orders, such as for 256-QAM. The nonlinear transmittance reduces the symbol dispersion around the reference constellation symbols at the NMCMA-SDD output, minimizing the influence of the modulation order, a feature not available for the CMA-SDD.

In conclusion, the novel blind equalization scheme NMCMA-SDD for M-QAM single carrier systems proposed in this dissertation achieved both a lower steady state MSE and a faster convergence rate than the state of the art CMA-SDD. These results validate the effectiveness of the proposed approach architecture for dynamic multipath scenarios.

5.1. FUTURE WORKS

In the context of optical fiber with coherent transmission, the proposed NMCMA-SDD concurrent equalizer can be used to mitigate de chromatic and the polarization mode dispersions. Moreover, the NMCMA-SDD can reduce the phase random walk originated from both the transmitter and the receiver oscillators (PFAU, 2009).

This dissertation addresses some important topics concerning blind equalization algorithms for dynamic scenarios. Nevertheless, the proposed equalizer

presented here may be further improved by the use of some additional techniques. It is suggested for future research that a mathematical approach for an optimum adaptive step definition (KIM, 2010) be implemented. Another technique that is suggested is the use of a fuzzy controller (CHEN et al., 2010) or a neuro-fuzzy system (ABIYEV; AL-SHANABLEH, 2006) in order to control the adaptive steps of the proposed NMCMA-SDD concurrent equalizer.

REFERENCES

ABIYEV, R.; AL-SHANABLEH, T. **Neuro-Fuzzy Network for Adaptive Channel Equalization**. 2006 Fifth Mexican International Conference on Artificial Intelligence. Anais...IEEE, Nov. 2006.

ATSC. **Digital Television Standard (A/53) Revision E, with Amendment No. 1**., 2006.

CHEN, S. **Low complexity concurrent constant modulus algorithm and soft decision directed scheme for blind equalisation**. IEE Proceedings - Vision, Image, and Signal Processing, v. 150, n. 5, p. 312, 2003.

CHEN, S. et al. **Fuzzy-logic tuned constant modulus algorithm and soft decision-directed scheme for blind equalisation**. Digital Signal Processing, v. 20, n. 3, p. 846–859, May 2010.

CHEN, S.; CHNG, E. S. **Concurrent constant modulus algorithm and soft decision directed scheme for fractionally-spaced blind equalization**. 2004 IEEE International Conference on Communications. **Anais**...IEEE, 2004.

DE CASTRO, F. C. C.; DE CASTRO, M. C. F.; ARANTES, D. S. **Concurrent blind deconvolution for channel equalization**. ICC 2001. IEEE International Conference on Communications. Conference Record (Cat. No.01CH37240). **Anais**...IEEE, 2001.

ENDRES, T. J. **Equalizing With Fractionally-Spaced Constant Modulus and Second-Order-Statistics Blind Receivers**. Ph.D. Thesis, Cornell University, 1997.

GARDNER, W. A. **A new method of channel identification**. IEEE Transactions on Communications, v. 39, n. 6, p. 813–817, Jun. 1991.

GITLIN, R. D.; WEINSTEIN, S. B. **Fractionally-Spaced Equalization: An Improved Digital Transversal Equalizer**. Bell System Technical Journal, v. 60, n. 2, p. 275–296, Feb. 1981.

GODARD, D. **Self-Recovering Equalization and Carrier Tracking in Two-Dimensional Data Communication Systems**. IEEE Transactions on Communications, v. 28, n. 11, p. 1867–1875, Nov. 1980.

HAYKIN, S. **Digital Communication Systems**. 1. ed. Hoboken: Wiley, 2013.

HAYKIN, S. **Adaptive filter theory**. 5. ed. Upper Saddle River: Pearson, 2014.

ITU. **ITU-R BT.2035-2: Guidelines and techniques for the evaluation of digital terrestrial television broadcasting systems including assessment of their**

coverage areas, 2008.

JOHNSON, R. et al. **Blind equalization using the constant modulus criterion: a review**. Proceedings of the IEEE, v. 86, n. 10, p. 1927–1950, 1998.

KIM, N. **Step-size control for width adaptation in radial basis function networks for nonlinear channel equalization**. Journal of Communications and Networks, v. 12, n. 6, p. 600–604, 2010.

LEBLANC, J. P. et al. **Fractionally spaced CMA equalizers under periodic and correlated inputs**. 1995 International Conference on Acoustics, Speech, and Signal Processing. **Anais**...IEEE, Jun. 1995.

NORONHA, T. B. **Equalização Concorrente de Canal para Sistemas Monoportadora com Acesso Múltiplo por Divisão de Frequência**. Ms.C. Dissertation. Pontifícia Universidade Católica do Rio Grande do Sul, 2012.

OH, K. N.; CHIN, Y. O. **Modified constant modulus algorithm: blind equalization and carrier phase recovery algorithm**. Proceedings IEEE International Conference on Communications ICC ’95. **Anais**...IEEE, 1995.

PAPOULIS, A.; PILLAI, S. U. **Probability, Random Variables and Stochastic Processes**. 4. ed., McGraw-Hill, 2002.

PFAU, T. **Development and Real-time Implementation of Digital Signal Algorithms for Coherent Optical Receivers**. Ph.D. Thesis. University of Paderborn, 2009.

PRESS, W. H. et al. **Numerical Recipes: The Art of Scientific Computing**. 3. ed., Cambridge University Press, 2007.

PROAKIS, J. G.; SALEHI, M. **Digital Communications**. 5. ed. New York: McGraw-Hill, 2008.

SMITH, S. W. **The Scientist and Engineering’s Guide to Digital Signal Processing**. 2. ed. San Diego: California Technical Publishing, 1999.

WANG, D. **A nonlinear modified constant modulus algorithm for blind equalization**. CCECE 2010. **Anais**...IEEE, May 2010.

WIDROW, B.; HOFF, M. E. **Adaptive Switching Circuits**. IRE WESCON Convention Record, n. 4, p. 96–104, 1960.

YOU, C.; HONG, D. **Nonlinear blind equalization schemes using complex-valued multilayer feedforward neural networks.** IEEE Transactions on Neural Networks, v. 9, n. 6, p. 1442–1455, 1998.

APPENDIX A - 16-QAM MSE and SER simulations for the static and dynamic Brazil channels.

Figure 84 – 16-QAM - MSE comparison of the CMA-SDD and NMCMA-SDD concurrent equalizers to the static Brazil A.

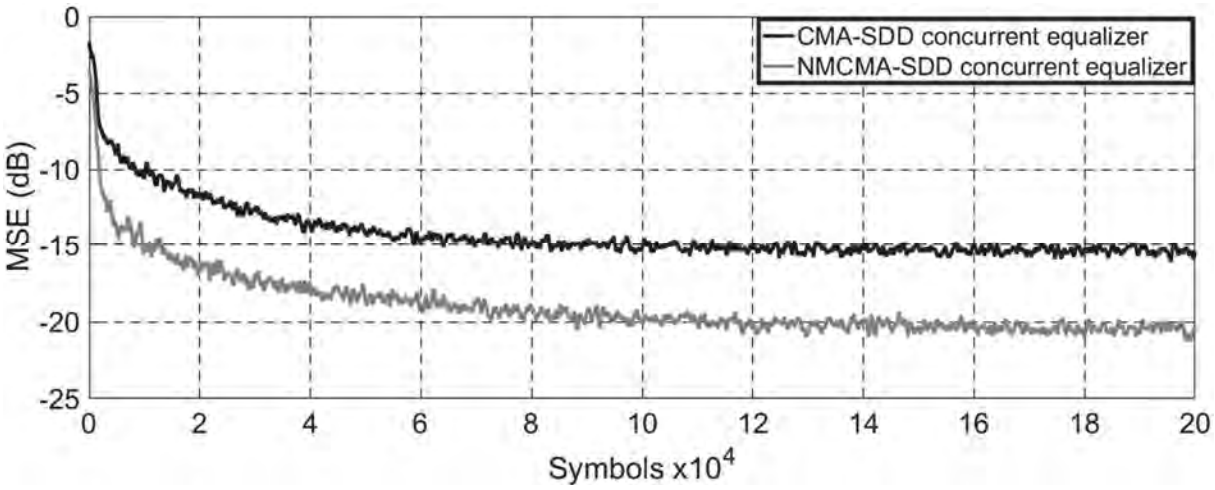

Source: Author (2018).

Figure 85 – 16-QAM - SER comparison of the CMA-SDD and NMCMA-SDD concurrent equalizers to the static Brazil A.

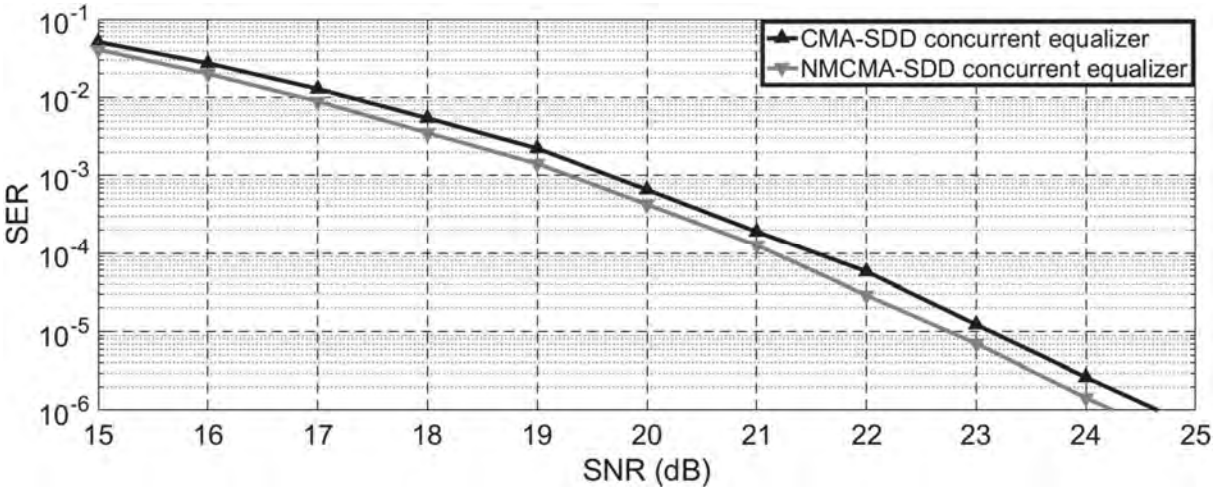

Source: Author (2018).

Figure 86 – 16-QAM - MSE comparison of the CMA-SDD and NMCMA-SDD concurrent equalizers to the dynamic Brazil A for $f_D = 20$ Hz.

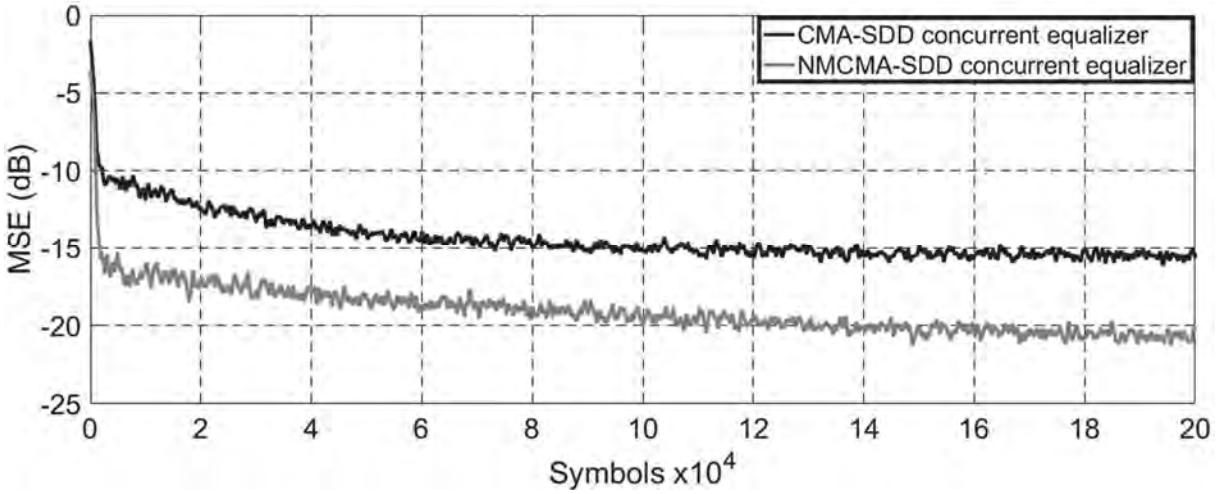

Source: Author (2018).

Figure 87 – 16-QAM - SER comparison of the CMA-SDD and NMCMA-SDD concurrent equalizers to the dynamic Brazil A for $f_D = 20$ Hz.

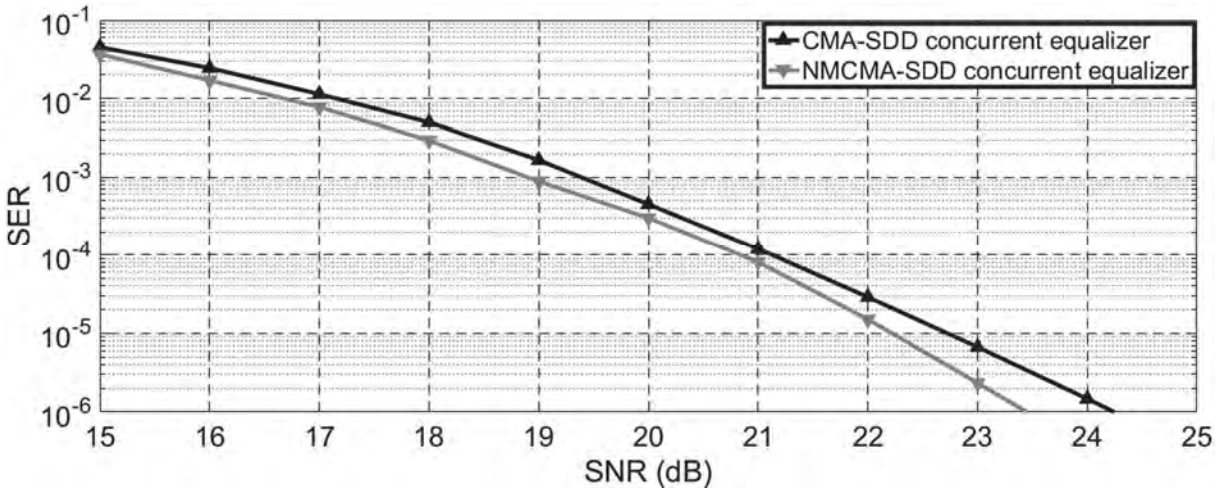

Source: Author (2018).

Figure 88 – 16-QAM - MSE comparison of the CMA-SDD and NMCMA-SDD concurrent equalizers to the static Brazil B.

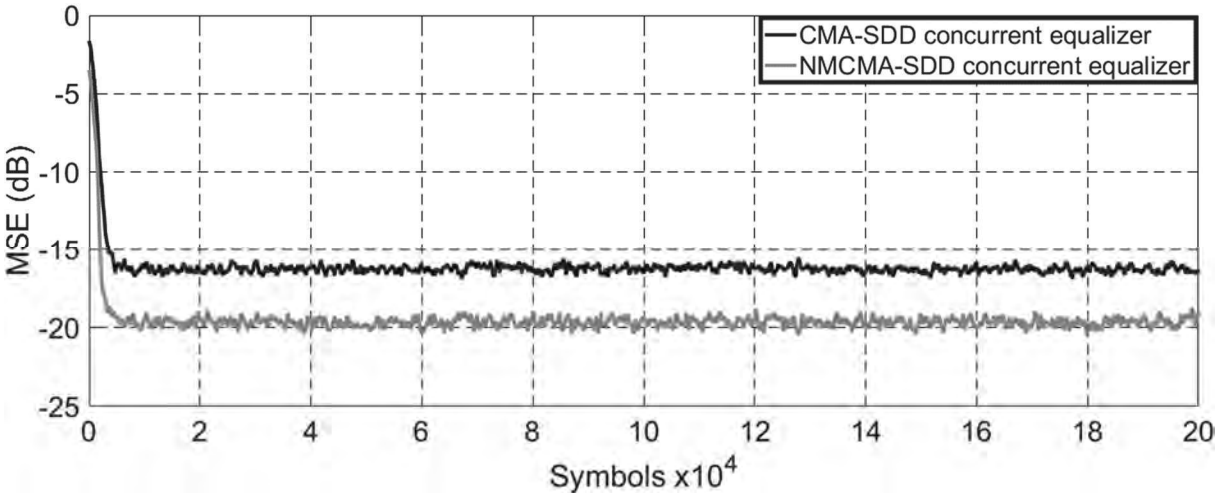

Source: Author (2018).

Figure 89 – 16-QAM - SER comparison of the CMA-SDD and NMCMA-SDD concurrent equalizers to the static Brazil B.

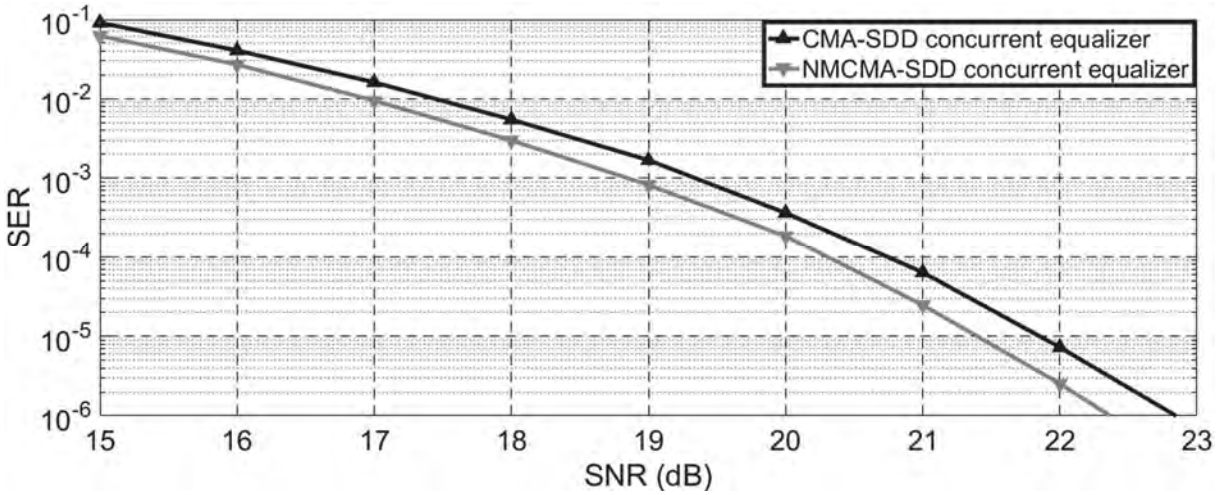

Source: Author (2018).

Figure 90 – 16-QAM - MSE comparison of the CMA-SDD and NMCMA-SDD concurrent equalizers to the dynamic Brazil B for $f_D = 20$ Hz.

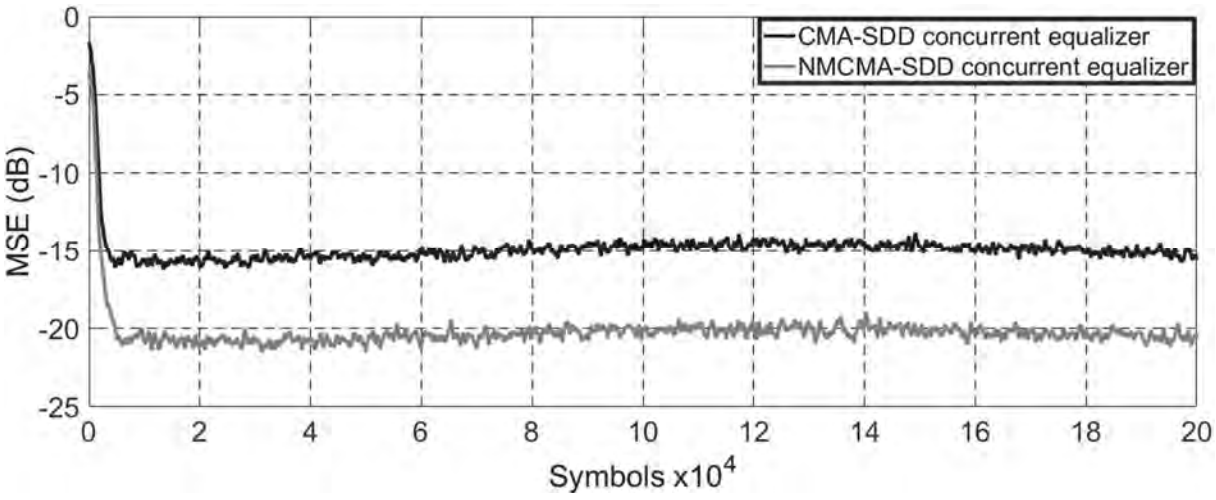

Source: Author (2018).

Figure 91 – 16-QAM - SER comparison of the CMA-SDD and NMCMA-SDD concurrent equalizers to the dynamic Brazil B for $f_D = 20$ Hz.

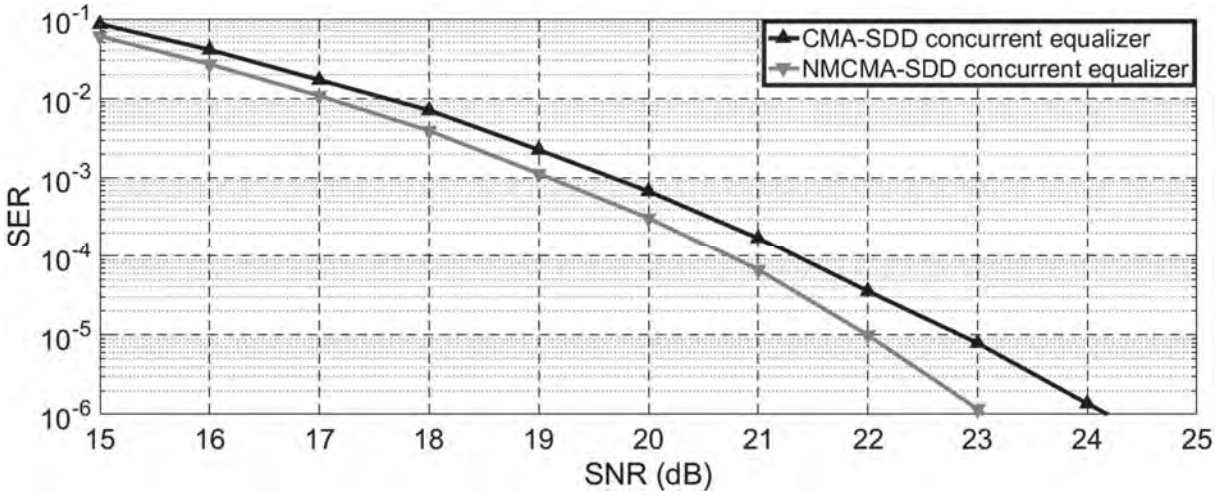

Source: Author (2018).

Figure 92 – 16-QAM - MSE comparison of the CMA-SDD and NMCMA-SDD concurrent equalizers to the static Brazil C.

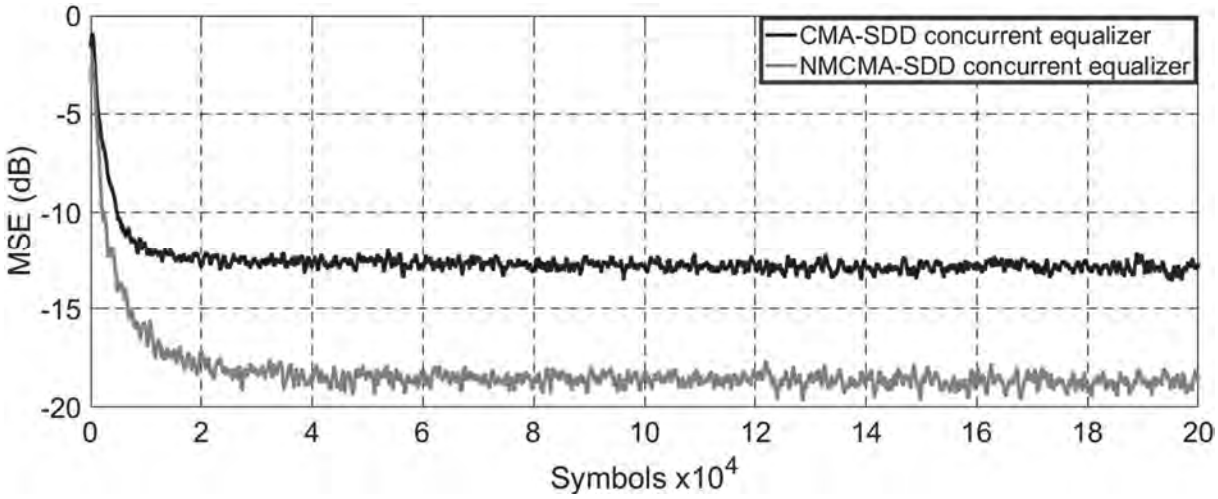

Source: Author (2018).

Figure 93 – 16-QAM - SER comparison of the CMA-SDD and NMCMA-SDD concurrent equalizers to the static Brazil C.

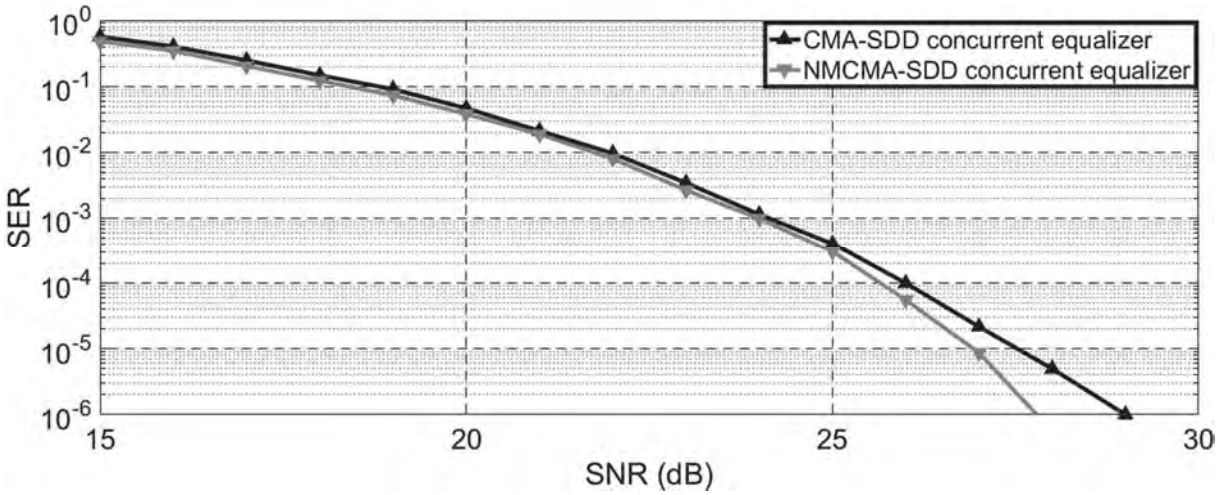

Source: Author (2018).

Figure 94 – 16-QAM - MSE comparison of the CMA-SDD and NMCMA-SDD concurrent equalizers to the dynamic Brazil C for $f_D = 20$ Hz.

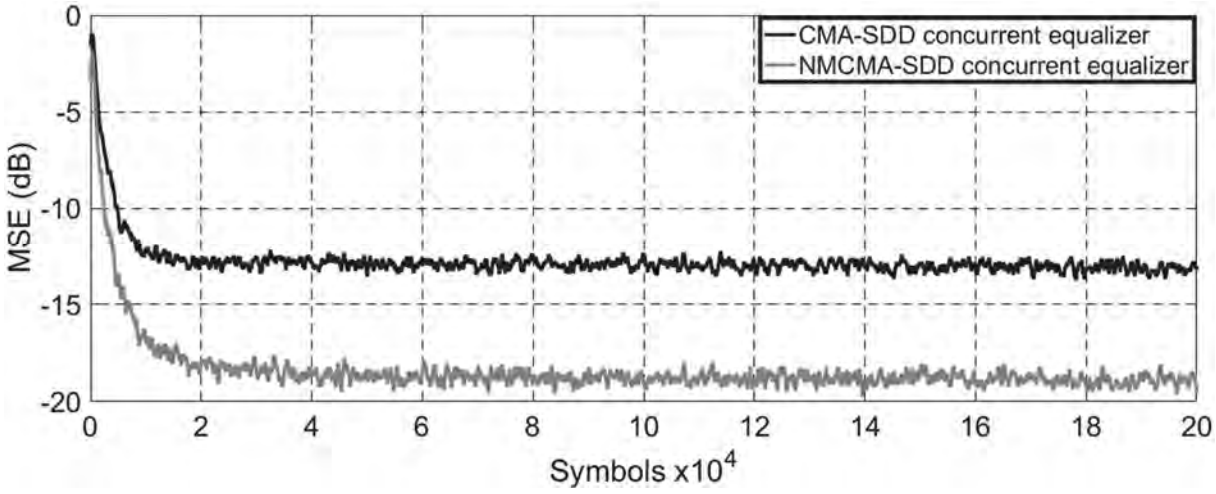

Source: Author (2018).

Figure 95 – 16-QAM - SER comparison of the CMA-SDD and NMCMA-SDD concurrent equalizers to the dynamic Brazil C for $f_D = 20$ Hz.

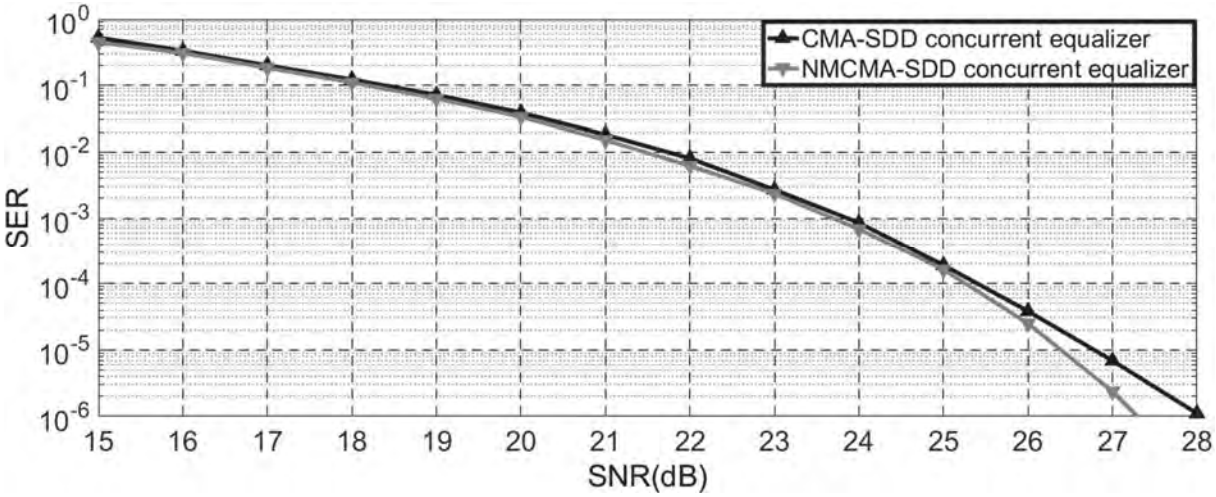

Source: Author (2018).

Figure 96 – 16-QAM - MSE comparison of the CMA-SDD and NMCMA-SDD concurrent equalizers to the static Brazil D.

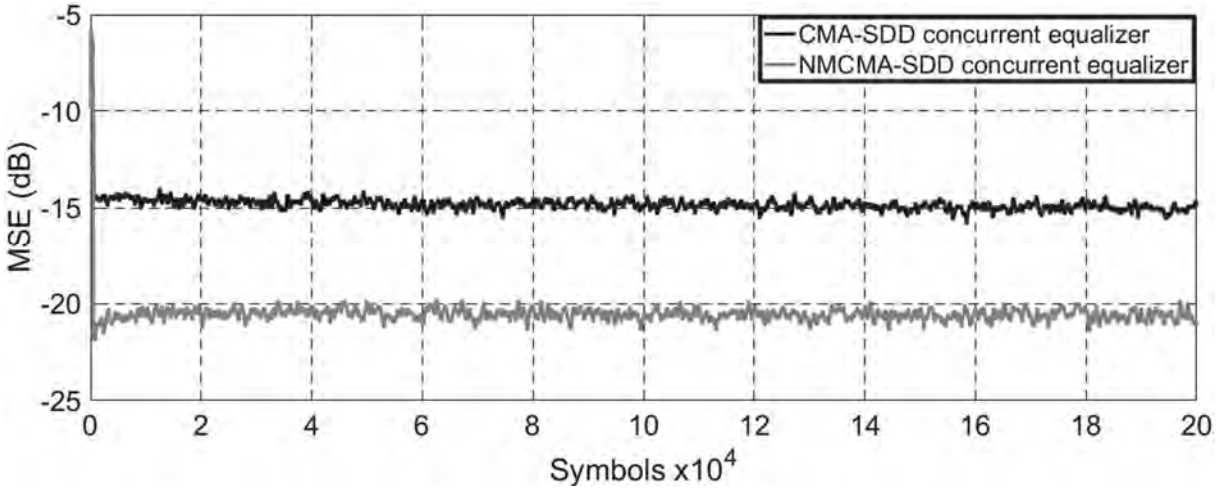

Source: Author (2018).

Figure 97 – 16-QAM - SER comparison of the CMA-SDD and NMCMA-SDD concurrent equalizers to the static Brazil D.

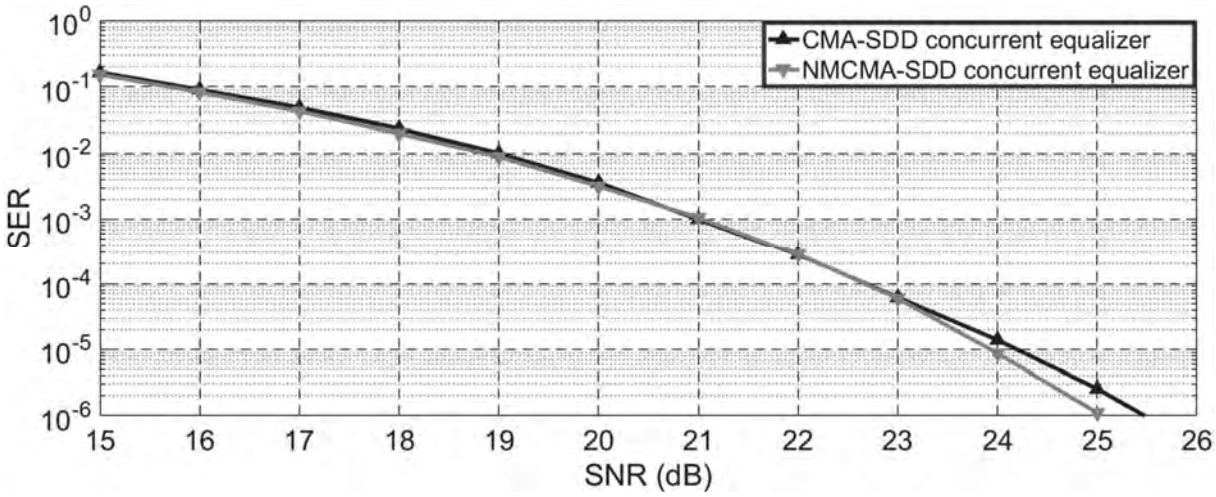

Source: Author (2018).

Figure 98 – 16-QAM - MSE comparison of the CMA-SDD and NMCMA-SDD concurrent equalizers to the dynamic Brazil D for $f_D = 20$ Hz.

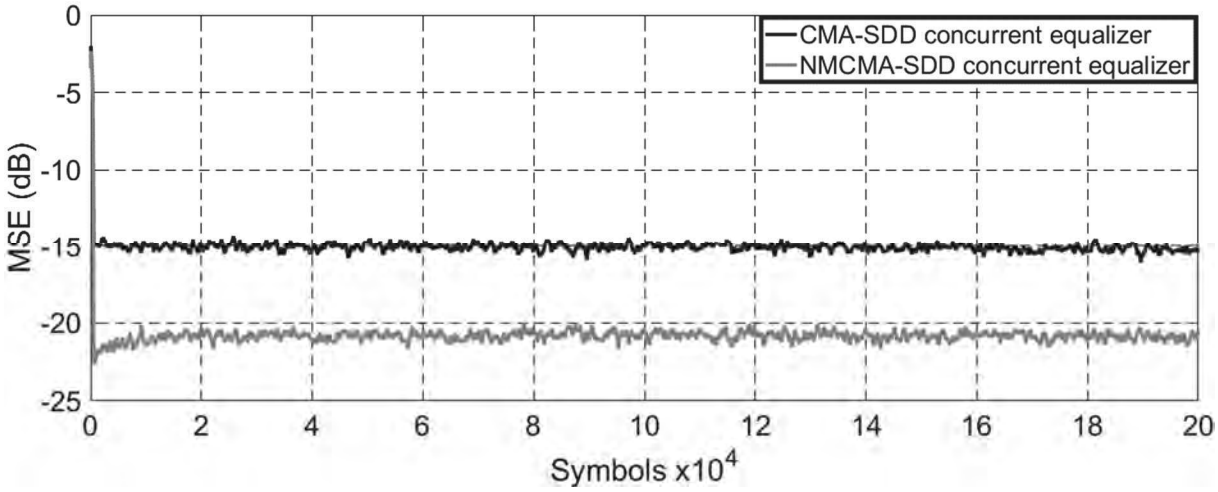

Source: Author (2018).

Figure 99 – 16-QAM - SER comparison of the CMA-SDD and NMCMA-SDD concurrent equalizers to the dynamic Brazil D for $f_D = 20$ Hz.

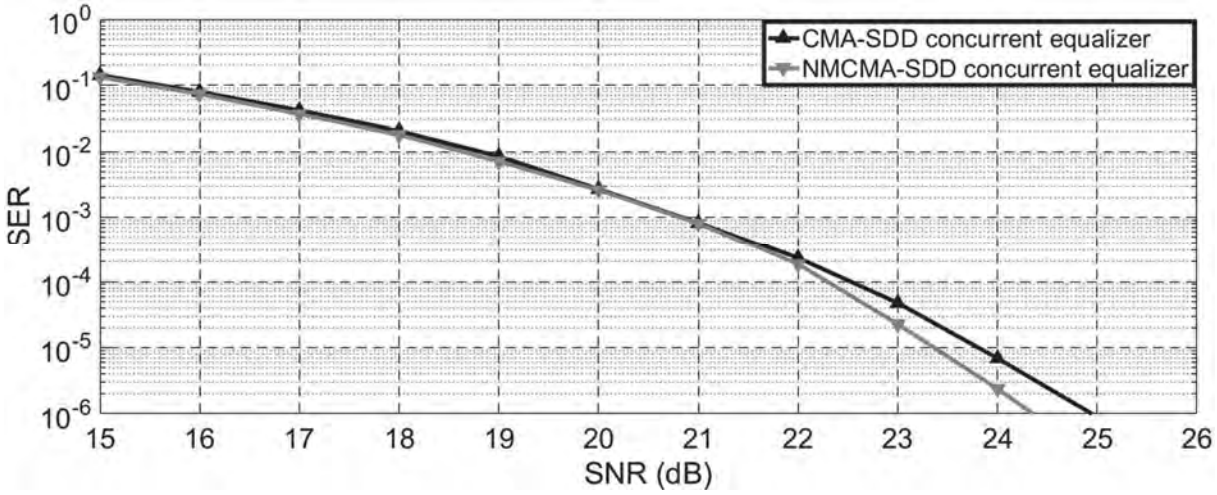

Source: Author (2018).

Figure 100 – 16-QAM - MSE comparison of the CMA-SDD and NMCMA-SDD concurrent equalizers to the static Brazil E.

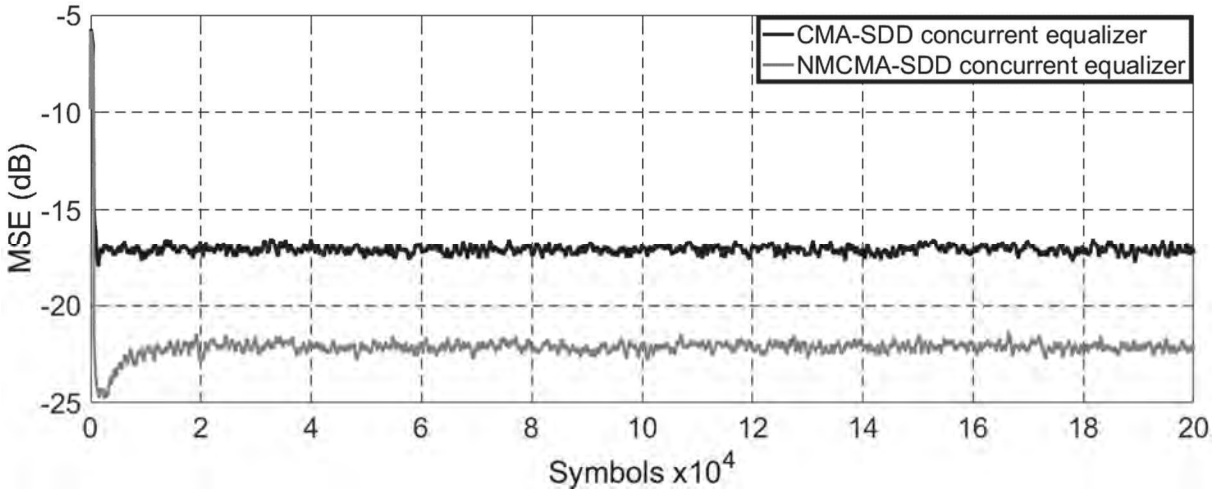

Source: Author (2018).

Figure 101 – 16-QAM - SER comparison of the CMA-SDD and NMCMA-SDD concurrent equalizers to the static Brazil E.

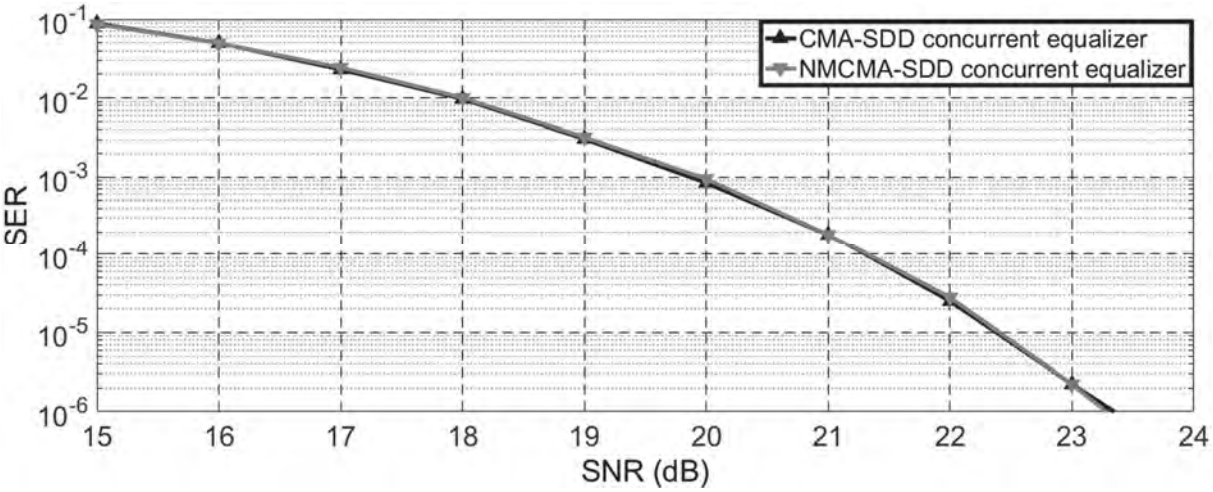

Source: Author (2018).

Figure 102 – 16-QAM - MSE comparison of the CMA-SDD and NMCMA-SDD concurrent equalizers to the dynamic Brazil E for $f_D = 20$ Hz.

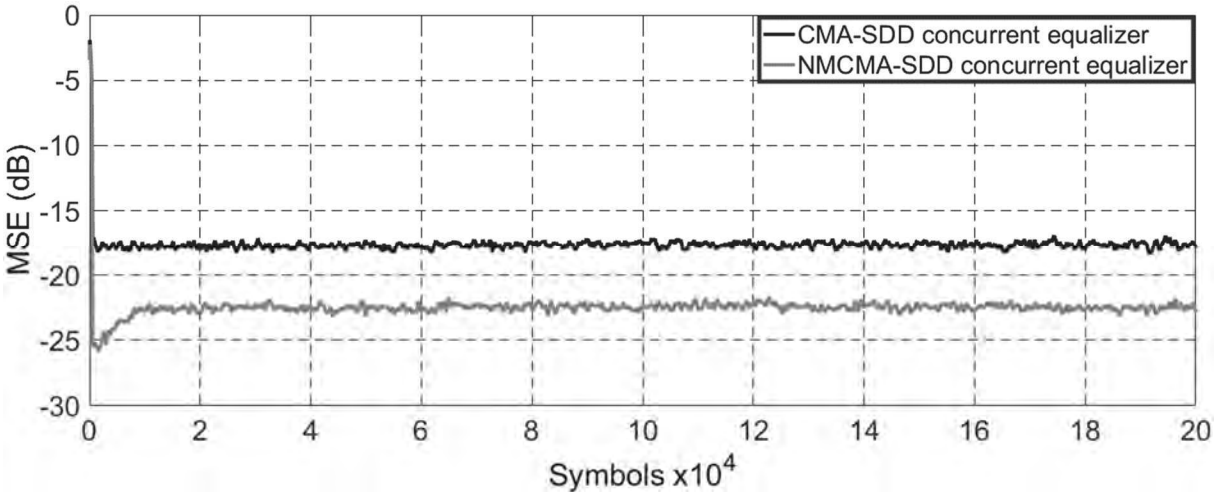

Source: Author (2018).

Figure 103 – 16-QAM - SER comparison of the CMA-SDD and NMCMA-SDD concurrent equalizers to the dynamic Brazil E for $f_D = 20$ Hz.

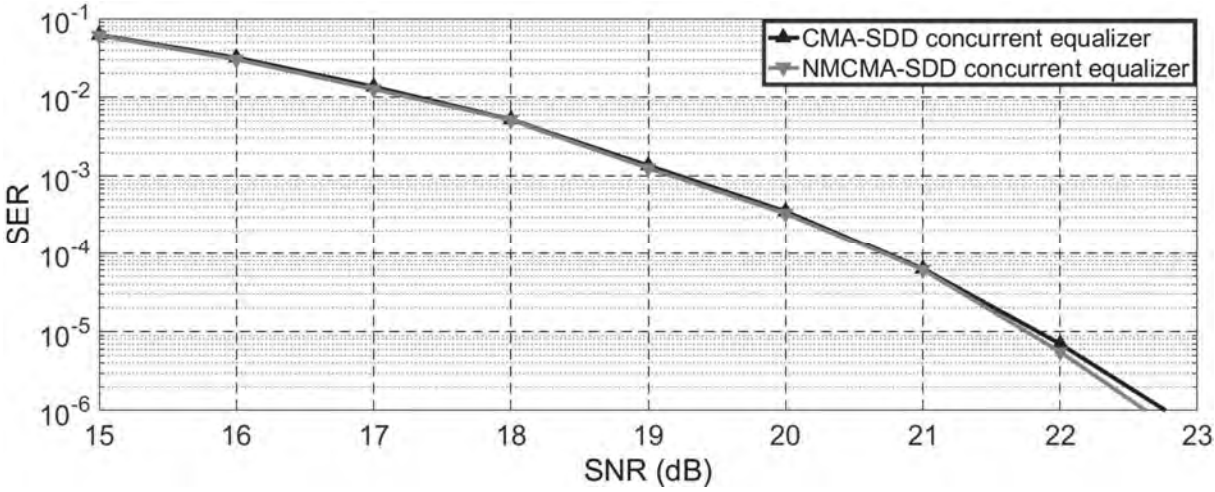

Source: Author (2018).

APPENDIX B - 64-QAM MSE and SER simulations for the static and dynamic Brazil channels.

Figure 104 – 64-QAM - MSE comparison of the CMA-SDD and NMCMA-SDD concurrent equalizers to the static Brazil A.

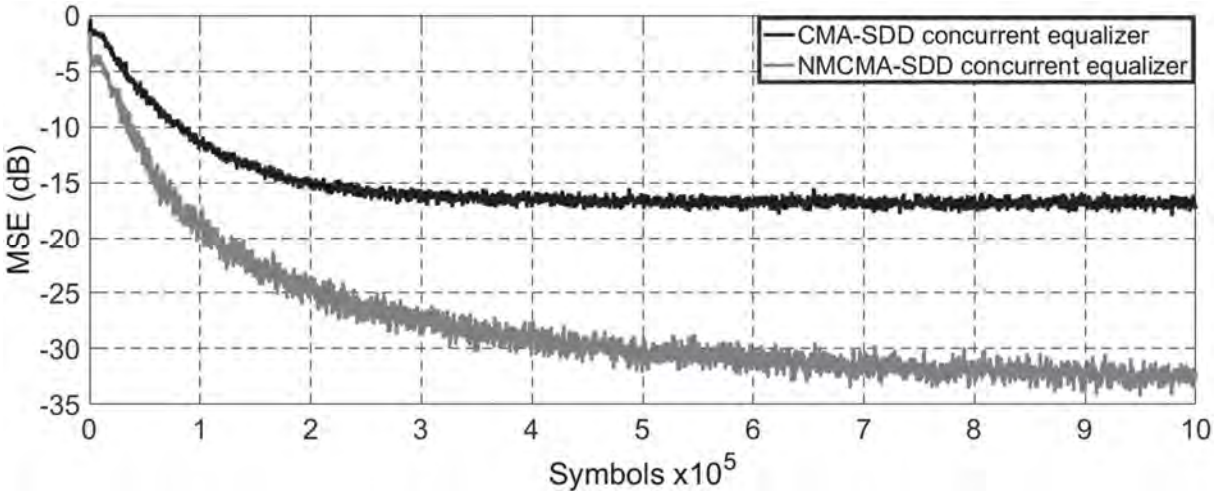

Source: Author (2018).

Figure 105 – 64-QAM - SER comparison of the CMA-SDD and NMCMA-SDD concurrent equalizers to the static Brazil A.

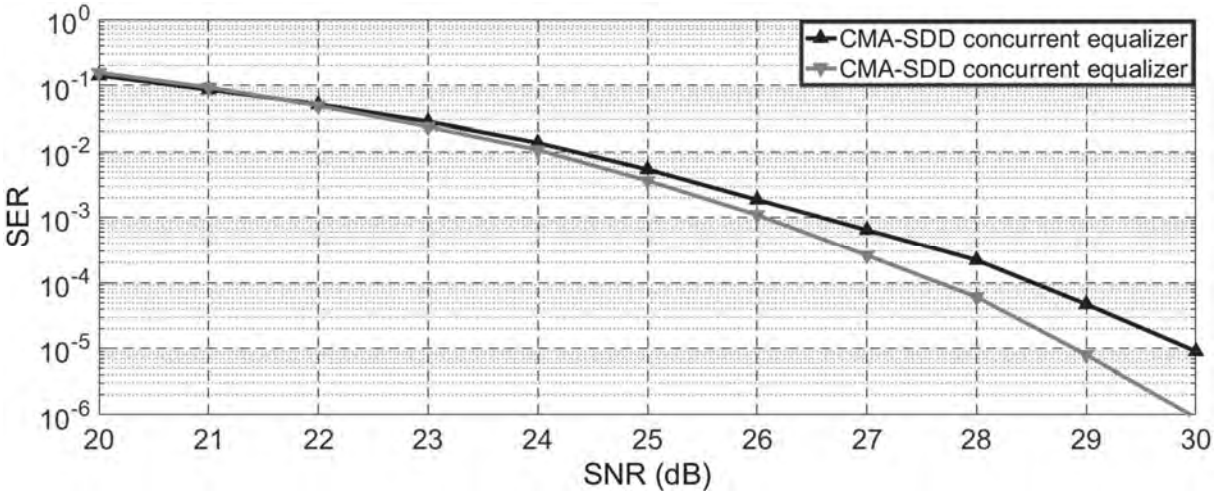

Source: Author (2018).

Figure 106 – 64-QAM - MSE comparison of the CMA-SDD and NMCMA-SDD concurrent equalizers to the dynamic Brazil A for $f_D = 20$ Hz.

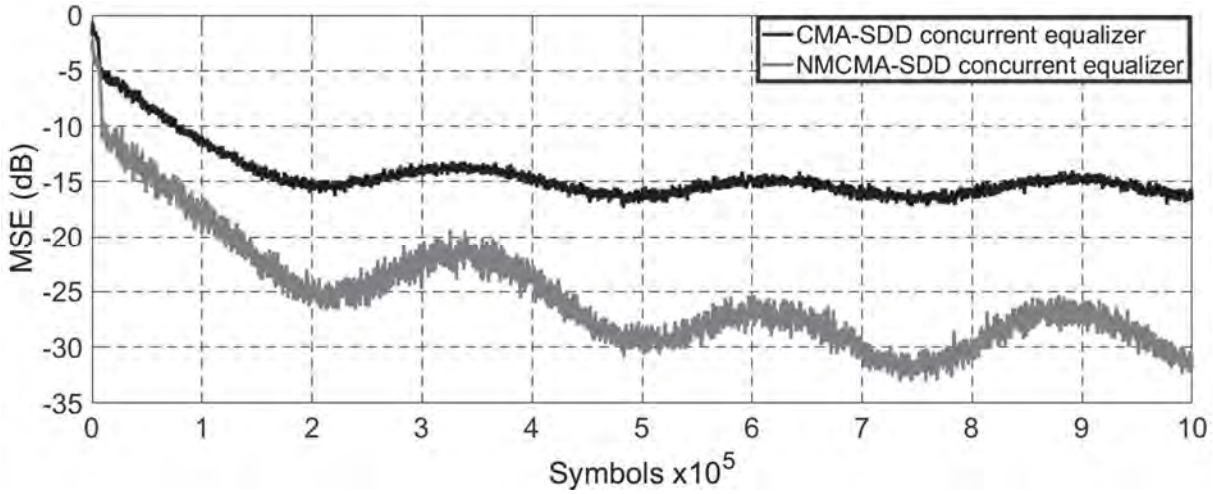

Source: Author (2018).

Figure 107 – 64-QAM - SER comparison of the CMA-SDD and NMCMA-SDD concurrent equalizers to the dynamic Brazil A for $f_D = 20$ Hz.

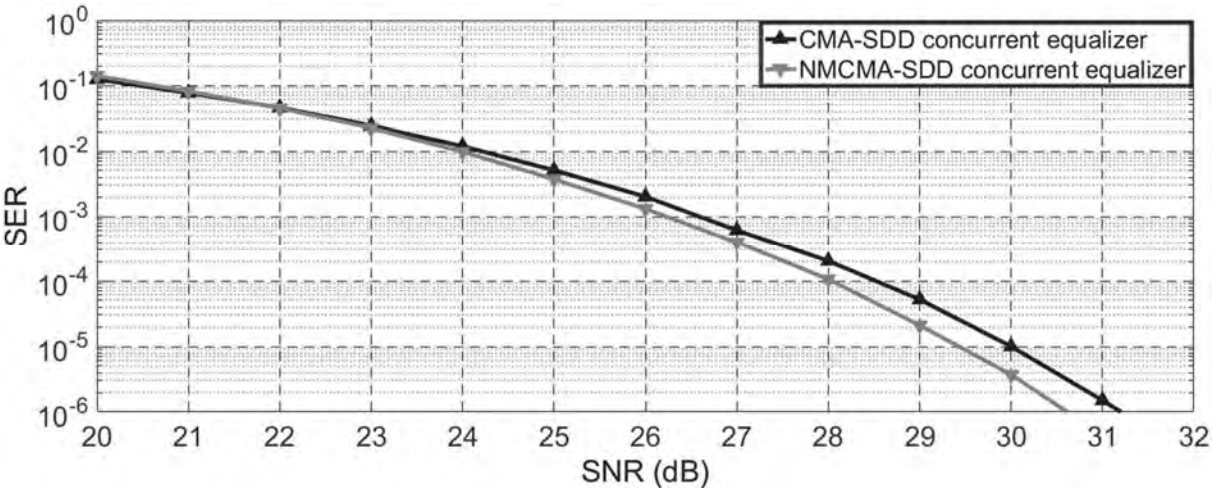

Source: Author (2018).

Figure 108 – 64-QAM - MSE comparison of the CMA-SDD and NMCMA-SDD concurrent equalizers to the static Brazil B.

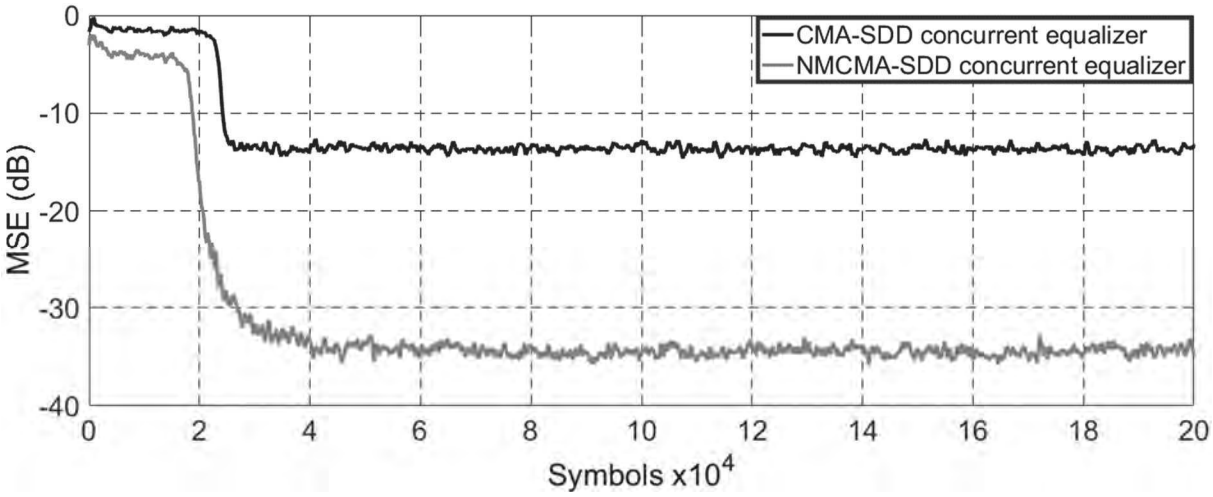

Source: Author (2018).

Figure 109 – 64-QAM - SER comparison of the CMA-SDD and NMCMA-SDD concurrent equalizers to the static Brazil B.

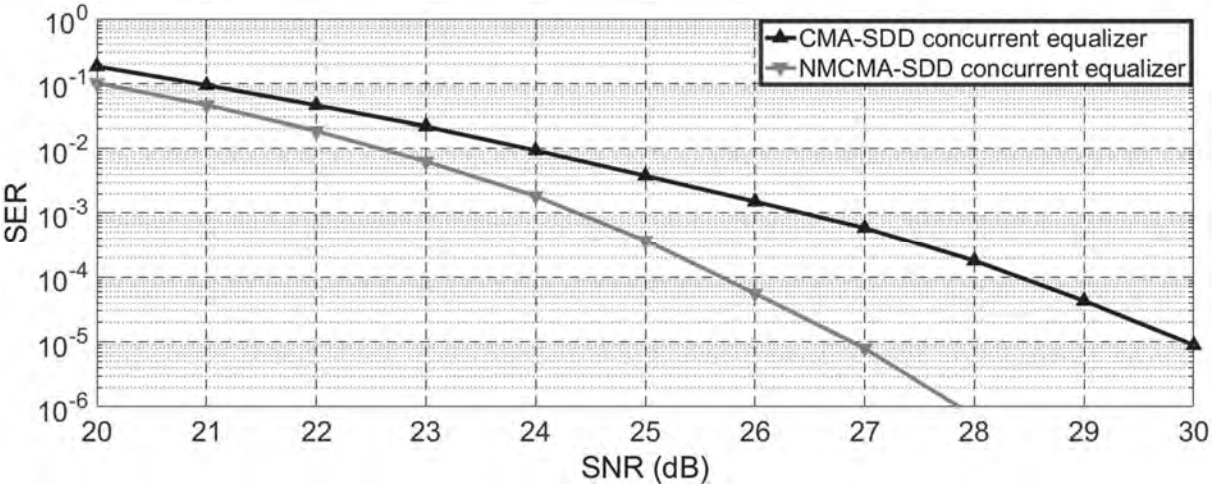

Source: Author (2018).

Figure 110 – 64-QAM - MSE comparison of the CMA-SDD and NMCMA-SDD concurrent equalizers to the dynamic Brazil B for $f_D = 20$ Hz.

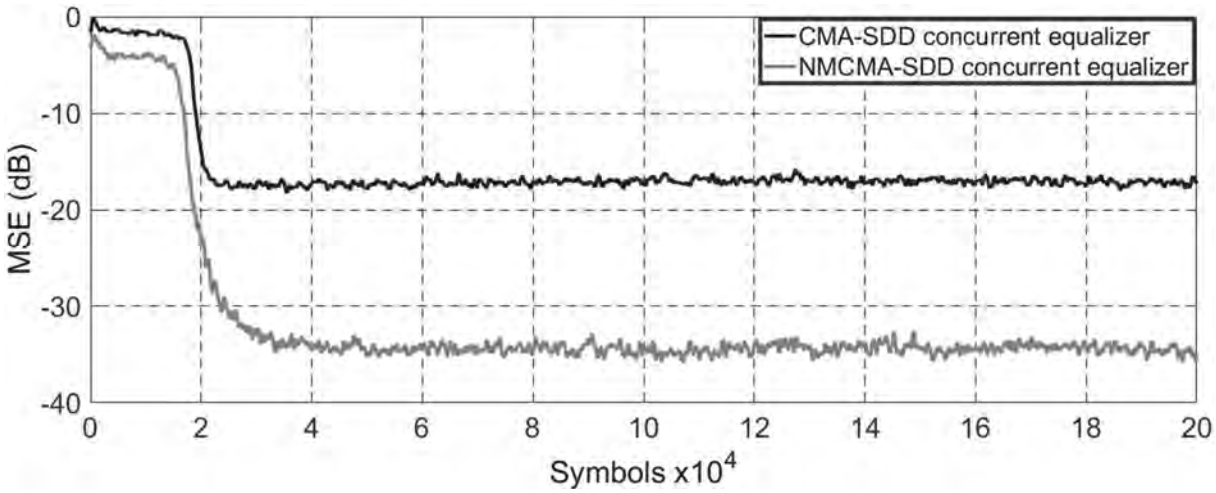

Source: Author (2018).

Figure 111 – 64-QAM - SER comparison of the CMA-SDD and NMCMA-SDD concurrent equalizers to the dynamic Brazil B for $f_D = 20$ Hz.

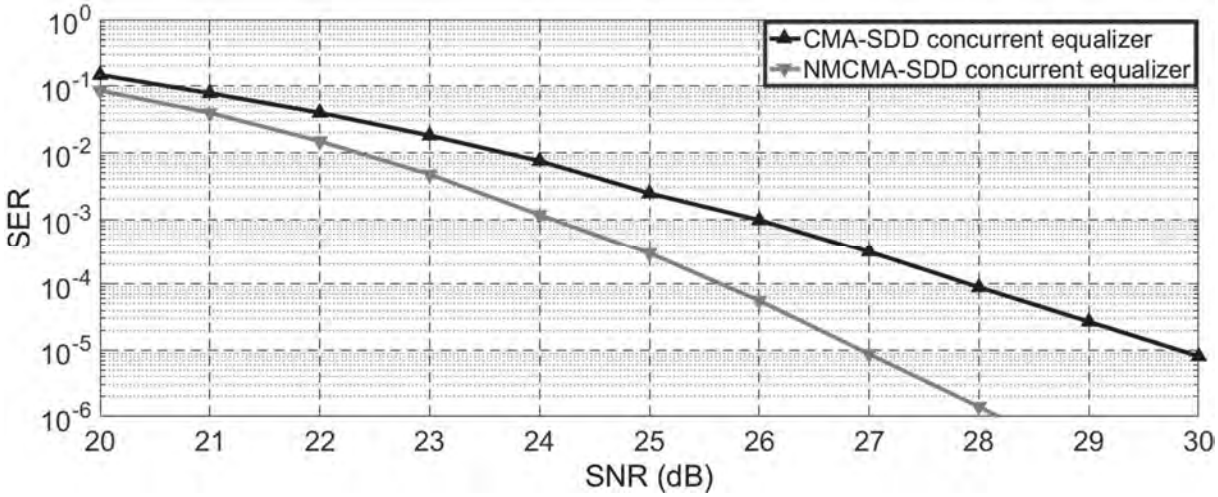

Source: Author (2018).

Figure 112 – 64-QAM - MSE comparison of the CMA-SDD and NMCMA-SDD concurrent equalizers to the static Brazil C.

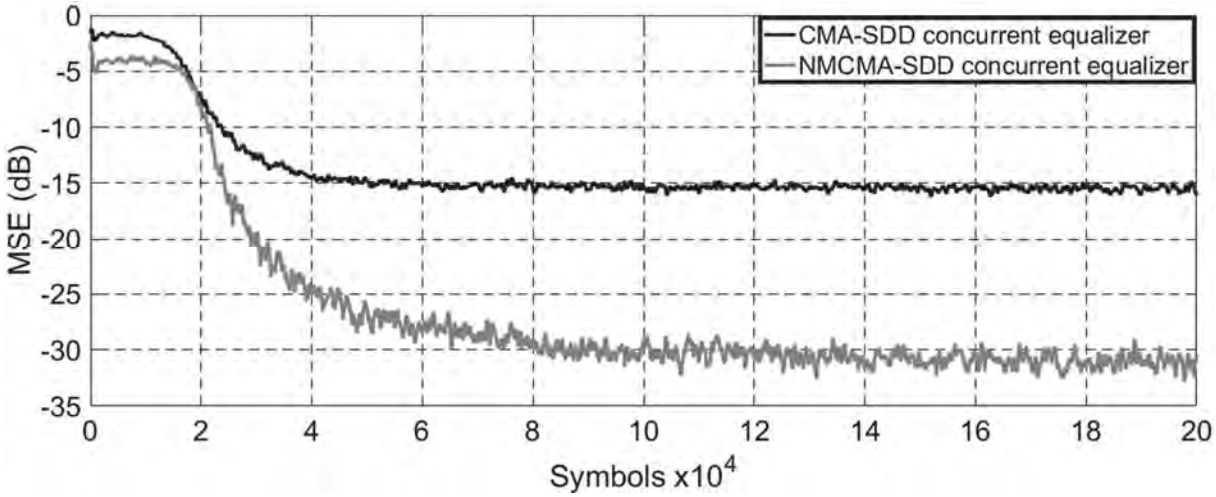

Source: Author (2018).

Figure 113 – 64-QAM - SER comparison of the CMA-SDD and NMCMA-SDD concurrent equalizers to the static Brazil C.

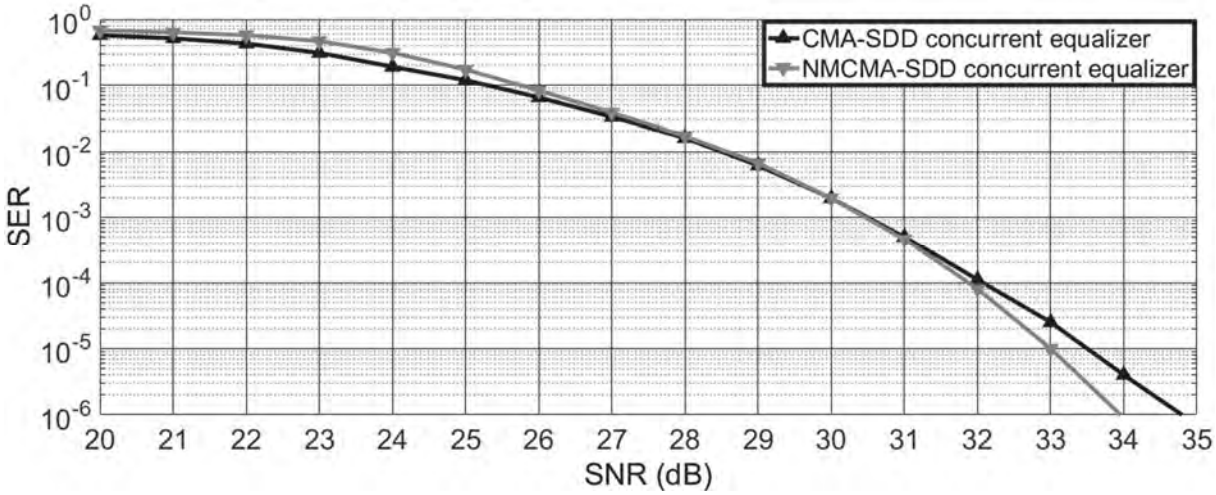

Source: Author (2018).

Figure 114 – 64-QAM - MSE comparison of the CMA-SDD and NMCMA-SDD concurrent equalizers to the dynamic Brazil C for $f_D = 20$ Hz.

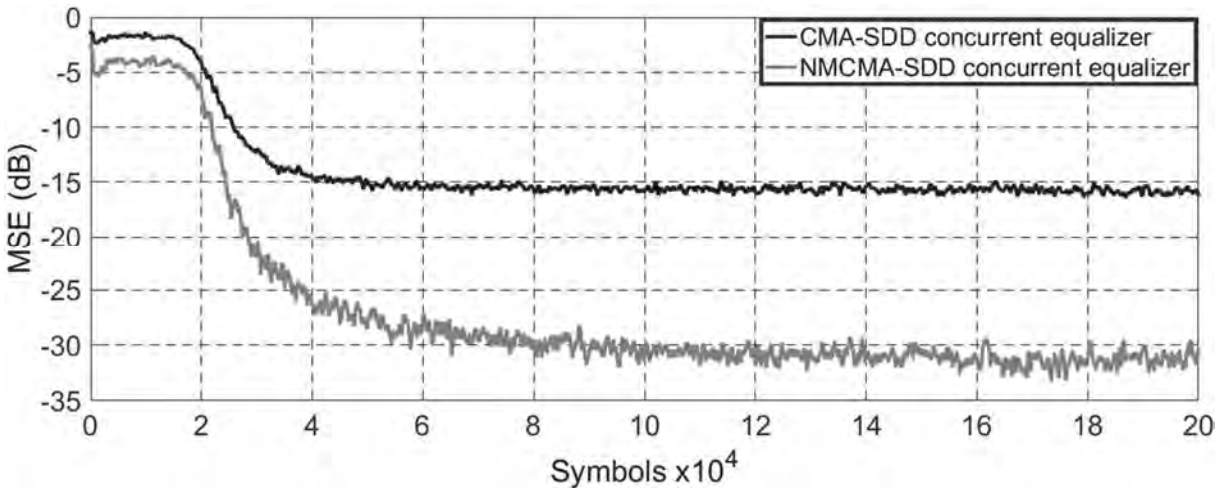

Source: Author (2018).

Figure 115 – 64-QAM - SER comparison of the CMA-SDD and NMCMA-SDD concurrent equalizers to the dynamic Brazil C for $f_D = 20$ Hz.

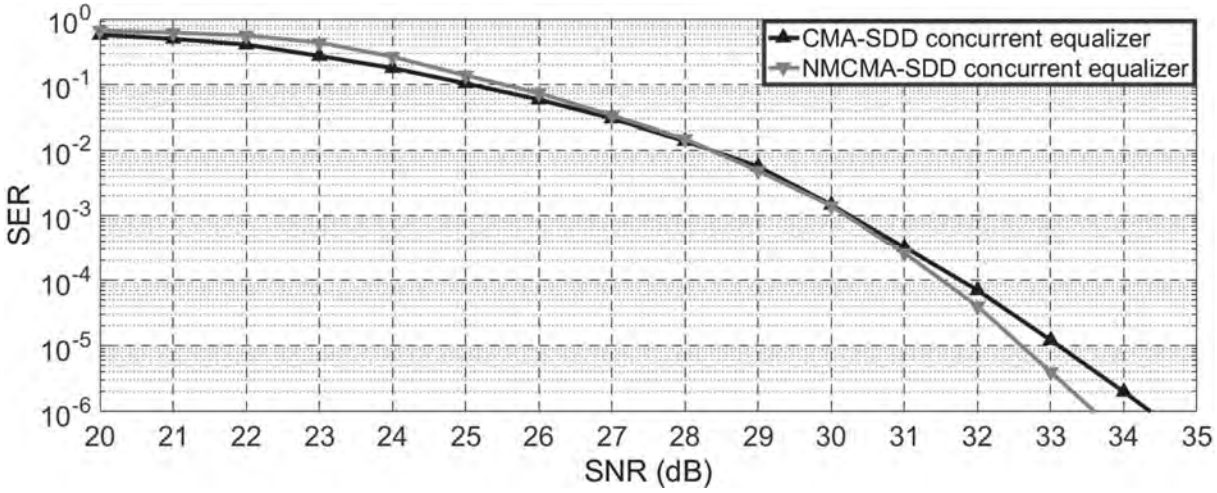

Source: Author (2018).

Figure 116 – 64-QAM - MSE comparison of the CMA-SDD and NMCMA-SDD concurrent equalizers to the static Brazil D.

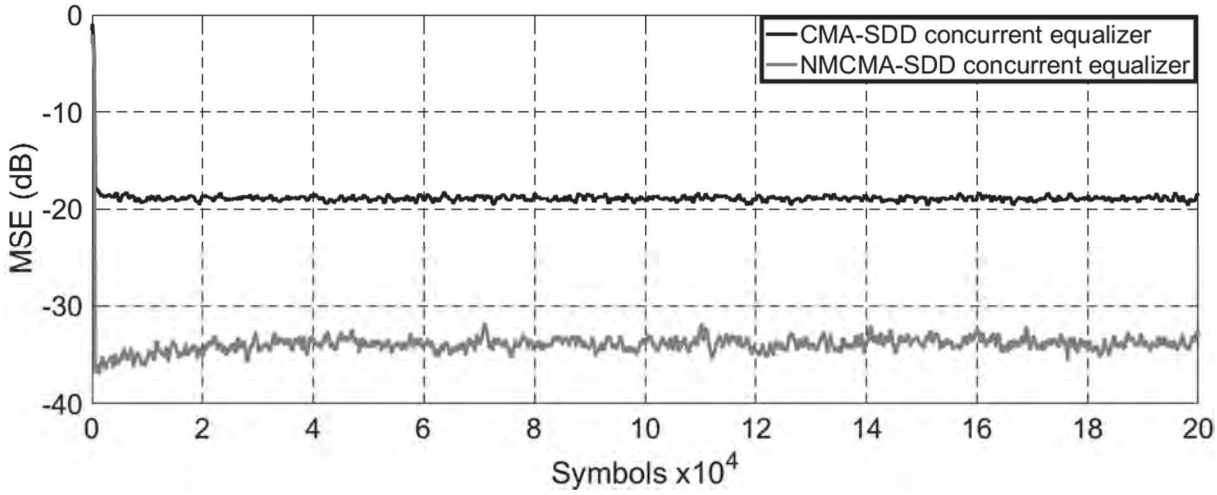

Source: Author (2018).

Figure 117 – 64-QAM - SER comparison of the CMA-SDD and NMCMA-SDD concurrent equalizers to the static Brazil D.

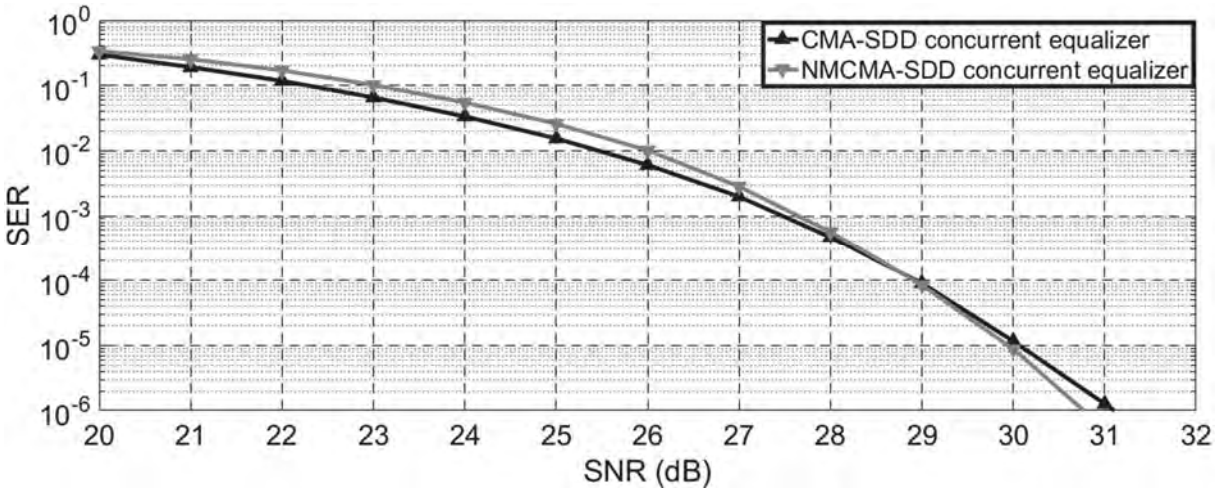

Source: Author (2018).

Figure 118 – 64-QAM - MSE comparison of the CMA-SDD and NMCMA-SDD concurrent equalizers to the dynamic Brazil D for $f_D = 20$ Hz.

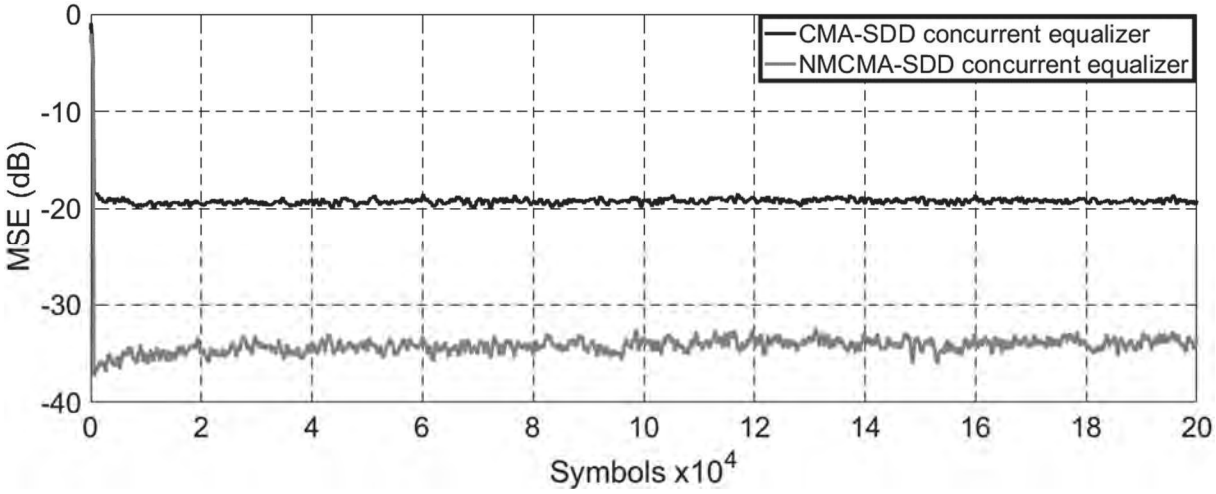

Source: Author (2018).

Figure 119 – 64-QAM - SER comparison of the CMA-SDD and NMCMA-SDD concurrent equalizers to the dynamic Brazil D for $f_D = 20$ Hz.

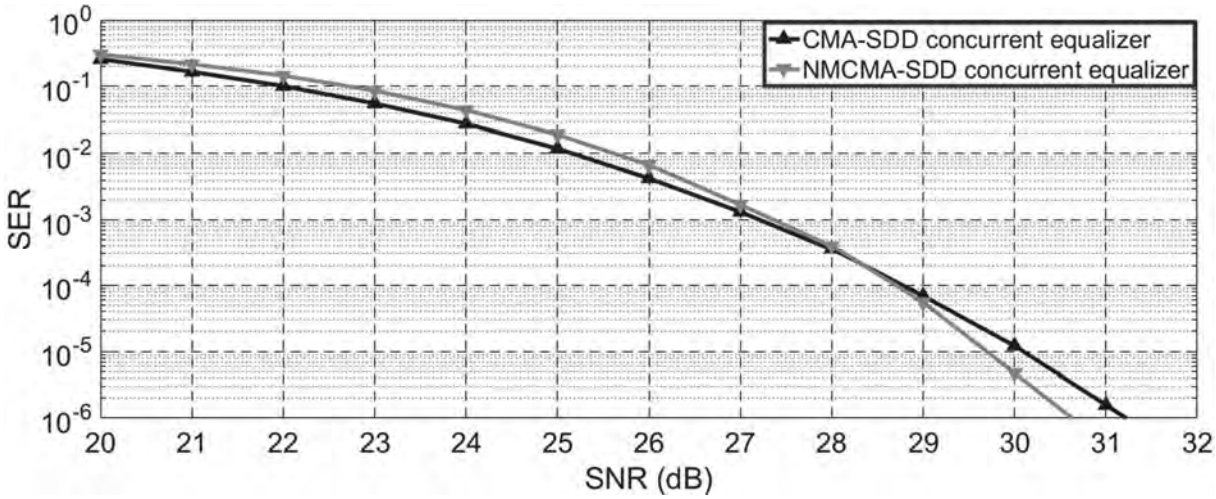

Source: Author (2018).

Figure 120 – 64-QAM - MSE comparison of the CMA-SDD and NMCMA-SDD concurrent equalizers to the static Brazil E.

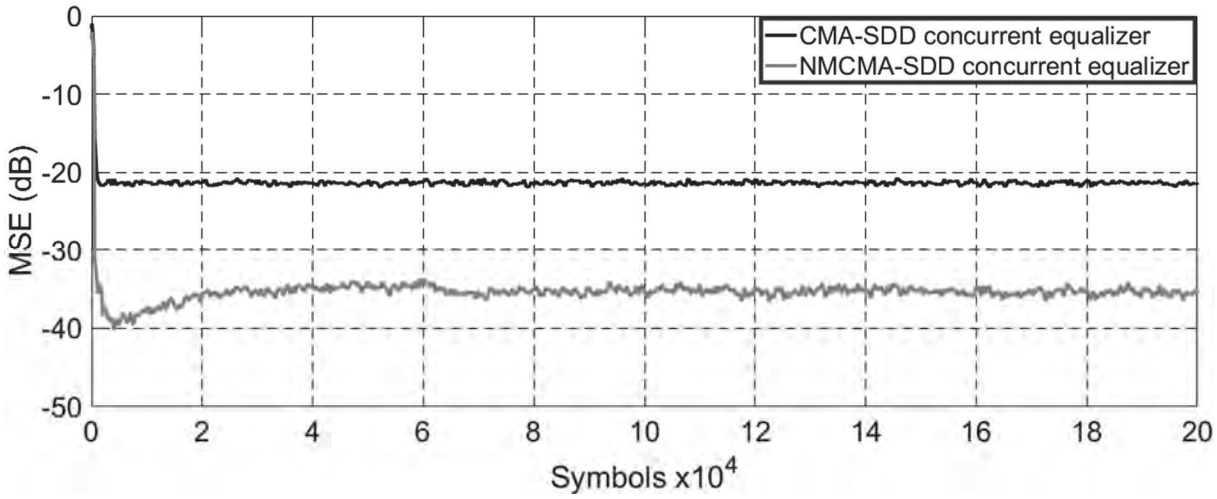

Source: Author (2018).

Figure 121 – 64-QAM - SER comparison of the CMA-SDD and NMCMA-SDD concurrent equalizers to the static Brazil E.

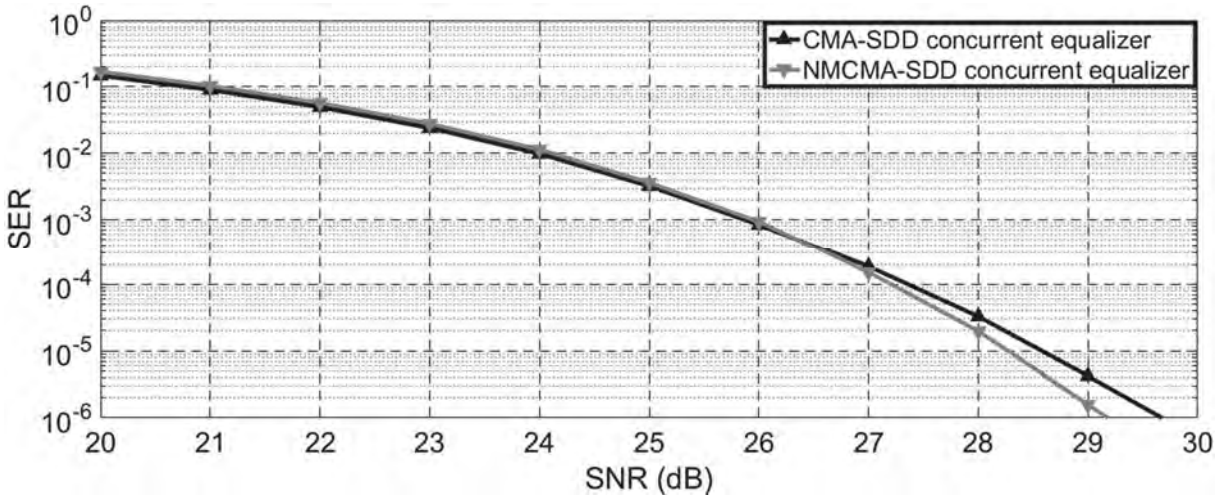

Source: Author (2018).

Figure 122 – 64-QAM - MSE comparison of the CMA-SDD and NMCMA-SDD concurrent equalizers to the dynamic Brazil E for $f_D = 20$ Hz.

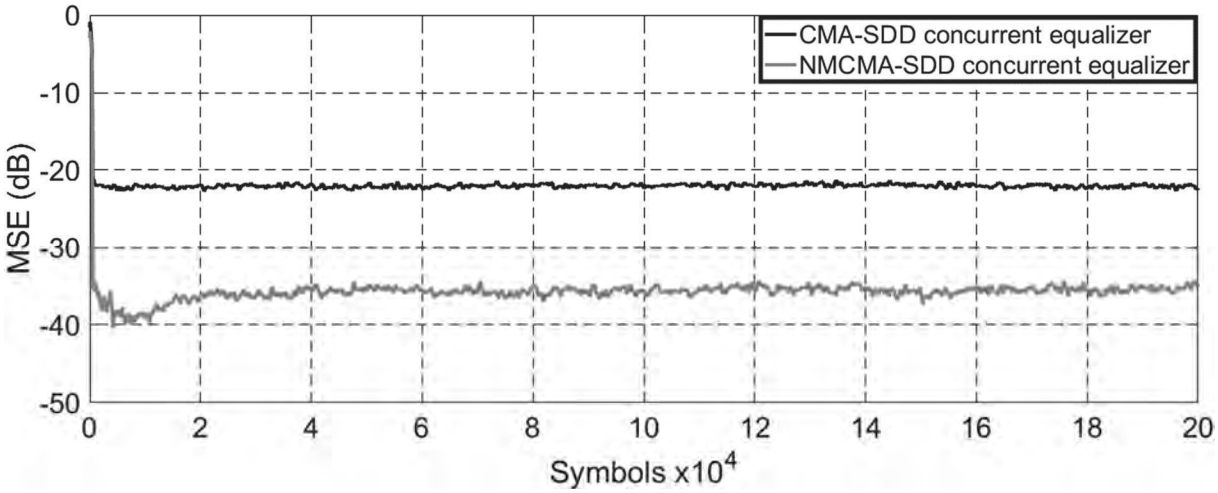

Source: Author (2018).

Figure 123 – 64-QAM - SER comparison of the CMA-SDD and NMCMA-SDD concurrent equalizers to the dynamic Brazil E for $f_D = 20$ Hz.

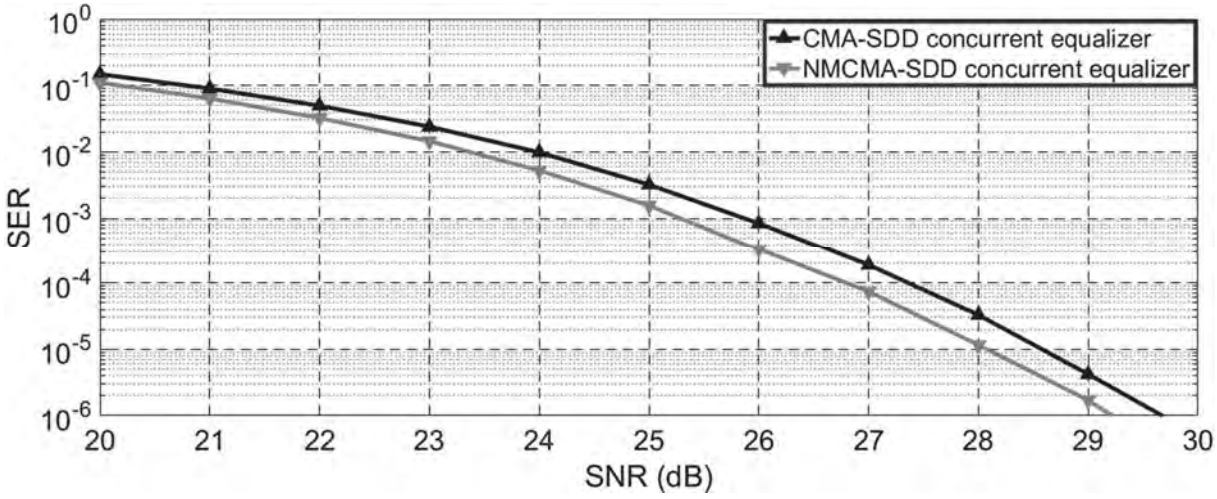

Source: Author (2018).

APPENDIX C - 256-QAM MSE and SER simulations for the static and dynamic Brazil channels.

Figure 124 – 256-QAM - MSE comparison of the CMA-SDD and NMCMA-SDD concurrent equalizers to the static Brazil A.

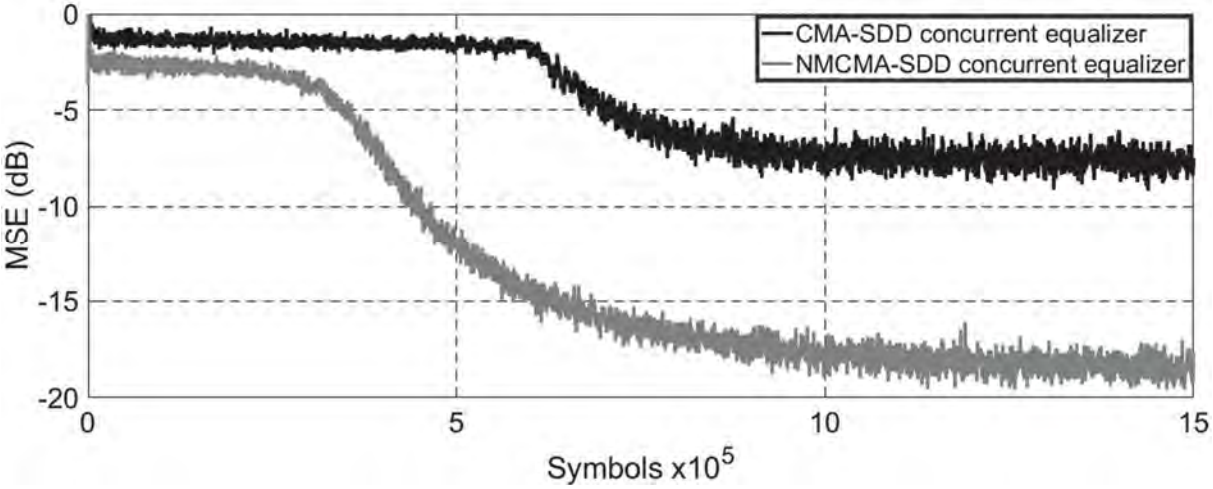

Source: Author (2018).

Figure 125 – 256-QAM - SER comparison of the CMA-SDD and NMCMA-SDD concurrent equalizers to the static Brazil A.

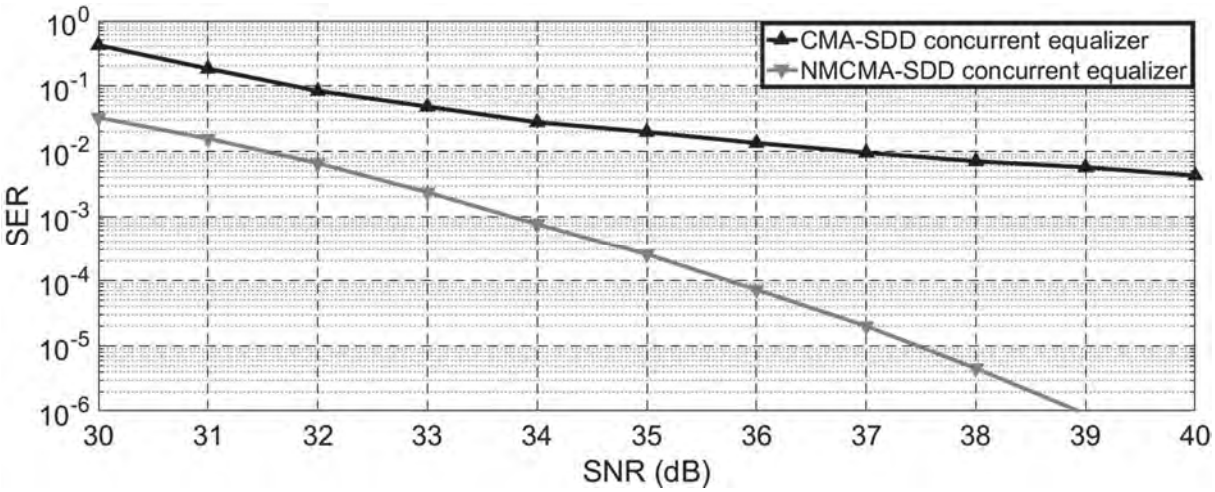

Source: Author (2018).

Figure 126 – 256-QAM - MSE comparison of the CMA-SDD and NMCMA-SDD concurrent equalizers to the dynamic Brazil A for $f_D = 20$ Hz.

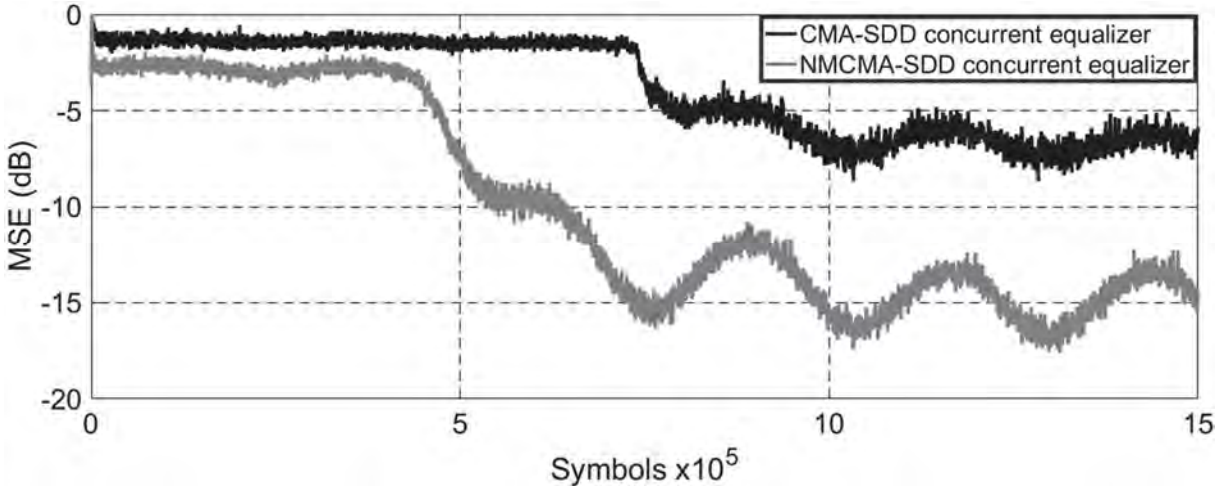

Source: Author (2018).

Figure 127 – 256-QAM - SER comparison of the CMA-SDD and NMCMA-SDD concurrent equalizers to the dynamic Brazil A for $f_D = 20$ Hz.

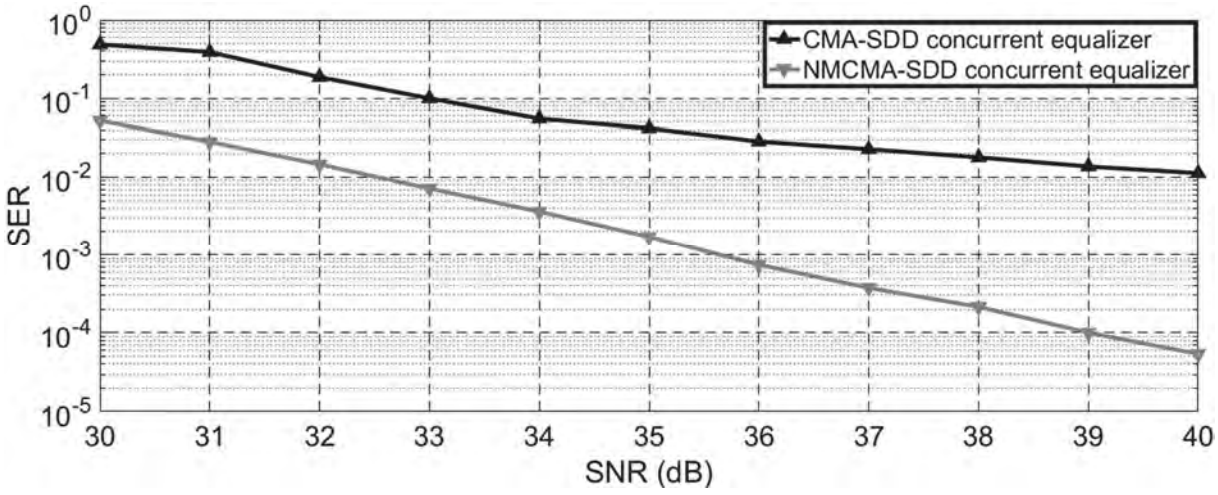

Source: Author (2018).

Figure 128 – 256-QAM - MSE comparison of the CMA-SDD and NMCMA-SDD concurrent equalizers to the static Brazil B.

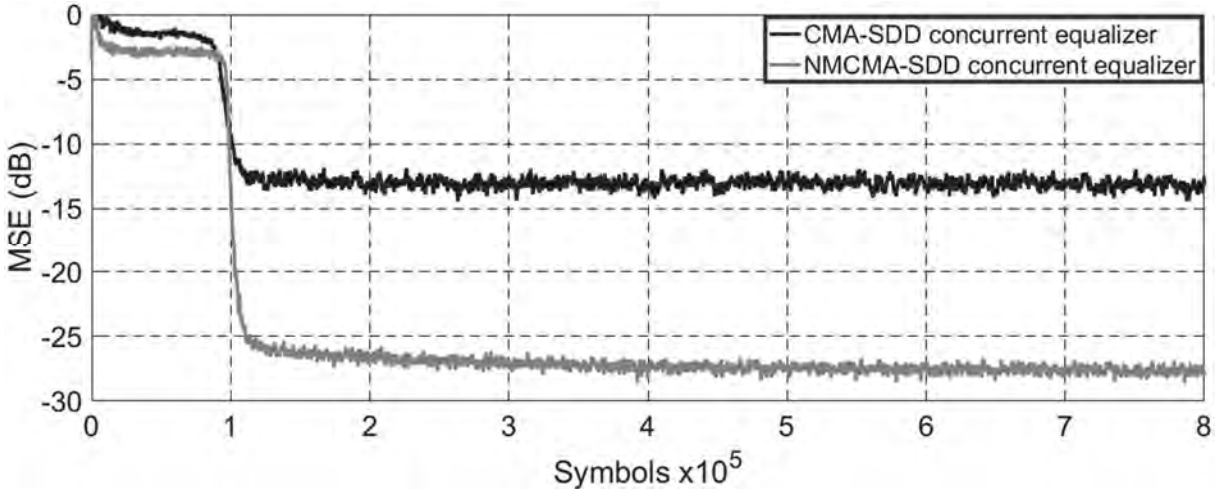

Source: Author (2018).

Figure 129 – 256-QAM - SER comparison of the CMA-SDD and NMCMA-SDD concurrent equalizers to the static Brazil B.

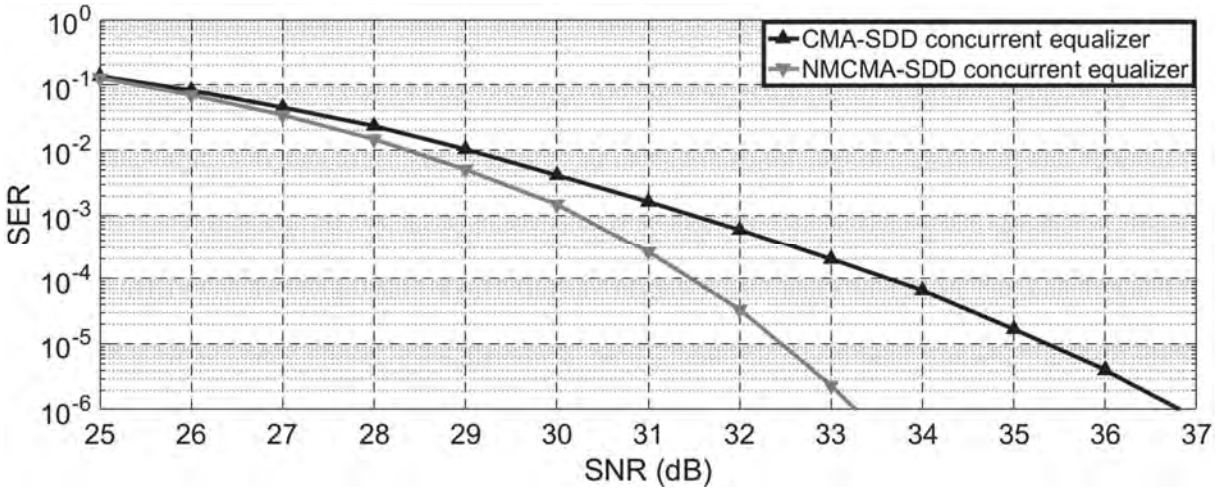

Source: Author (2018).

Figure 130 – 256-QAM - MSE comparison of the CMA-SDD and NMCMA-SDD concurrent equalizers to the dynamic Brazil B for $f_D = 20$ Hz.

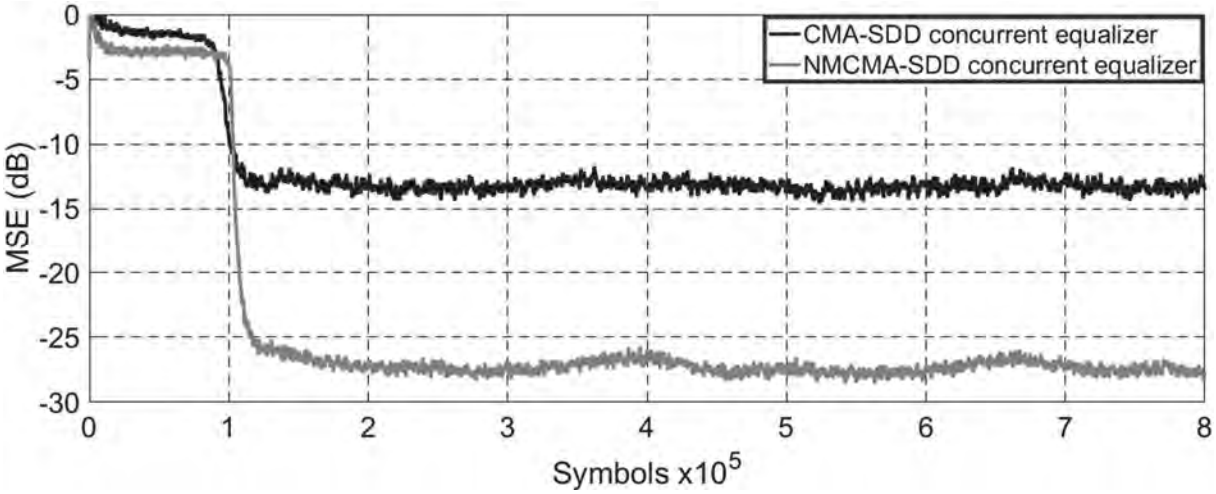

Source: Author (2018).

Figure 131 – 256-QAM - SER comparison of the CMA-SDD and NMCMA-SDD concurrent equalizers to the dynamic Brazil B for $f_D = 20$ Hz.

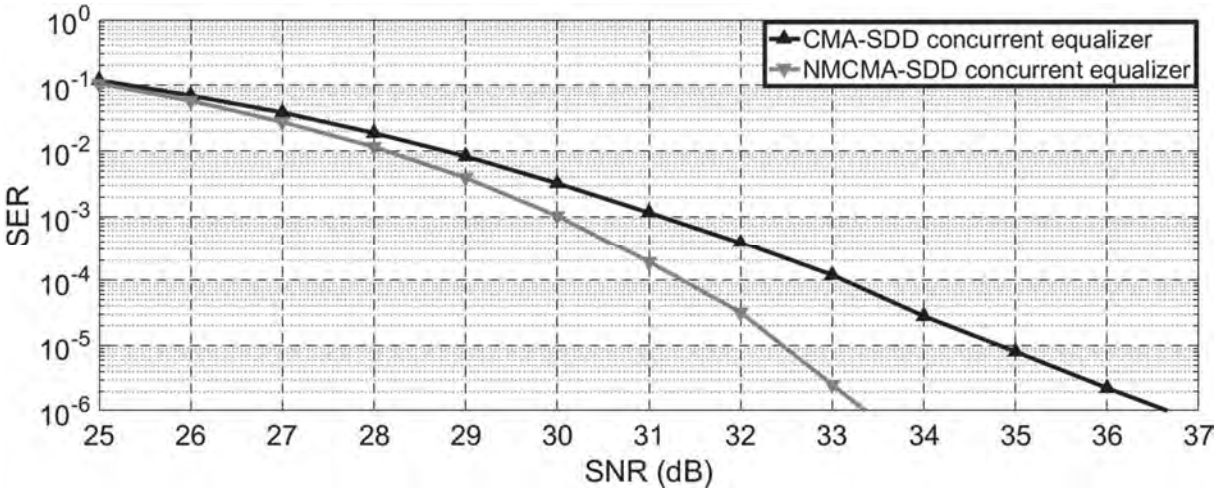

Source: Author (2018).

Figure 132 – 256-QAM - MSE comparison of the CMA-SDD and NMCMA-SDD concurrent equalizers to the static Brazil C.

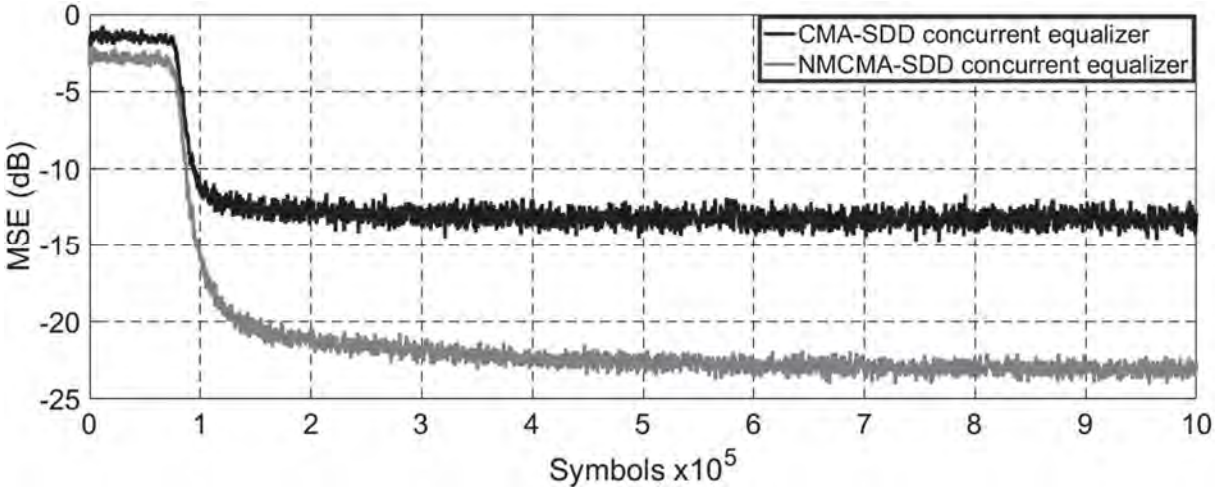

Source: Author (2018).

Figure 133 – 256-QAM - SER comparison of the CMA-SDD and NMCMA-SDD concurrent equalizers to the static Brazil C.

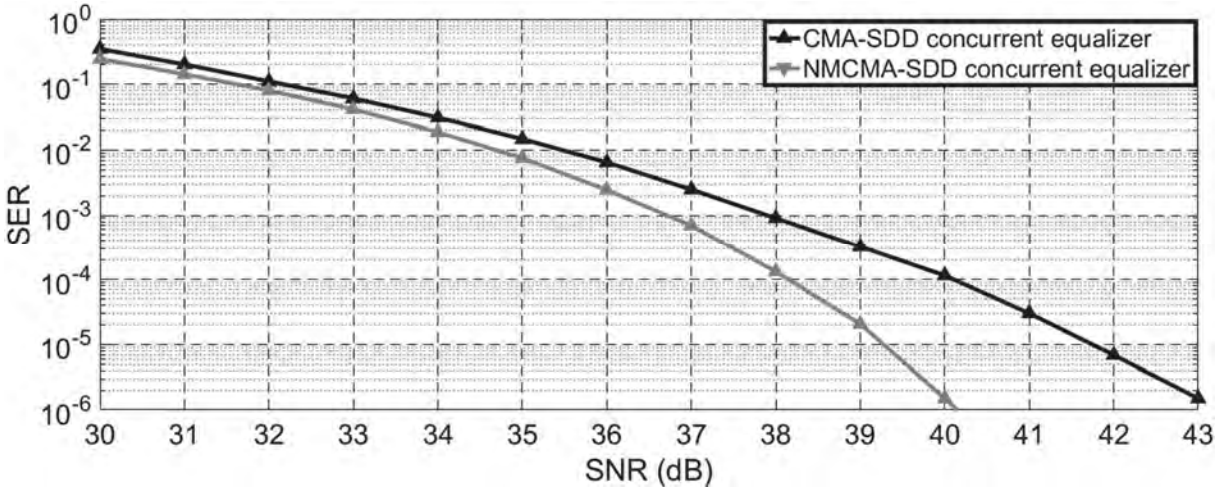

Source: Author (2018).

Figure 134 – 256-QAM - MSE comparison of the CMA-SDD and NMCMA-SDD concurrent equalizers to the dynamic Brazil C for $f_D = 20$ Hz.

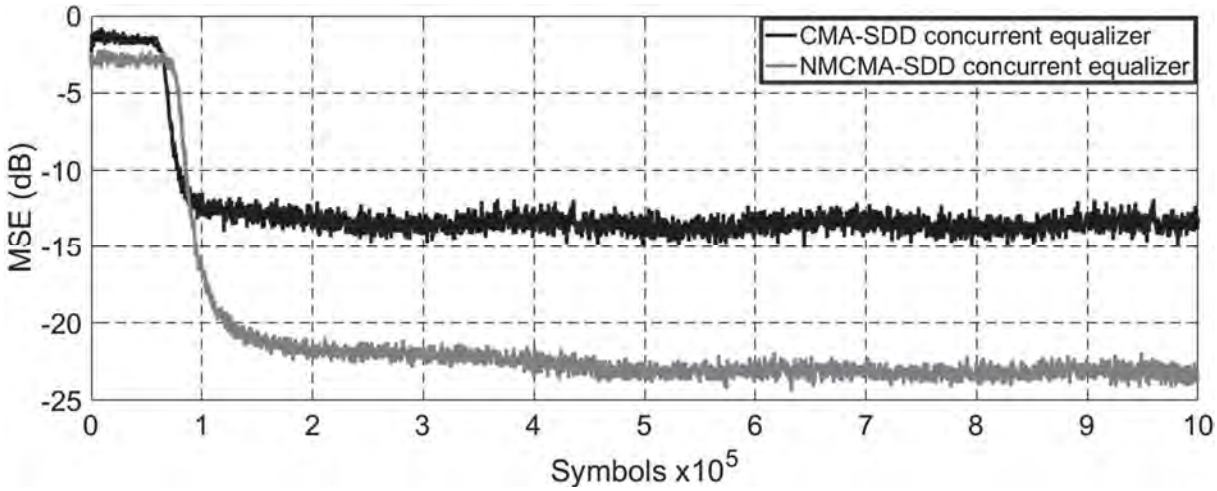

Source: Author (2018).

Figure 135 – 256-QAM - SER comparison of the CMA-SDD and NMCMA-SDD concurrent equalizers to the dynamic Brazil C for $f_D = 20$ Hz.

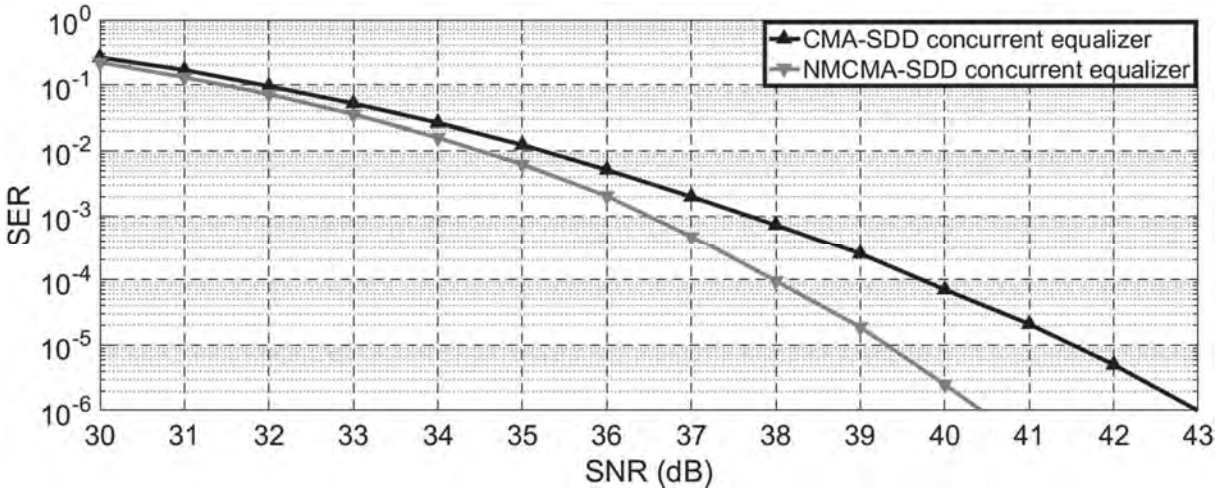

Source: Author (2018).

Figure 136 – 256-QAM - MSE comparison of the CMA-SDD and NMCMA-SDD concurrent equalizers to the static Brazil D.

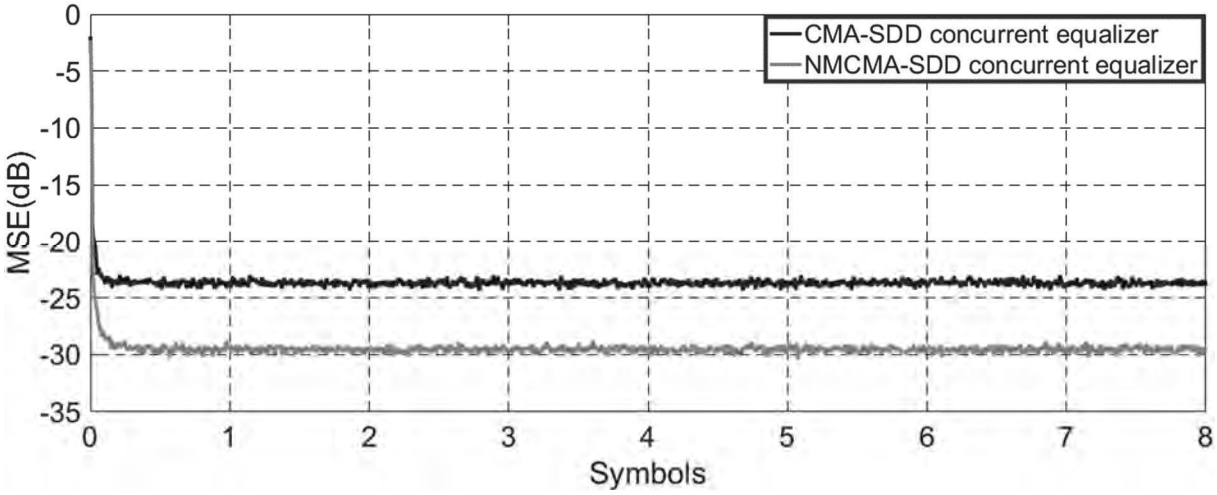

Source: Author (2018).

Figure 137 – 256-QAM - SER comparison of the CMA-SDD and NMCMA-SDD concurrent equalizers to the static Brazil D.

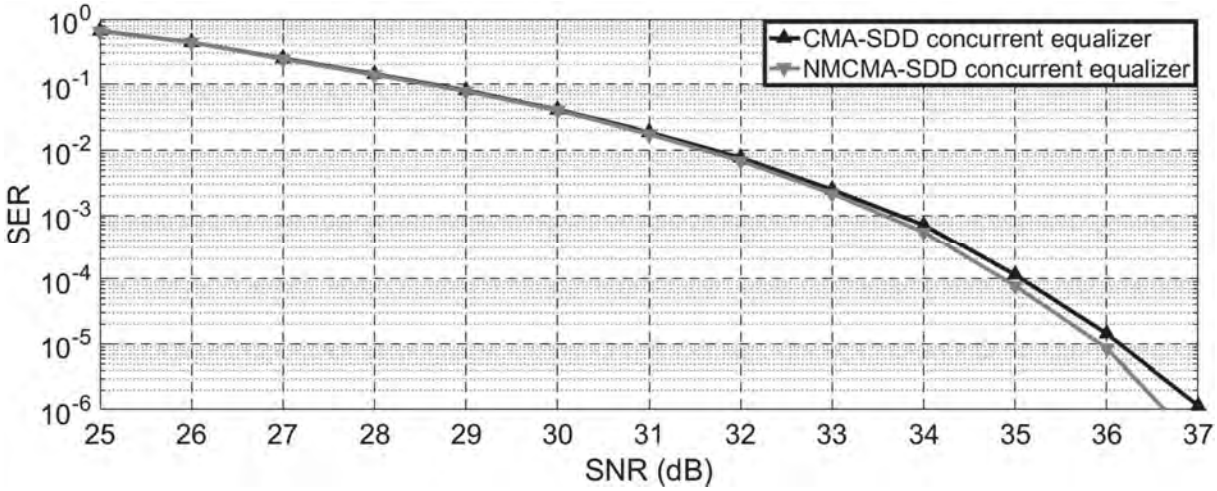

Source: Author (2018).

Figure 138 – 256-QAM - MSE comparison of the CMA-SDD and NMCMA-SDD concurrent equalizers to the dynamic Brazil D to $f_D = 20$ Hz.

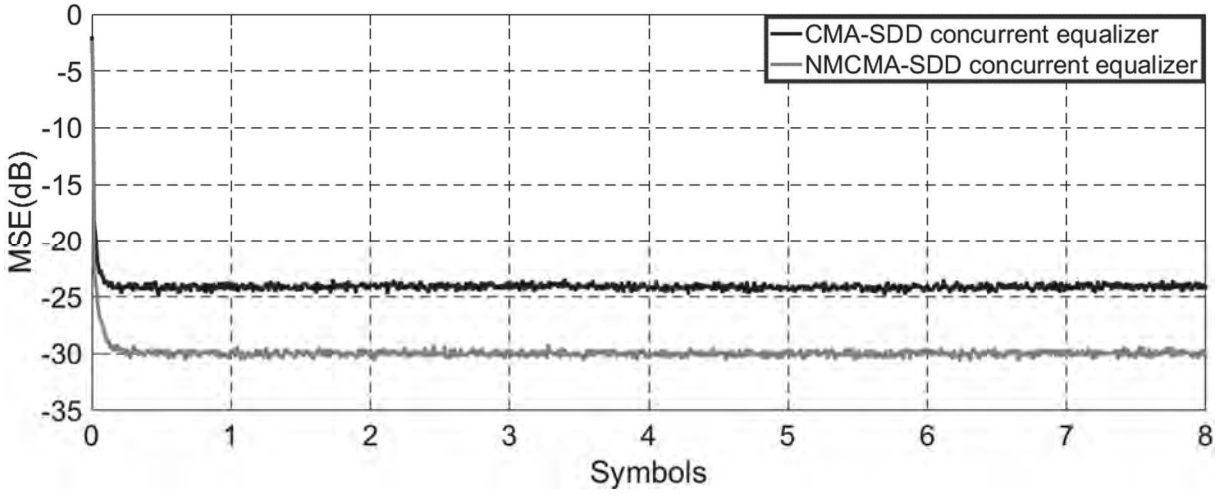

Source: Author (2018).

Figure 139 – 256-QAM - SER comparison of the CMA-SDD and NMCMA-SDD concurrent equalizers to the dynamic Brazil D to $f_D = 20$ Hz.

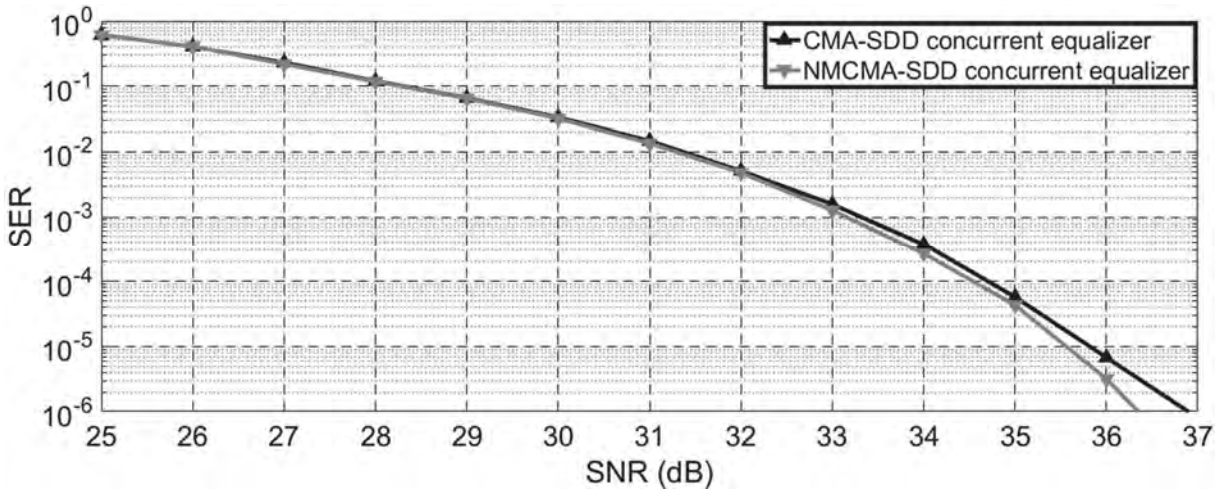

Source: Author (2018).

Figure 140 – 256-QAM - MSE comparison of the CMA-SDD and NMCMA-SDD concurrent equalizers to the static Brazil E.

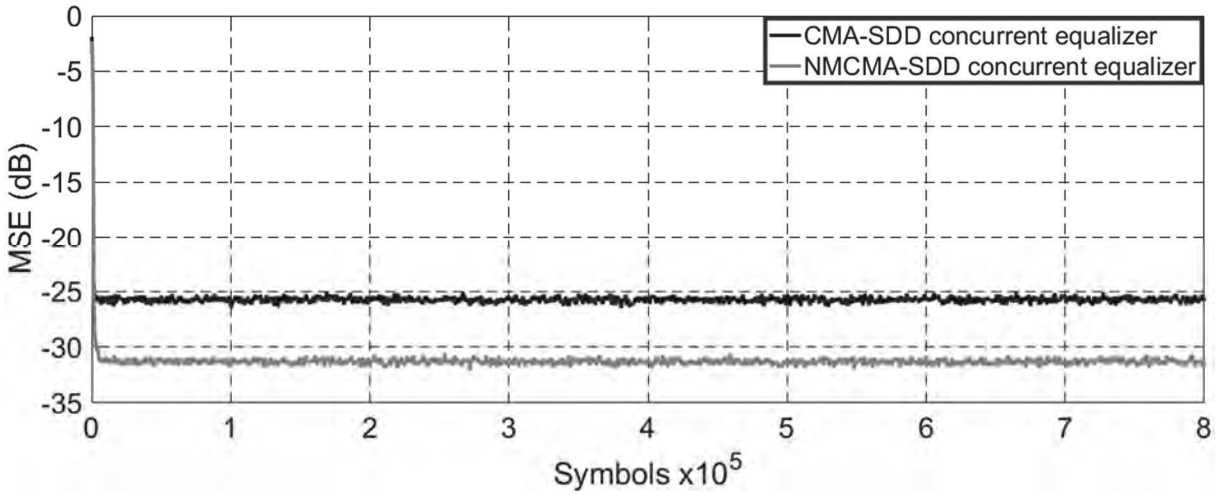

Source: Author (2018).

Figure 141 – 256-QAM - SER comparison of the CMA-SDD and NMCMA-SDD concurrent equalizers to the static Brazil E.

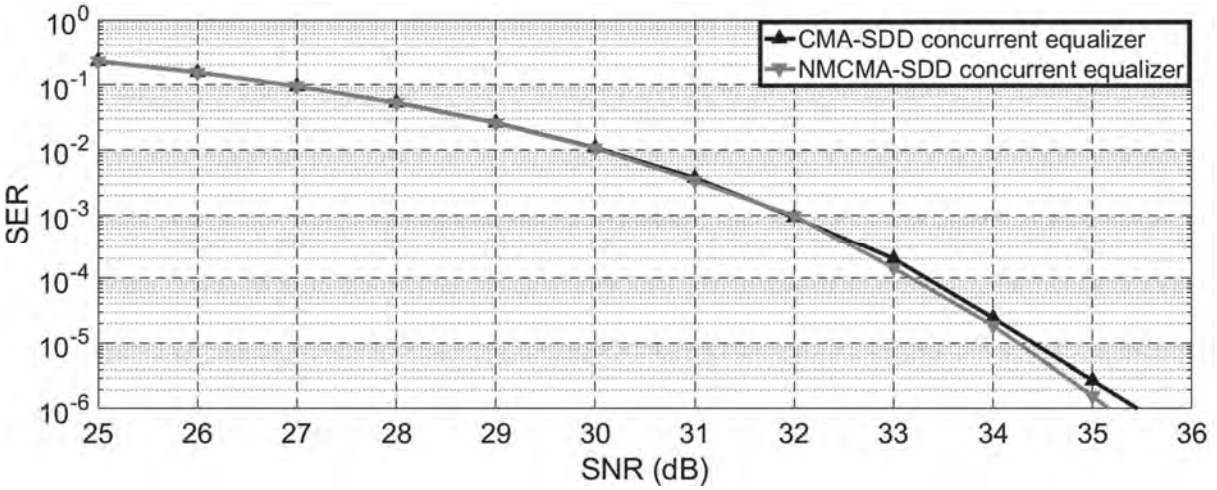

Source: Author (2018).

Figure 142 – 256-QAM - MSE comparison of the CMA-SDD and NMCMA-SDD concurrent equalizers to the dynamic Brazil E for $f_D = 20$ Hz.

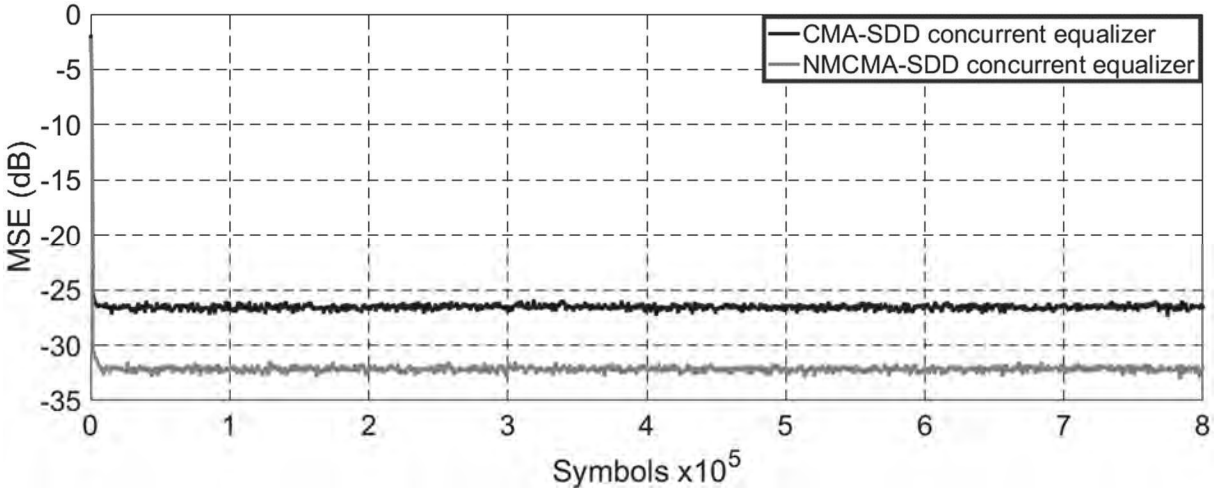

Source: Author (2018).

Figure 143 – 256-QAM - SER comparison of the CMA-SDD and NMCMA-SDD concurrent equalizers to the dynamic Brazil E for $f_D = 20$ Hz.

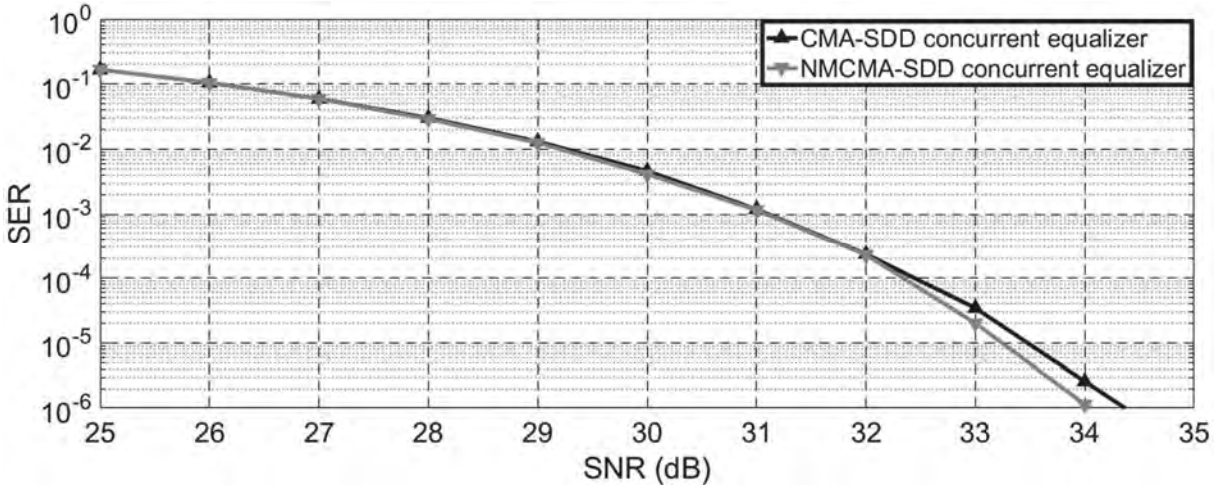

Source: Author (2018).

Pontifícia Universidade Católica do Rio Grande do Sul
Pró-Reitoria de Graduação
Av. Ipiranga, 6681 - Prédio 1 - 3º. andar
Porto Alegre - RS - Brasil
Fone: (51) 3320-3500 - Fax: (51) 3339-1564
E-mail: prograd@pucrs.br
Site: www.pucrs.br